FERMILAB-THESIS-2017-19

Phenomenology and Astrophysics of Gravitationally-Bound Condensates of Axion-Like Particles

Joshua Armstrong Eby
B.S. Physics, Indiana University South Bend (2011)

A dissertation submitted to the
Graduate School
of the University of Cincinnati
in partial fulfillment of the
requirements for the degree of
Doctor of Philosophy
in the Department of Physics
of the College of Arts and Sciences

Committee Chair: L.C.R. Wijewardhana, Ph.D

Date: 4/24/2017

Abstract

Light, spin-0 particles are ubiquitous in theories of physics beyond the Standard Model, and many of these make good candidates for the identity of dark matter. One very well-motivated candidate of this type is the axion. Due to their small mass and adherence to Bose statistics, axions can coalesce into heavy, gravitationally-bound condensates known as boson stars, also known as axion stars (in particular). In this work, we outline our recent progress in attempts to determine the properties of axion stars. We begin with a brief overview of the Standard Model, axions, and bosonic condensates in general. Then, in the context of axion stars, we will present our recent work, which includes: numerical estimates of the macroscopic properties (mass, radius, and particle number) of gravitationally stable axion stars; a calculation of their decay lifetime through number-changing interactions; an analysis of the gravitational collapse process for very heavy states; and an investigation of the implications of axion stars as dark matter. The basic conclusions of our work are that weakly-bound axion stars are only stable up to some calculable maximum mass, whereas states with larger masses collapse to a small radius, but do not form black holes. During collapse, a rapidly increasing binding energy implies a fast rate of decay to relativistic particles, giving rise to a Bosenova. Axion stars that are otherwise stable could be caused to collapse either by accretion of free particles to masses above the maximum, or through astrophysical collisions; in the latter case, we estimate the rate of collisions and the parameter space relevant to induced collapse.

Acknowledgements

I would first like to thank my advisor, L.C.R. Wijewardhana, who as a mentor and role-model, pushed me to be successful; I could not have asked for a more supportive, encouraging, or dedicated advisor. I would also like to thank Peter Suranyi, from whom I have learned a great deal and without whom this work would not have been possible.

I also thank my family, for providing encouragement throughout this process; where friendship is fragile, family is robust, and I thank them for their unwavering support.

In my development as a physicist, I am indebted to Philip Argyres, Paddy Fox, Roni Harnik, Frank Pinski, and Jure Zupan, who provided important guidance, as well as many opportunities that would not have existed otherwise.

In my development as a person, I sincerely thank Stephanie Burkus, Carrie Doyle, Matteo Lotito, Brian Maddock, Patrick Malsom, Jonathan Thompson, Douglas Tuckler, Kelsey Turner, and Sarah Unser, who were by my side as I traversed the best and worst of graduate school. This road would have been much more difficult without them.

I further thank Kay Kinoshita, Chris Kouvaris, Madelyn Leembruggen, Joseph Leeney, Michael Ma, Niklas Gronlund Nielsen, and Cenalo Vaz, who made crucial contributions to this work as well.

Finally, I would like to thank Jerry Hinnefeld, Ilan Levine, Monika Lynker, and Rolf Schimmrigk, for guidance in my very early years of studying science, and for nurturing the potential they saw in me. To the latter, I have not forgotten that I owe a paper on the topic of General Relativity. Though it is now more than six years late, I hope this will suffice.

Preface

This dissertation describes my research related to axions and axion stars as a component of dark matter. Chapter 1 gives a basic introduction to the Standard Model of particle physics and the ΛCDM model of cosmology, and briefly outlines the relevant successes and failures of both. Axions are introduced in Chapter 2, which is followed by a historical and pedagogical introduction to boson stars in Chapter 3. We turn then to the particular case of axion stars. The macroscopic properties, including mass and radius, of weakly-bound axion stars are calculated in Chapter 4. In Chapter 5, we take into account axion self-interactions which lead to number-changing transitions in an axion star, leading to a nontrivial lifetime for axion stars to decay to relativistic free particles. The collapse of gravitationally unstable states is detailed in Chapter 6, and in Chapter 7, the question is considered whether collapse can be triggered by astrophysical collisions. Concluding remarks are found in Chapter 8.

In what follows, we will use Greek characters (α, β, γ, etc.) to denote Lorentz indices, early-alphabet Latin characters (a, b, c, etc.) for gauge indices, and later-alphabet Latin characters (i, j, k, etc.) for other indices. We employ the Einstein summation convention, and use natural units, where $\hbar = c = 1$.

Contents

List of Figures

List of Tables

List of Abbreviations

ΛCDM	Standard Model of Cosmology
CP	Charge-Parity Symmetry
ALP	Axion-Like Particle
ASt	Axion Star
BE	Bose-Einstein
BEC	Bose-Einstein Condensate
DM	Dark Matter
EDM	Electric Dipole Moment
EKG	Einstein+Klein-Gordon
FD	Fermi-Dirac
FDM	Fuzzy Dark Matter
FRB	Fast Radio Burst
GP	Gross-Pitäevskii
GPP	Gross-Pitäevskii+Poisson
GR	General Relativity
KG	Klein-Gordon
NFW	Navarro-Frenk-White
NSt	Neutron Star
OSt	Ordinary Star
PQ	Peccei-Quinn
QCD	Quantum Chromodynamics
QFT	Quantum Field Theory
RB	Ruffini-Bonazzola
SM	Standard Model of Particle Physics
TF	Thomas-Fermi
vev	Vacuum Expectation Value

"The scientist does not study nature because it is useful; he studies it because he takes pleasure in it, and he takes pleasure in it because it is beautiful. If nature was not beautiful, it would not be worth knowing, life would not be worth living. I am not speaking here, of course, of that beauty which strikes the senses, of the beauty of qualities and appearances; nor that I should deny it, far from it, but it has nothing to do with science. I mean the more intimate beauty which comes from the harmonious order of the parts, and which a pure intelligence can grasp."

— Henri Poincaré

Chapter 1.

Introduction

"Science is built up of facts, as a house is built of stones; but an accumulation of facts is no more a science than a heap of stones is a house."

— Henri Poincaré

In this chapter, we review the well-understood properties of the Standard Model of particle physics, and the ΛCDM model of cosmology. We then discuss open questions and unexplained observations which will be relevant to this work.

1.1. The Standard Model of Particle Physics

The Standard Model of particle physics (SM) forms the basis of all investigations of the fundamental properties of particles in the universe (for recent reviews, see [1, 2]). The Higgs particle, discovered at the LHC in 2012 [3, 4], constituted the last major piece of the quantum picture of the SM, as it provides a consistent dynamical mechanism for generating the masses of the rest of the fundamental particles [5, 6]. The SM describes well a vast array of current experimental observations, including small-scale observations of the inner structure and forces inside of nuclei (e.g. for strong force see [7], for weak force see [8, 9]), as well as numerous observations in astrophysics and cosmology [10–12].

The basic interactions between particles in the SM are defined by Quantum Field Theory (QFT) [14, 15], which describes the electromagnetic, strong nuclear, and weak nuclear forces, as well as General Relativity (GR) [16, 17]. GR describes gravity through the connection of the curvature of spacetime to the mass-energy density, as encapsulated

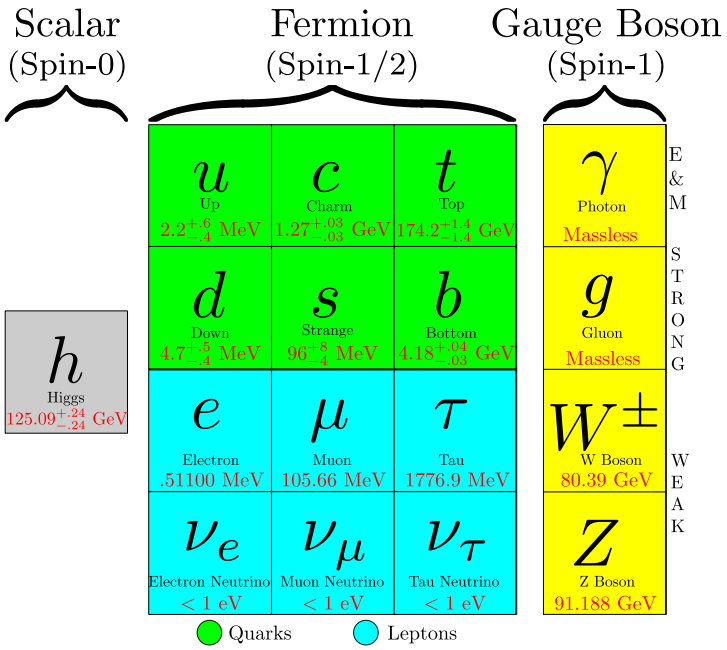

Figure 1.1.: The particle content of the Standard Model of particle physics. For each particle, both their spin class (spin = 0, 1/2, or 1) and mass [13] are included. Lepton and gauge boson mass uncertainties are at the $< 10^{-4}$ level and are omitted.

by the Einstein field equations:

$$G_{\mu\nu} = 8\,\pi\,G\,T_{\mu\nu} \tag{1.1}$$

where $G = 1/M_P^2$ is Newton's gravitational constant and $M_P = 1.22 \times 10^{19}$ GeV is the Planck mass. In Einstein's equations, the curvature tensor $G_{\mu\nu}$ is proportional to the stress-energy tensor $T_{\mu\nu}$, which contains the matter and energy content of the underlying system.

In QFT, particles of different spin are described by different quantum equations. Of particular interest here, scalar (spin-0) fields $\phi(x^\mu)$ satisfy the Klein-Gordon (KG) equation,

$$\mathcal{D}\,\phi - \frac{\partial\,V(\phi)}{\partial\,\phi} = 0, \tag{1.2}$$

where $V(\phi)$ is the potential for the scalar field ϕ, and $\mathcal{D}\,\phi = g^{\mu\nu}\,\partial_\mu\,\partial_\nu\,\phi$ is a covariant second derivative in curved spacetime with a metric $g^{\mu\nu}$.[1] This equation determines the dynamics of scalar particles on mass-shell; that is, particles which satisfy the relationship $E^2 - p^2 = m^2$ between their momentum p, energy E, and mass m. The

[1] Fermionic particles are described by the Dirac equation, but we will not need to consider such particles much further for the purposes of this work.

gauge interactions of particles in the SM are defined by their charges under the SM gauge group, $SU(3)_{color} \times SU(2)_{weak} \times U(1)_{EM}$.

Of paramount importance in the SM is Lorentz invariance, which ensures energy and momentum conservation in fundamental interactions. In four spacetime dimensions, it also provides an important classification of particles by their spin, into bosons (which have integer spins $s = 0, 1, 2, ...$) and fermions (which have half-integer spins $s = \frac{1}{2}, \frac{3}{2}, ...$). Fermions, satisfying the Pauli Exclusion Principle, exist in quantum states that can be occupied by at most one particle. On the other hand, quantum states can be occupied by an arbitrary number of bosons, leading to special properties for bosonic systems.

When a very large collection of bosons is cooled to low temperatures, an $\mathcal{O}(1)$ fraction of them coalesce into the ground state of the system [18–20]. The resulting state, known as a Bose-Einstein condensate (BEC), has been observed in atomic systems [21, 22]. These are quantum states in which every ground state boson subscribes to the same wavefunction localized on some radius R. They can have superfluid properties [23], form vortices with nontrivial angular momentum [24–26], and in some cases, collapse under perturbations or when they exceed a critical number of occupying bosons [27–29]. Recently, non-atomic BECs composed of light bosonic particles in theories beyond the SM have been investigated in an astrophysical context; such theories are relevant to the work presented here. We will return to the topic of BECs in Chapter 3.

The SM, successful though it is, does not succeed in answering a number of open questions, a few of which are of particular interest here. For example, there are strong experimental upper limits on the magnitude of the neutron electric dipole moment; because its magnitude is theoretically unconstrained, it is unknown within the SM why this dipole moment should be so small. This discrepancy between observation and expectation, known as the Strong CP Problem (see [30] and references therein), motivates the addition of particles known as *axions* to the SM. This problem and its solution through the addition of the axion is central to this work; these issues will be discussed in detail in Chapter 2.

The consistent application of the SM can, through the known particle content and interactions, explain a vast collection of observations in astrophysics and cosmology. However, in this application there also exist unanswered questions, as well as discrepancies with observation. For example, the epoch of the formation of galaxies predicted by the SM alone does not match with what is observed, and the SM does not explain the observation of late-time accelerated expansion of the universe. An extended model of cosmology, consistent with these observations and known as the ΛCDM model, is detailed in the next section.

1.2. The ΛCDM Model of Cosmology

In the early 1930s, astronomer Fritz Zwicky made an astounding discovery, by using two distinct methods to measure the mass of the Coma Cluster [31][2]. On one hand, he used the virial theorem to estimate the gravitational mass in the Cluster, using the velocities of galaxies estimated using their Doppler shifts. On the other hand, he also estimated the total mass of the visible matter, using the total light output of the trillions of stars in the Cluster's galaxies. If the known stars and gas, the luminous matter, were all there was, then these two estimates should have agreed. However, Zwicky found a large discrepancy: the gravitational mass he estimated was several times larger than the luminous mass! He concluded that the Coma Cluster must contain a large amount of matter not accounted for by the stars and gas, which he referred to as "dark matter."

Several decades later, Vera Rubin and others [33, 34] made very careful measurements of the rotation speeds of stars around galaxies out to very large radial distances r. It was expected, by the standard Newtonian gravitational theory, that these rotation speeds would drop quickly at large r, because a large fraction of the visible matter (stars and gas) in galaxies is concentrated in the central regions. To the contrary, the observations suggested *flat rotation curves*: stars very far from the galactic center were revolving with nearly the same speed as those closer to the center. Modern observations of a similar kind are consistent with this observation (see e.g. the recent publication [35]). It is now believed that these large rotation speeds are due to Zwicky's "dark matter" as well, a new form of non-luminous matter which exists in an extended halo enveloping galaxies.

Modern measurements of numerous kinds have corroborated this story. Observations of colliding galaxy clusters (one notable example being the so-called Bullet Cluster Collision) have shown a separation between the luminous matter, slowed by electromagnetic friction, and a significant nonluminous gravitational component which passes nearly unslowed by the collision [36]. The additional gravitational mass here is consistently identified as dark matter. Additionally, temperature correlations of the low-energy background of photons from the early universe (the *Cosmic Microwave Background*) are fit by a matter distribution which contains a DM component with roughly five times the mass of the SM contribution [37]. The modern view, consistent with the above observations, is that dark matter (which we now recognize as the DM of the ΛCDM model) consists of some particle(s) not contained within the SM, and which can only interact weakly (or not at all) with the electromagnetic force.

[2] For recent republication in English, see [32]

While there are numerous theories of possible constituents of DM in galaxies, one can constrain the space of DM models in particle physics using astrophysical and cosmological observations. As mentioned briefly in the previous section, the cosmological evolution of the SM particles from the early universe is not consistent with the known epoch of galaxy formation. Numerical simulations, performed both with and without a dark matter component, lead to the expectation that galaxies form from small density perturbations in the very dense background of the early universe. These perturbations are too small and come too late if the SM particle content is all that exists, but simulations containing a dark matter component show that DM can solve this problem if it constitutes a very large fraction of the mass of the early universe [38]. This conclusion comes with a caveat, however: the DM must be sufficiently *cold*, that is, nonrelativistic early enough in the universe so that it clumps together to form the seeds of future galaxies. The "C" in the ΛCDM cosmological model represents the requirement that DM particles be cold.

These same numerical simulations also give hints regarding the structure of dark matter halos. Generically, the density distribution for dark matter that emerges from simulation is well-approximated by a simple function known as the Navarro-Frenk-White (NFW) profile [39, 40], which has the form

$$\rho_m(r) = \frac{\rho_0}{\left(\frac{r}{R_0}\right)\left(1+\frac{r}{R_0}\right)^2}. \tag{1.3}$$

The free parameters ρ_0 and R_0 are the scale density and radius (respectively), which vary from galaxy to galaxy. Note that the NFW form of the density distribution implies a spherically symmetric dark matter halo.

As alluded to above, DM cannot couple strongly to the electromagnetic force, because it does not appear to emit or absorb light (it is "dark"). It similarly cannot couple strongly to the strong nuclear force; such couplings would conflict with a number of observations, including the galaxy cluster collisions discussed above. In the "worst-case" scenario (that is, the most difficult case experimentally), DM might not couple to the weak nuclear interaction either, implying that its only connection to the SM might be gravitational. For a recent review of constraints on DM couplings to the SM from direct detection experiments, see [41].

There are also constraints on the *self*-interactions among DM particles. These arise from, again, the observation of large, gravitating masses passing directly without interaction in galaxy cluster collisions [36]. The upper bound on the DM cross section

σ_{SI} is of the form

$$\frac{\sigma_{SI}}{m} \lesssim 1 \frac{\text{cm}^2}{\text{gram}}, \tag{1.4}$$

where m is the DM particle mass. Larger cross sections than the bound in eq. (1.4) have also been found to overflatten the cores of dwarf galaxies [42]. In many models of DM, the self-interaction cross section is set effectively to zero (making DM collisionless), but recently self-interactions in the DM sector have received renewed interest (for recent reviews and comparisons, see [43, 44]).

One reason self-interacting DM has received attention of late is that there exist discrepancies between observations and simulations of collisionless DM. The first discrepancy, known as the cusp-core problem, is related to the fact that dwarf galaxies are observed to have flat density profiles in their central regions [45, 46], while N-body simulations predict cuspy profiles for collisionless DM (as in the NFW profile of eq. (1.3) [39, 40]). Second, the number of satellite galaxies in the Milky Way is far fewer than the number predicted in simulations [47–52]. Last is the so-called "too big to fail" problem: simulations predict dwarf galaxies in a mass range that we have not observed, but which are too large to have not yet produced stars [53]. (For a recent review of the status of these problems, see [54].) The solution of these problems is currently unknown, but simulations including DM self-interactions suggest that they have the effect of smoothing out cuspy density profiles, and could solve the other problems of collisionless DM as well [42, 44, 55].

Clearly, there is very strong evidence for some non-SM particle (or particles) which constitute DM. While we have learned much about the nature and structure of DM halos, there are many unanswered questions. For a review of modern models and constraints on DM, see [56, 57]. We will return to some of these issues throughout this work.

Finally, we come to the Λ in ΛCDM. The field equations of GR, when applied to the universe as a whole, relate the total energy density to the overall curvature (see, e.g. [10]). The relative contributions of different forms of energy, e.g. matter and radiation, give rise to different expansion rates of the universe. Both matter and radiation give rise to positive pressure terms, i.e. they tend to cause the universe to contract; as a result, it was expected for many years that the universe's outward expansion, a remnant of the hot Big Bang, should be slowing due to gravity. Measurements of this expansion rate, conducted in the late 1990s, gave a startling conclusion: that the universe was expanding at an *accelerated rate* [58, 59]. In modern terms, this is understood to arise from a term with negative pressure in the Einstein equations, which would arise from

a so-called Cosmological Constant energy density, often referred to as "dark energy" and typically denoted by Λ. To be consistent with the observed acceleration rate and other cosmological observables, this "dark energy" should constitute nearly 70% of the total energy content of the universe, the remaining 30% being in the form of DM and ordinary SM particles [37]. We will not discuss the issue of dark energy any further here, but for recent reviews see [60, 61].

1.3. Summary

In this chapter, we have reviewed the standard picture of the universe, both in particle physics (using the Standard Model), as well as in astrophysics and cosmology (using ΛCDM). The SM is defined by the particle content shown in Figure 1.1, along with a symmetry group $SU(3) \times SU(2) \times U(1)$ defining gauge interactions. The SM is defined in part by to a small set of interactions and their corresponding force-carrier particles. Certain open questions, including the Strong CP Problem, suggest extensions of the SM which include additional particles, symmetries, or interactions.

Consistency with astrophysical and cosmological data requires the extension of the SM to include two very mysterious additional components: a cold "dark matter", which takes the form of some new, nonluminous particle(s); and a "dark energy" suffusing empty space and giving rise to the accelerated expansion of the universe. While the latter is interesting and important, the topic of this work will be a particular class of models for the particle content of DM. The particular DM candidate considered here, known as the *axion*, is also a well-motivated solution of a fine-tuning problem in the SM. We will describe the motivation and consequences of axion field theory in Chapter 2.

Chapter 2.

Axions in the Early Universe

"Laws were made to be broken."
— Christopher North

Axions are very light scalar particles which, if they exist, can solve multiple problems in the Standard Model at once: The Strong *CP* Problem, and the problem of dark matter (both reviewed in Chapter 1). In this section, we review the history of the axion as it connects to these problems, and in doing so, outline the important properties and the allowed parameter space for the axion. We also mention briefly axion-like particles which emerge from other theories.

2.1. The Strong *CP* Problem

Successful though it is, the SM does contain a few discrepancies in comparison to observation, as well as unsolved puzzles. One such puzzle goes by the name of the Strong *CP* Problem (for recent reviews, see [62, 63]). This is one of a number of fine-tuning problems in the SM; it can be summarized by the observation that a free parameter in the model is constrained to be significantly smaller than what would "naturally" be expected from the theory. While not strictly in conflict with observation, fine tuning problems often point us in the direction of new physics, or to a deeper understanding of existing results [64–66].

The Strong *CP* Problem is, as the name suggests, connected to the strong nuclear force, which is described by the theory of Quantum Chromodynamics (QCD).[1] The most generic Lagrangian allowed by the SM field content and gauge symmetries contains a

[1] Our discussion in this section will follow mostly [62], though other good reviews exist.

term of the form

$$\mathcal{L}_\theta = \frac{\theta\, g_s^2}{32\,\pi^2}\, G^{a\mu\nu}\, \tilde{G}^a_{\mu\nu}, \tag{2.1}$$

where $G^{a\mu\nu} = \partial^\mu\, G^{a\nu} - \partial^\nu\, G^{a\mu} - g_s\, f^{abc}\left[G^{b\mu}, G^{c\nu}\right]$ is the field strength tensor built from the gluon field $G^{a\mu}$, $\tilde{G}^{a\mu\nu} = \frac{1}{2}\epsilon^{\mu\nu\alpha\beta}\, G^a_{\alpha\beta}$ is the dual field strength, and where g_s and f^{abc} are the coupling and structure constants (respectively) of the gauge group of QCD, namely $SU(3)$. The brackets $[X, Y]$ denote the commutator of X and Y. Finally, θ is a dimensionless free parameter which, unconstrained by any dynamics that would fix its value, would be expected to take a "natural" value of $\mathcal{O}(1)$.

There is a second dimensionless parameter that mixes with θ, which originates in the fermion mass sector. The quark mass Lagrangian is

$$\mathcal{L}_M = \bar{q}_{iR}\, M_{ij}\, q_{jL} + h.c., \tag{2.2}$$

where R (L) labels the right-handed (left-handed) helicity state of the quark field q. The mass matrix M_{ij} is in general complex, but can be transformed by chiral rotations of the quark fields

$$q \to e^{i\,\alpha\,\gamma_5/2}\, q \tag{2.3}$$

with $\gamma_5 = i\,\gamma_0\,\gamma_1\,\gamma_2\,\gamma_3$ the usual product of γ-matrices. These chiral transformations also rotate the θ-vacuum, as

$$e^{i\,\alpha\,\gamma_5}\,|\theta\rangle = |\theta + \alpha\rangle. \tag{2.4}$$

A shift of θ by an amount $ArgDetM$ is required to make the quark mass matrix M_{ij} real and positive. Because these two contributions are inexorably connected, the single physical parameter is the combination

$$\bar{\theta} = \theta + ArgDetM. \tag{2.5}$$

The $\bar{\theta}$ parameter in eq. (2.5) has measurable effects. In particular, it should give rise to a nonzero electric dipole moment (EDM) for the neutron [30, 67, 68], which violates time-reversal symmetry T and parity P. The interaction must also violate charge-parity symmetry CP, since the composite symmetry CPT is conserved in any quantum field theory (see [69] and references therein). Because the axion mixes with the SM pion fields, the neutron EDM $d_n \propto g_{\pi NN}$, where $g_{\pi NN}$ effective pion-nucleon CP-violating coupling. Estimates somewhat vary (within about an order of magnitude);

for example, [70] finds $g_{\pi NN} \approx -0.023\,\bar{\theta}$, whereas a more recent estimate [30] gives $g_{\pi NN} \approx -0.3\,\bar{\theta}$. The precise numerical factor does not concern us here; the upshot is that the neutron EDM and the parameter $\bar{\theta}$ are related by

$$d_n \approx \left(10^{-16} - 10^{-14}\right) \bar{\theta}\ \mathrm{e}\cdot\ \mathrm{cm}, \tag{2.6}$$

where e is the magnitude of the electron charge.

If $\bar{\theta} = \mathcal{O}(1)$, then the neutron EDM should be observable with present-day experiments. However, the experimental non-observation of this EDM have constrained it to very small values, $d_n \lesssim 10^{-26}$ e·cm [71–73], which implies $\bar{\theta} \lesssim 10^{-10}$; contrary to expectation, the θ-parameter is not $\mathcal{O}(1)$, but rather remarkably close to zero. In short, the expectation of, and lack of experimental evidence for, a violation of CP in the strong nuclear interaction is the essence of the Strong CP Problem.

The Strong CP Problem would be easily solved if one of the quarks (say, the up quark) in the SM were massless [74,75]. This is because in that case, $DetM = 0$, rendering $ArgDetM$ arbitrary and the parameter $\bar{\theta}$ unphysical. This can also be understood from the standpoint of quark phases: a massless up quark can be rotated by an arbitrary, unphysical phase, which allows one to absorb the the CP-violating phase and effectively set $\bar{\theta} = 0$ without affecting any observable quantity. However, there is good experimental reason to believe that all quarks in the SM are massive [74], implying that the massless up quark solution is not viable.

A more viable solution was proposed by Peccei and Quinn (PQ) in the 1970s [76,77]. The essence of the PQ proposal was to introduce a new $U(1)$ symmetry to the SM, under which a new scalar

$$\phi(x) = \phi_0(x)\, e^{i\,a(x)/f} \tag{2.7}$$

transforms as

$$\phi(x) \to e^{i\,\alpha}\, \phi(x). \tag{2.8}$$

This complex scalar field, as written above, is decomposed into two real scalars $\phi_0(x)$ and $a(x)$. However, at low energy, the $U(1)_{PQ}$ symmetry is broken spontaneously by the vacuum expectation value (vev) of the field $\langle\phi\rangle = f$. This gives rise to a massless Nambu-Goldstone boson $a(x)$, known as the *axion* [78,79].

We can also think of the PQ solution as promoting of the static parameter θ to a dynamical field $\theta \to a(x)/f$. Then, the smallness of θ is explained as a relaxation of the axion field to its low-energy minimum, which happens to be CP-conserving. Then

the vanishing neutron EDM is no mystery at all: the ground state of QCD, with the addition of the axion field and at scales below f, conserves CP.

To complete the picture, the field ϕ must be coupled to the SM in such a way that the QCD vacuum is CP-conserving. At low energy and at leading order in $1/f$, the resulting axion potential has the form [80]

$$\mathcal{L}_a = \frac{1}{2}\left(\partial_\mu a\right)^2 + \frac{\alpha_s}{8\pi}\frac{a}{f}\, G^{a\mu\nu}\,\tilde{G}_{a\mu\nu} + \frac{E}{N}\frac{\alpha_{em}}{8\pi}\frac{a}{f}\, F^{\mu\nu}\,\tilde{F}_{\mu\nu} + \frac{c_q}{2f}\left(\partial_\mu a\right)\left(\bar{q}\gamma^\mu\gamma_5 q\right), \tag{2.9}$$

where E/N is the ratio of electromagnetic and color anomalies, F ($\tilde{F}$) is the (dual) field strength tensor for electromagnetism, and c_q is a model-dependent coupling of the axion to the quark axial current. Note that the axion field $a(x)$, despite its lack of any direct electromagnetic or color charge, is coupled through nonperturbative dynamics to the gluon, photon, and quark fields. This fact makes detection of the axion much more viable.

Note that the couplings to the SM fields are proportional to the decay constant f. In the original models of axions, the scale f was assumed to be of the order of the electroweak scale, $\mathcal{O}(100)$ GeV. However, it was quickly noted that such models would be ruled out by constraints on these couplings (see Section 2.3.2). So called "invisible axions", with very large f and thus very small SM couplings, were proposed by two different groups near the same time, which are now known as the KSVZ model [81, 82] and DFSZ model [83, 84]. They differ in certain details (including the value of c_q above), but the discussion of this chapter does not depend on which of these models we consider.

2.2. Axion Mass and Self-Interactions

While the axion is massless at the high scale where $U(1)_{PQ}$ is broken, it acquires a mass after the QCD phase transition through couplings to the light quarks and their bound states, the QCD pions. In order to determine the axion mass and any self-coupling terms, we use the chiral effective theory which couples the effective axion field to pions.

Using the two-flavor effective theory of only two light quarks u and d, the axion dynamics in the broken $U(1)_{PQ}$-phase are determined by the effective field

$$M_a = \exp\left(i\,\frac{a}{2f}\,Q_a\right)\, M_q\, \exp\left(i\,\frac{a}{2f}\,Q_a\right), \tag{2.10}$$

with

$$M_q = \begin{bmatrix} m_u & 0 \\ 0 & m_d \end{bmatrix}, \qquad Q_a = \begin{bmatrix} 2/3 & 0 \\ 0 & -1/3 \end{bmatrix}. \tag{2.11}$$

At leading order $\mathcal{O}(p^2)$ in the chiral expansion, the field M_a couples to the pion field operator

$$\Pi = \begin{bmatrix} \pi^0 & \sqrt{2}\,\pi^+ \\ \sqrt{2}\,\pi^- & -\pi^0 \end{bmatrix} \tag{2.12}$$

through effective mass terms

$$\mathcal{L}_{p^2} = B_0 \frac{{f_\pi}^2}{2} Tr\left[\exp\left(\frac{i\,\Pi}{f_\pi}\right) {M_a}^\dagger + M_a \exp\left(-\frac{i\,\Pi^\dagger}{f_\pi}\right)\right], \tag{2.13}$$

where $B_0 \sim \langle \bar{q}\, q \rangle$ is proportional to the chiral condensate, and $f_\pi \approx 92$ MeV is the pion decay constant. Neglecting also the charged pion terms, we obtain the following potential for the neutral pion π^0 and the axion field a:

$$V(a, \pi^0) = {m_\pi}^2 {f_\pi}^2 \sqrt{1 - \frac{4\, m_u\, m_d}{(m_u + m_d)^2} \sin^2\left(\frac{a}{2f}\right)} \cos\left(\frac{\pi^0}{f} - \varphi_a\right) \tag{2.14}$$

with $m_\pi \approx 135$ MeV and $\tan\varphi_a \propto \tan(a/2f)$.

In the vacuum state, the potential must be extremized, and the last cosine in eq. (2.14) is equal to 1. Thus the axion field decouples from the pions, giving an effective axion potential

$$\begin{aligned} V_C(a) &= m_\pi^2 f_\pi^2 \sqrt{1 - \frac{4\, m_u\, m_d}{(m_u + m_d)^2} \sin^2\left(\frac{a}{2f}\right)} \\ &= \frac{m_\pi^2 f_\pi^2}{1+z}\left[1 + z - \sqrt{1 + z^2 + 2z\,\cos\left(\frac{a}{f}\right)}\right] \end{aligned} \tag{2.15}$$

with $z \equiv m_u/m_d \approx .457$. This is known as the "chiral potential" for the QCD axion. Expanding to quadratic order gives the following expression for the axion mass:

$$m^2 = \frac{m_u\, m_d}{(m_u + m_d)^2} \frac{m_\pi^2 f_\pi^2}{f^2}, \tag{2.16}$$

which implies the requirement

$$m^2 f^2 = \frac{z}{(1+z)^2} m_\pi^2 f_\pi^2 \approx (6 \times 10^{-3}\ \text{GeV})^2 \tag{2.17}$$

on the product $m f$. In this form, it is clear that the theory of QCD axions has a single free parameter, which can be chosen as either the axion mass m or the decay constant f.

In what follows, the requirement that eq. (2.17) be satisfied will define the term *QCD axion*. As explained in Section 2.4, other particles with similar potentials, but vastly different values for m and f, emerge often in theories of physics beyond the SM.

In the approximation $z \ll 1$ (which implies $m_u \ll m_d$), the chiral potential of eq. (2.15) has a simplified form:

$$V_I(a) = m^2 f^2 \left[1 - \cos\left(\frac{a}{f}\right)\right], \tag{2.18}$$

which is sometimes called the "instanton potential" for axions. Using this, or the chiral form in eq. (2.15), at small field values $a \ll f$ one can expand either potential in powers of a/f, the coefficients being coupling constants. What is typically done is to truncate the expansion at leading order in the self-interaction, which gives an attractive force with a coupling proportional to $m^2/f^2 \ll 1$. Subsequent couplings are suppressed by higher powers of f, so the truncation is justified in all but the most extreme cases. In the later chapters, we will examine critically this approximation.

Direct comparison of the couplings in the expansions of eqs. (2.18) and (2.15) shows that they differ significantly at higher orders, both in sign and in magnitude. The first few coefficients of both potentials are shown in Table 2.1. In spite of the differences in the couplings, many of the conclusions drawn from the simpler instanton potential of eq. (2.18) apply well to the chiral potential of eq. (2.15). An analysis of the two potentials, in the context of axion star energy and gravitational collapse, will be presented in Chapter 6.

2.3. Axions as Dark Matter

2.3.1. The Primordial Axion Density

The evolution of the axion field on cosmological timescales is highly nontrivial, and is described by a series of broken symmetries [85]. At very high scales $T \gg f$, the $U(1)_{PQ}$ symmetry is exact, but as the universe expands and cools to $T \sim f$, $U(1)_{PQ}$ is broken.

Expansion Order	$V_I(a)$	$V_C(a)$
c_4	$-.0417$	$-.0148$
c_6	$+.00139$	-1.99×10^{-4}
c_8	-2.48×10^{-5}	-2.28×10^{-5}
c_{10}	$+2.76 \times 10^{-7}$	-1.59×10^{-6}

Table 2.1.: The dimensionless coupling constants c_n in the expansion of $V_I(a)$ and $V_C(a)$, where each term has the form $c_n\, m^2\, f^2\, (a/f)^n$; in addition to decreasing dimensionless coupling strengths $|c_n|$, higher-order self-interactions terms are suppressed by higher powers of f^n.

As described above, the axion arises as the massless Nambu-Goldstone boson of the global symmetry breaking. Since it does not couple strongly to the thermal SM and its potential is flat, axion particles are not produced at that time.[2]

At a much lower scale, near the QCD phase transition $T_1 \sim \Lambda_{QCD}$, non-perturbative effects give rise to a temperature-dependent axion mass $m(T)$. At this time, the axion field a is homogeneous on horizon scales, and is characterized by a *misalignment angle*

$$\alpha_1 \equiv \left.\frac{a}{f}\right|_{T=T_1} \equiv \frac{a_1}{f}. \tag{2.19}$$

The emergence of an axion mass leads to a mapping of large/small values of α_1 to over-/under-densities (respectively) in the axion field between one horizon and the next.

In order to estimate the magnitude of the axion field density, we need to examine the the cosmological evolution of the axion field $a(x,t)$ near the transition temperature T_1. This evolution can be described by the KG equation of eq. (1.2) with the axion potential of eq. (2.18), which gives

$$\left(\partial_t{}^2 + 3\,\frac{\dot{R}(t)}{R(t)}\,\partial_t - \frac{1}{R(t)^2}\,\partial_r{}^2\right) a(x,t) + m(T)^2\, f\, \sin\left(\frac{a(x,t)}{f}\right) = 0 \tag{2.20}$$

where $R(t)$ is the scale factor of the universe at time t. As stated above, the axion mass term is negligible until a time t_1 such that $m(T_1) = m(T)|_{t=t_1} \sim 1/t_1$, i.e. at the temperature T_1. It has been shown that the temperature-dependent mass near this

[2] This is true unless, in inflation scenarios, the axion couples directly to the inflaton *and* inflation occurs after $U(1)_{PQ}$-symmetry breaking. In that case a thermal population of axions could be produced during reheating in addition to the nonthermal component considered here.

transition has the form [86]

$$m(T) \approx 4 \times 10^{-9}\ \text{eV} \left(\frac{10^{12}\ \text{GeV}}{f}\right)\left(\frac{\text{GeV}}{T}\right)^4, \tag{2.21}$$

which implies an approximate temperature at which the transition occurs

$$T_1 \approx 1\ \text{GeV} \left(\frac{10^{12}\ \text{GeV}}{f}\right)^{1/6}. \tag{2.22}$$

At zero-temperature, the axion mass is given by eq. (2.16), and the total matter content contained in axions makes up a possible contribution of axions to cold DM. This production mechanism is known as the *misalignment mechanism*; these misalignment axions are naturally very cold and are decoupled from the thermal background of SM particles.

Two cases should be distinguished when discussing the cosmological evolution of the axion field: where $U(1)_{PQ}$-breaking occurs (I) before inflation, or (II) after inflation.[3] In case (I), the misalignment angle α_1 is selected effectively at random, then smoothed out across multiple horizons during inflation. In that case one can neglect the ${\partial_r}^2$ term in eq. (2.20), so that we can estimate the average number density of axions as [85]

$$\bar{n}_a(T_1) \sim \frac{m(T_1)}{2}\,{a_1}^2 = \frac{f^2}{2\,t_1}\,{\alpha_1}^2. \tag{2.23}$$

In case (II), the form of the axion number density is similar, but the misalignment angle takes a random value $\alpha_1 \in [0, 2\pi]$ in a given horizon, and as a result, the number density varies as well. In that case, eq. (2.23) is approximately equal to the average axion density across multiple horizons, though relatively large fluctuations are possible.

The number density of eq. (2.23) is the contribution of the ground state, but in case (II), there are additional states of higher momentum which are populated after at T_1. The contribution of these states can be an $\mathcal{O}(1)$ fraction of that of the ground state [85], and in the generic axion DM picture this is an important factor to take into account. However, when we discuss axion condensates in the chapters that follow, the lowest momentum states produced at this epoch will be the dominant factor, and we will neglect higher momentum modes.

There is a third potential contribution to the primordial axion density, which originates in the topological defects generated by the original PQ symmetry breaking. Firstly, the original $U(1)_{PQ}$ is a continuous global symmetry, which implies that the

[3] For our purposes, models with no inflation at all would fall into class (II).

vacuum state in different Hubble volumes will be characterized by different values of the misalignment angle $\alpha_1 \in [0, 2\pi]$. *Cosmic strings* are topological defects connecting those volumes, and having a finite energy density, they can eventually decay to axions in a thermal distribution.

Finally, in the breaking of $U(1)_{PQ}$, there is generically some residual $\mathbb{Z}_N$ symmetry which is preserved by non-perturbative QCD effects, but nevertheless broken spontaneously; said differently, in the flat direction of the axion potential labeled by $\alpha_1 \in [0, 2\pi]$, there can be N-degenerate vacua which are preserved by QCD effects. *Domain walls* are low-energy, two dimensional configurations which connect these vacua, and are exhibited as topological defects.

In case (I), where PQ-breaking happens before inflation, the subsequent inflation dilutes the density of cosmological defects (both cosmic strings and domain walls) so that their relative contribution to the final axion density is negligible. However, in case (II), both can have an important effect [85]. In some axion theories, the prevalence of domain walls gives an energy density so large that the universe would be overclosed; this constrains the space of viable models. Cosmic strings, on the other hand, are completely generic and their energy density can be computed; their contribution to the low-temperature present-day background of axions scales also as f^2 (similarly to other contributions) [85]. More precise simulations of axion production through decay of topological defects can be found in [87, 88].

To summarize: axions can be produced in a number of ways in the early universe: (1) through the misalignment mechanism, which produces very cold axions in Hubble-sized configurations resembling a classical field; (2) through production of thermally excited states on top of this cold background; (3) and through decay of topological defects. Because the main goal of this work will be to analyze the BEC configuration of axions, which are known as axion stars, we will focus primarily on those axions produced via (1), the misalignment mechanism. While axions produced in the two latter ways can be an $\mathcal{O}(1)$ contribution to DM axions, they will have a thermal distribution and will not necessarily relax to the ground state on short enough timescales; as a result, they will have a subleading effect on the production of axion stars. For the purposes of the outline given in this chapter, we will not elaborate further on the topic of the thermal contributions.

At temperatures $T > T_1$, even though the average density of misalignment axions is fixed by α_1 as given in eq. (2.23), there are large isocurvature fluctuations which later collapse into what are called axion "miniclusters" [89, 90]. Prior to the epoch of matter-radiation equality, the fluctuations become nonlinear and the miniclusters collapse. Initially, it was believed that the maximum overdensity was roughly $2\,\bar{n}_a$, twice the

background density, corresponding to a maximal misalignment angle $\alpha_1 = 2\pi$ [89]. However, nonlinear effects in the axion potential at $\alpha_1 \sim 2\pi$ cause a large enhancement in the corresponding overdensity [90]. These miniclusters are generally understood to become unstable at or before the epoch of matter-radiation equality, so that miniclusters collapse or dissipate shortly after they form.[4] The very largest miniclusters may fracture and fragment during collapse, possibly leading to the formation of primordial axion stars [93]. This is the basic picture of early-universe axion star formation. Significant open questions remain, however, including the fraction of axions which end up in this fractured BEC state, as well as their mass distribution.

2.3.2. Constraints on Cosmic Axions

There are nontrivial constraints on the mass m (and by association, f) of QCD axions from astrophysical observation. Firstly, we have already pointed out that the mass and decay constant of the axion are not independent, being mutually determined by the constraint of eq. (2.17). Further, as we will explain in detail in Chapter 5, axion particles are not stable, as there is no quantum symmetry protecting axion particle number. As a result, free axions can decay through a process

$$a \to 2\,\gamma, \tag{2.24}$$

as a result of the photon coupling $\sim a\,\tilde{F}\,F$ in eq. (2.9). The decay rate of axions through this process is

$$\Gamma_a = \frac{(E/N)^2\,{\alpha_{em}}^2\,m^3}{64\,\pi^3\,f^2}, \tag{2.25}$$

quickly growing with particle mass m. As a result, QCD axions with masses $m \gtrsim 20$ eV will decay with a lifetime shorter than the age of the universe, and thus cannot contribute to dark matter.

There are other constraints originating in the axion-photon coupling of eq. (2.9). In particular, the observation of the length of the supernova SN 1987A imply important bounds on the axion coupling to photons [94, 95]. Axions, like neutrinos, could be produced in the core of collapsing stars but have a large mean free path. If such particles are emitted from the star, they can carry away significant energy and cause the supernova to end prematurely. The requirement that axion production and emission

[4] There do exist recent works which examine the possibility that these miniclusters remain stable and form a component of dark matter in the present day [91, 92]. These considerations are related to the open question of axion star formation.

from SN 1987A not conflict with observation leads to the bound

$$f \gtrsim 4 \times 10^8 \text{ GeV} \qquad \text{[SN 1987A]}. \tag{2.26}$$

This bound is complemented by other astrophysical and detector constraints (including e.g. white dwarf cooling) which set competitive bounds on f through the axion-photon coupling (see e.g. [96] and references therein). Because of the relation between m and f in QCD via eq. (2.17), this implies an equivalent upper bound on the axion mass

$$m \lesssim 16 \times 10^{-3} \text{ eV} \qquad \text{[SN 1987A]}. \tag{2.27}$$

An upper bound on f can be set by cosmological considerations. The axion density at time t_1, given in eq. (2.23), along with the fact that these cold axions redshift as the scale factor $R(t)^{-3}$ (appropriate for pressureless matter), allows us to compute the mass density at present time t_0 in axions over cosmological distances. The result is [85]

$$\rho_a(t_0) \sim \begin{cases} \frac{m f^2}{t_1} {\alpha_1}^2 \left(\frac{R(t_1)}{R(t_0)}\right)^3 & \text{(case I)}, \\ \frac{m f^2}{t_1} \langle {\alpha_1}^2 \rangle \left(\frac{R(t_1)}{R(t_0)}\right)^3 & \text{(case II)} \end{cases} \tag{2.28}$$

where in case II we must take the average $\langle {\alpha_1}^2 \rangle \approx \pi^2/3$ over many QCD horizons. In both cases, we have neglected some $\mathcal{O}(1)$ factors which set the overall numerical value, but it is the scaling that concerns us here. Since the universe is very close to being flat on cosmological scales, we expect $\rho_a \lesssim \rho_c \equiv 3 {H_0}^2/8\pi G$. If axions are to constitute a significant fraction of DM, then $\rho_{a,0}/\rho_c \sim \mathcal{O}(1)$. Using the present temperature of the universe, we find a relic density in axions today of [85]

$$\Omega_{a,0} \equiv \frac{\rho_{a,0}}{\rho_c} \sim \begin{cases} \left(\frac{f}{10^{12} \text{ GeV}}\right)^{7/6} \left(\frac{0.7}{h}\right)^2 {\alpha_1}^2 & \text{(case I)}, \\ \left(\frac{f}{10^{12} \text{ GeV}}\right)^{7/6} \left(\frac{0.7}{h}\right)^2 \frac{\pi^2}{3} & \text{(case II)} \end{cases} . \tag{2.29}$$

More recent estimates, which include anharmonic effects during the QCD phase transition, give more precise numerical factors but a very similar functional form [97].

In case (II), the requirement that axions not overclose the universe (i.e. that $\Omega_{a,0} \lesssim 1$) give the complimentary bounds

$$f \lesssim 10^{12} \text{ GeV} \Leftrightarrow m \gtrsim 10^{-6} \text{ eV} \qquad \text{[Overclosure, case II]}, \tag{2.30}$$

The situation is somewhat different in case (I), because a small value of the misalignment angle α_1 can further suppress the axion relic density. For this reason, authors sometimes

speak of QCD axions with very small masses, even $m < 10^{-12}$ eV [98, 99]. For these theories to be compatible with $\Omega_a < 1$ in eq. (2.29), the misalignment angle has to be tuned to a very small value $\alpha_1 \lesssim 10^{-4}$. Though not in conflict with observation, this reintroduces an element of fine-tuning into the theory that the axion, through the PQ solution of the Strong CP Problem, was designed originally to solve.

For very light QCD axions, bounds of a very different type can be set. Very light scalars can generally be produced in the ergosphere of rapidly rotating black holes, in a process known as *superradiance* [100]. The newly-created axions populate energy and angular momentum states in a "gravitational atom", an analogue of electron states a hydrogen atom; conservation of energy and angular momentum dictates that the black hole mass and rotation speed decrease as a result. This mechanism is especially interesting because it does not rely on the assumption that axions are a large component of DM; if axions exist, even if their cosmological abundance is very close to zero, they can be produced through superradiance effects. Thus bounds set in this way would be relatively model-independent.

In particular, black holes of solar mass (or larger) will superradiate QCD axions with masses $m \lesssim 10^{-11}$ eV[5] very efficiently, because the process is enhanced when the Compton wavelength of the axion is very close to the Schwarzschild radius of the black hole [98, 99]. Monochromatic gravitational waves would be emitted by axions transitioning between energy levels in this "gravitational atom", or by annihilation of axions in states of very high occupancy. Gravitational wave detectors like LIGO [101, 102] or LISA [103] could possibly detect signals of this type in the next decade [98, 99]. This could lead to nontrivial constraints on the very low-mass region of the QCD axion parameter space.

2.4. Other Types of Axions

As described above, axions were originally motivated as a solution of the Strong CP Problem. However, other theories of physics beyond the SM give rise to axion-like particles (ALPs) ; whereas QCD axions restricted by the requirement (2.17), other ALPs can have vastly different masses and decay constants. Though this work will focus primarily on QCD axions, for completeness we include a brief discussion of other ALPs below.

[5] As pointed out above, such theories require PQ breaking after inflation, and considerable fine-tuning of the misalignment angle α_1.

Recall that the QCD axion emerged as a pseudo Nambu-Goldstone of a broken $U(1)_{PQ}$ symmetry. Generically, physics beyond the SM brings with it a variety of new global symmetries, whose breaking at high scales gives rise to massless Nambu-Goldstone bosons. In certain cases, the theory will also include some explicit breaking of the global symmetry, giving the Goldstone boson a small mass, and often, a potential very similar to that of the QCD axion. Particles of this kind are referred to here as ALPs.

For example, ALPs exist in string theoretic models which require compactification with antisymmetric tensors [104–108]. These theories can have decay constants $f \sim M_P$, and some even have super-Planckian decay constants $f \gtrsim M_P$. We will comment briefly in later chapters on ALPs with $f \sim M_P$ and how this parameter space is reflected in the spectrum and the properties of bound states, known as axion stars.

Often theories of ALPs with very large decay constants will also imply very small masses. The cosmology of axions, and particularly axion condensates, is very different in this regime. Some authors use ultralight ALPs with masses in the range $m \sim 10^{-22} - 10^{-21}$ eV to describe dark matter halos [109–117], because in that regime the de Broglie wavelength of the ALPs is $\mathcal{O}(kpc)$, of the order of the radius of a typical galaxy. This paradigm has become known as *Fuzzy Dark Matter* [112], and occupies the corner of DM parameter space with the very lowest possible DM particle masses. Axion condensates in this regime correspond to solitonic cores of DM halos. We will discuss such theories in Chapter 5.

2.5. Summary

The QCD axion was proposed to address the Strong CP Problem, and remains among the best and simplest solutions. Because of its small mass and peculiar production mechanism, axion particles are copiously produced early in the universe, and naturally a large fraction of the total energy density is in a population of cold (low energy) particles; this makes them ideal candidates for the identity of DM. Due to the ability of the axion to solve both of these problems at once, it has attracted a great deal of attention and remains an interesting topic for research today.

QCD axions are constrained by the relation of their mass m to their decay constant f, as given in eq. (2.17). This defines a one-parameter family of theories which can both solve the Strong CP and DM problems at once. Astrophysical and cosmological constraints, outlined in Section 2.3, further constrain the parameter space; current and future axion experiments (not reviewed here) have and will set important constraints as well. Axion-like particles, or ALPs, for which m and f are independent parameters,

emerge in a variety of theories of physics beyond the SM; such particles can have distinct experimental signatures, in terrestrial or astrophysical observations.

Axions are produced with low energy, with a density that varies across different Hubble volumes. Overdensities on the axion field are known as *miniclusters*, and they are believed to collapse (at a time close to matter-radiation equality) to some combination of gravitationally bound condensates, known as axion stars, and a dilute background of axions. The fraction of the total axion mass density that is contained in axion stars, and what their primordial mass distribution was, remain open questions. Nonetheless, if these states exist in the present day, their properties are interesting and can they serve to distinguish axions from other light scalars as a component of dark matter. Condensates formed from light scalars are reviewed in a generic way in Chapter 3, before returning to axion condensates in particular in Chapters 4, 5, 6, and 7.

Chapter 3.

Methods in Investigations of Boson Stars

"There, sir! that is the perfection of vessels!"
— Jules Verne

Boson stars are macroscopic, self-gravitating condensates of bosonic particles. While their sizes and masses vary significantly, depending on the properties of the constituent particles, they can be analyzed in fairly generic ways, based on the principles of quantum statistical mechanics and field theory. In this section, we review the basic mechanics of Bose-Einstein condensation as it applies to very light scalar particles, and detail several relevant methods for the determination of the properties of the resulting boson stars.

3.1. Bose Statistics and Field Theory

Bosons and fermions have a number of different properties. For example, no two fermions can occupy the same quantum state, a fact known as the Pauli Exclusion Principle. In the mathematical formulation of QFT, this can be understood by the fact that fermions are represented by anticommuting fields, implying that the combined wavefunction of two identical fermions is odd under particle exchange. Thus, such a wavefunction can only be nonzero if the two fermions occupy different states. This is one of the basic facts underlying Fermi-Dirac (FD) statistics, to which all fermions

subscribe. The fermion occupation number for a state of energy E is

$$\mathcal{N}_{FD} = \frac{1}{e^{\beta E} + 1}, \tag{3.1}$$

where $\beta = 1/kT$ and k is the Boltzmann constant. The fact that $0 \leq \mathcal{N}_{FD} \leq 1$ is a reflection of the Pauli Exclusion Principle: no more than one fermion may occupy a given quantum state.

Bosonic fields are commuting (not anticommuting), allowing two or more bosons to occupy the same quantum state. The boson occupation number, based in Bose-Einstein (BE) statistics, for a state of energy E is

$$\mathcal{N}_{BE} = \frac{1}{e^{\beta E} - 1}. \tag{3.2}$$

The fact that $\exp(\beta E) = \mathcal{O}(1)$ when $E \ll kT$ implies that the boson occupation number can be very large for sufficiently low-energy states. When the occupation number of the ground state is an $\mathcal{O}(1)$ fraction of the total number of particles, the system undergoes a phase transition to a Bose-Einstein Condensate (BEC) state [20].

Condensates have been observed in condensed matter systems with ultracold atoms [21,22]. These atomic BECs typically have very small sizes, and the condensates have to be cooled very close to $T = 0$K (absolute zero temperature). However, both of these properties (size and critical temperature) are governed by the mass of the bosons in the BEC. First, as explained in detail in the coming sections, the size of a condensate typically scales inversely with the particle mass m. Second, the critical temperature for transition to the BEC phase is

$$kT_c = \frac{2\pi}{m}\left(\frac{\bar{n}}{\zeta(3/2)}\right)^{2/3}, \tag{3.3}$$

where $\bar{n}$ is the average particle density of the condensate and $\zeta(x)$ is the Riemann zeta function. This is approximately the temperature at which the thermal de Broglie wavelength becomes equal to the average interparticle spacing. For atomic condensates, the relatively large[1] mass m_A of the condensing atoms implies a critical temperature T_c very close to 0K.

In many theories of physics beyond the SM, very light bosonic states are predicted which may be able to condense as well. For example, the axion described in Chapter 2 has a mass many orders of magnitude smaller than an atomic mass m_A, implying a significantly larger size and a much higher critical temperature for condensation.

[1] "Large" relative to the bosons of interest in this work.

Condensates composed of particles with such small masses can in fact be macroscopic, and are referred to as *boson stars* [118]. In theories of bosonic DM, boson stars could potentially be a significant fraction of the total DM mass, and in some scenarios, could be constrained by gravitational or electromagnetic observables [119]. These macroscopic condensates of very light bosonic particles are the topic of this chapter.

An investigation into boson stars must begin with a quantum description of the constituent particles. Scalar particles in QFT come in two types: real (or Hermitian) scalars, and complex scalars. A complex scalar has two degrees of freedom, which can be represented by two real scalars. If a field ϕ is complex, then $\phi^\dagger \neq \phi$, which implies its Lagrangian must be built out of bilinears $(\phi^\dagger \phi)$, rather than $\phi^\dagger$ or ϕ separately. There is thus a natural symmetry of the Lagrangian under transformations of the form [15]

$$\phi \to e^{i\alpha}\phi, \qquad \alpha \in \mathbb{R}. \tag{3.4}$$

The conserved Noether charge of this symmetry is the total *particle number* N of the system.

For real scalars, no such symmetry exists; in general, any ϕ^n ($n \in \mathbb{Z}$ and $n > 0$) is a valid (gauge and Lorentz invariant) operator in the Lagrangian for a real scalar ϕ. Axions, the fields reviewed in Chapter 2, are in fact *real* scalars. This fact implies that number-changing operations in axion field theory are allowed, both through couplings of the axion to SM fields, and through transitions generated by the axion self-interaction potential. This point will be made more strongly in Chapter 5. Because this work focuses on axions as the constituents of boson stars, we will specialize to the case of real scalars for the remainder of this work.

A simple interacting Lagrangian for a real scalar field ϕ can be written as[2]

$$\mathcal{L} = \frac{1}{2}\left(\partial_\mu \phi\right)\left(\partial^\mu \phi\right) - \frac{m^2}{2}\phi^2 - \frac{\lambda}{4!}\phi^4 \tag{3.5}$$

where m is the boson mass and λ is the dimensionless coupling constant. Note, for later use, that $\lambda > 0$ corresponds to an effective repulsive interaction between the bosons, while $\lambda < 0$ gives an attractive one. Of course, $\lambda = 0$ is the non-interacting limit. Theories of each of these three types will be of interest in the next few sections. The equation of motion generated by the Lagrangian in eq. (3.5) is the Klein-Gordon equation introduced in Chapter 1, i.e. eq. (1.2).

[2] We specialize to the case of a leading four-scalar operator ϕ^4 in this chapter. An operator proportional to ϕ^3 would also be allowed, and can affect the dynamics.

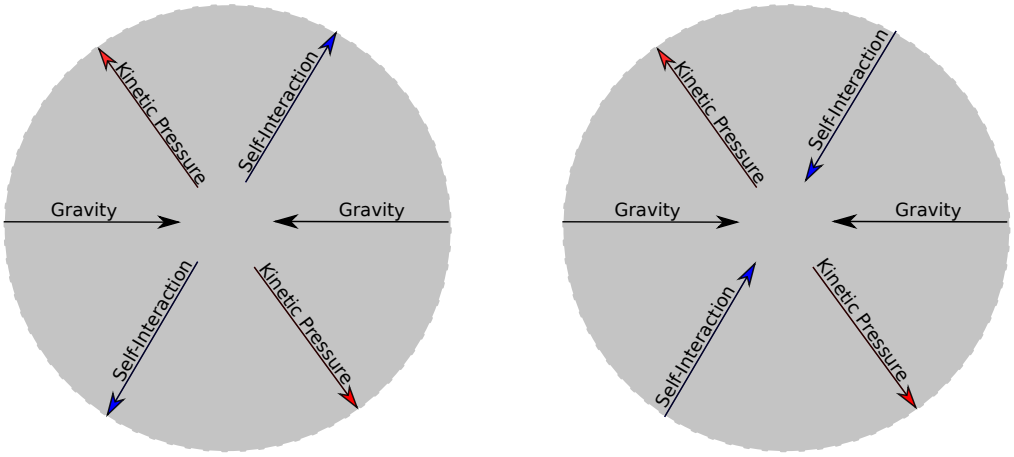

Figure 3.1.: An illustration of the balance of forces for boson stars with repulsive (left) and attractive (right) self-interactions. The gravitational force is always attractive, represented by inward-pointing arrows, and the quantum kinetic pressure is always repulsive, represented by outward-pointing arrows.

The balance of forces supporting a stable boson star is somewhat different depending on the nature of the self-interaction potential; see Figure 3.1. There are generically three relevant forces: gravitation F_g (which is always attractive); the quantum pressure F_q, which originates from the Heisenberg Uncertainty Principle (which is always repulsive); and self-interaction F_{SI} (which can be attractive or repulsive). Of course, in equilibrium, the sum of the magnitudes of the repulsive forces must equal the sum of the magnitudes of the attractive forces. A stable state with a repulsive self-interaction implies the force magnitudes be balanced as

$$F_g = F_q + F_{SI}, \tag{3.6}$$

whereas for an attractive self-interaction,

$$F_g + F_{SI} = F_q. \tag{3.7}$$

The physical consequences of the different balance of forces in the attractive and repulsive cases will become clear in the next few sections.

All known theories of boson stars have a maximum mass allowed for gravitational stability [120]. Depending on the underlying theory and (in particular) the self-interactions allowed, the resulting states will take a variety of forms, and the maximum mass can vary by many orders of magnitude. As a result, observational signatures of boson stars differ greatly for different underlying theories. Some of these consequences are analyzed in Section 3.6.

3.2. Historical Overview

(This section is intended as a historical overview of boson star literature; many of the themes and specific ideas will be examined in greater detail in subsequent sections.)

The proposal of macroscopic BECs in the context of fundamental particle interactions began with the proposal of John Archibald Wheeler in 1955 [121], who suggested that photons (being spin-1 bosons) or gravitons (which have spin-2) could condense. While both photons and gravitons are massless, Wheeler suggested that their energy-momentum could be sufficient to form a gravitationally bound state, which he referred to as a *Geon*. Today, the viability of his proposal in an astrophysical setting remains an open question, although in condensed matter experiments, trapped condensates composed of photons have recently been observed [122].

A decade later, Kaup modified Wheeler's proposal to the application of scalar fields [123]; as detailed in Section 3.3, he considered a condensed boson star as a classical field, and solved the coupled Einstein and Klein-Gordon equations to determine its properties. His analysis assumed non-interacting bosons, and he called his solutions *Klein-Gordon Geons*. He found solutions describing gravitationally stable bound states for such bosons, up to a maximum mass which he determined numerically to high precision. A subsequent analysis by Colpi et al. [118] included the effects of repulsive self-interactions in the analysis of bosonic condensates; the solutions had a different scaling with the dimensionful parameters of the theory, and as a result, had a much larger maximum mass, possibly reaching solar masses.[3] This justified the term *boson star* coined by Colpi et al., which is still in use today.

A second method, pioneered by Ruffini and Bonazzola (RB) [125], for analyzing scalar boson stars appeared shortly after Kaup's original paper [123]. The RB approach treated a boson star semiclassically, second-quantizing the boson field and expanding in creation and annihilation operators. The condensate was then represented by an N-particle ground state; subsequently, RB took expectation values of the equations of motion to calculate the macroscopic properties of boson stars. Their result, which was also restricted to theories of non-interacting bosons, was numerically identical to Kaup's. However, when extended to interacting theories, the semiclassical RB method can give important new consequences, an important theme which will be revisited in Chapter 4. The RB method, as it originally appeared, is detailed in Section 3.4.

[3] The work done by [124], performed in the method of Kaup and prior to the work of Colpi et al., also included a nontrivial self-interaction potential. However, their potential included both an attractive and repulsive term, unlike our simple model of (3.20). This work is interesting but we will not comment further on it here.

Because boson stars are typically extremely cold, constituted of bosons whose wavefunctions peak at extremely low momentum, they can often be treated in the nonrelativistic limit as well (see e.g. [126]).[4] Such analyses are often computationally more tractable than the relativistic and/or semiclassical approaches outlined above, and give compatible results over a large region of parameter space. In Section 3.5, this method will be explained in detail. In this regime, we will also describe a variational method for finding extrema of the total energy of a boson star, as an approximation to its stable bound states.

In the remainder of this chapter, we review the methods described above in greater detail, with particular emphasis on the region of validity for each.

3.3. Boson Stars as Classical Fields

The first known solutions for stable, gravitationally bound configurations of scalar particles was found by Kaup [123], who considered spherically symmetric configurations composed of non-interacting bosons. In Kaup's original work, the bosons were assumed to be non-interacting, but a later work by Colpi et al. [118] extended the method to apply to theories with strong repulsive interactions. We will consider both limits in this section.

To describe the effect of the self-gravitation of the boson star, the boson field $\phi(r)$ is coupled to the components $A(r)$ and $B(r)$ of the gravitational metric, defined by

$$ds^2 = -B(r)\,dt^2 + A(r)\,dr^2 + r^2\left(\sin^2\theta\,d\theta^2 + d\varphi^2\right). \tag{3.8}$$

Of course, if $A(r) = B(r) = 1$, one recovers the vacuum Minkowski metric. The resulting Klein-Gordon equation, defined in eq. (1.2), and the Einstein equations, defined in eq. (1.1), are the equations of motion defining a complete set of solutions for the functions $A(r)$, $B(r)$, and $\phi(r)$:

$$\begin{aligned}
\frac{A'}{A^2 x} + \frac{1}{x^2}\left(1 - \frac{1}{A}\right) &= \left(\frac{\Omega^2}{B} + 1\right)\sigma^2 + \frac{\Lambda}{2}\sigma^4 + \frac{(\sigma')^2}{A} \\
\frac{B'}{B^2 x} + \frac{1}{x^2}\left(1 - \frac{1}{A}\right) &= \left(\frac{\Omega^2}{B} + 1\right)\sigma^2 - \frac{\Lambda}{2}\sigma^4 + \frac{(\sigma')^2}{A} \\
\sigma'' + \left(\frac{2}{x} + \frac{B'}{2B} - \frac{A'}{2A}\right)\sigma' + A\left[\left(\frac{\Omega^2}{B} - 1\right)\sigma - \Lambda\sigma^3\right] &= 0,
\end{aligned} \tag{3.9}$$

[4] In this regime, particle number is absolutely conserved, even if the high-energy underlying theory contains real bosons for which no number-conserving quantum number exists. This point will be important, and more clearly emphasized, later.

where the rescaled variables are $x = m\,r$, $\sigma = \sqrt{4\pi\,G}\,\phi$, $\Omega = \mu_0/m$ (μ_0 the eigenenergy of one boson), and $\Lambda = \lambda\,{M_P}^2/(4\,\pi\,m^2)$. The first (second) equation in (3.9) is the tt (rr) component of the Einstein equations, and the third is the KG equation. The other nontrivial Einstein equations $\theta\theta$ and $\varphi\varphi$ are related to the KG equation by a Bianchi identity.

For non-interacting theories where $\lambda \to 0$, the basic equations of motion are those of eqs. (3.9) with $\Lambda \to 0$; these were the equations considered originally by Kaup [123]. By solving these equations numerically, Kaup found a spectrum of gravitationally stable configurations for the boson field ϕ. Of particular interest was the existence of a maximum mass of non-interacting boson stars,

$$M_{max}^{NI} = .633\,\frac{{M_P}^2}{m}. \tag{3.10}$$

Because states with $M > M_{max}^{NI}$ did not exist in the spectrum, it was concluded that such states are gravitationally unstable.

The existence of a maximum mass was no surprise, as the fermionic analogue of a boson star (e.g. a neutron star) also has limitations on its mass from gravitational stability. However, the maximum mass of a "fermi star" scales as $M_{max} \sim {M_P}^3/m^2$ [127,128]; by comparison, the Kaup bound is diminished by the very small factor m/M_P, implying that boson stars must be relatively small and light. This can be qualitatively understood by the fact that fermi stars are partially supported by an outward pressure originating in the Pauli Exclusion requirement; the analogue for boson stars is the quantum pressure F_q originating in the kinetic energy of the cold bosons, which is comparatively weak.

Colpi et al. [118] expanded on the Kaup analysis by including a repulsive self-interaction coupling $\lambda > 0$, implying $\Lambda > 0$ in eq. (3.9). To investigate the solution, one can trade $A(r)$ for a mass distribution function $\mathcal{M}(x)$ by the relation $A(x) = [1 - 2\mathcal{M}(x)/x]^{-1}$.[5] In the limit that the interactions are strong (precisely, $\Lambda \gg 1$), the system can be simplified significantly, as one can perform a further rescaling of the equations: $\sigma_* = \sigma\Lambda^{1/2}$, $x_* = x\Lambda^{-1/2}$, and $\mathcal{M}_* = \mathcal{M}\Lambda^{-1/2}$. In this limit, and at leading

[5] In a broad class of metrics, for example, the mass function $\mathcal{M}(x) = 2\,G\,M(x)$, where $M(x)\,dx$ is the mass in a thin shell of thickness dx.

order in $1/\Lambda$, eqs. (3.9) simplify to

$$\begin{aligned} \sigma_* &= \sqrt{\frac{\Omega^2}{B} - 1} \\ \mathcal{M}'_* &= 4\pi x_*^2 \rho_* \\ \frac{B'}{B x_*}\left(1 - \frac{2\mathcal{M}_*}{x_*}\right) - \frac{2\mathcal{M}_*}{x_*^3} &= 8\pi p_*, \end{aligned} \tag{3.11}$$

where the dimensionless pressure p_* and density ρ_* are given by

$$\begin{aligned} \rho_* &= \frac{1}{16\pi}\left(\frac{3\Omega^2}{B} + 1\right)\left(\frac{\Omega^2}{B} - 1\right) \\ p_* &= \frac{1}{16\pi}\left(\frac{\Omega^2}{B} - 1\right)^2. \end{aligned} \tag{3.12}$$

Colpi et al. solved the simplified equations above, and like Kaup, found an upper bound on the mass. However, the inclusion of self-interactions implied a very different form for the maximum mass

$$M_{max}^{rep} = .22\sqrt{\frac{\lambda}{4\pi}}\frac{{M_P}^3}{m^2}. \tag{3.13}$$

There are two important things to note about the maximum mass derived by Colpi et al., reproduced in eq. (3.13). First, observe that when the coupling $\lambda = \mathcal{O}(1)$, the scaling ${M_P}^3/m^2$ is very similar to that of fermionic stars; thus, boson stars could potentially be as heavy as their designation seems to suggest, having possible masses as high as $M \sim M_\odot = 2 \times 10^{30}$ kg (the mass of the sun). Second, it may seem puzzling that the Colpi bound does not reduce to the Kaup (non-interacting) limit, defined in eq. (3.10), as $\lambda \to 0$. But this is no puzzle at all: the Colpi analysis assumed a sufficiently strong repulsive self-interaction, defined by the requirement $\Lambda \gg 1$, or $\lambda/4\pi \gg m^2/{M_P}^2$. This requirement necessarily breaks down before one reaches $\lambda = 0$. Some further constraints on this framework can be found in [129], and a general review by the same authors is [130].

The essence of the method employed by Kaup and Colpi et al. is to treat a BEC as a classical field described by relativistic equations. The field described in this section is a coherent state, essentially classical, whereas a BEC is a quantum state. In general, the distinction between the boson stars as classical fields and in the context of BECs is somewhat murky, and remains the topic of discussion. See for example the discussions in [131, 132].[6]

[6] As recently as this year, there has been debate in the literature regarding whether high-occupancy boson systems can be described precisely as classical fields [133, 134].

For our purposes, it may be sufficient to note that although the classical field described in this section is not an exact N-particle state, it is sharply peaked near the average value; its constituent N-states are approximately Poisson distributed with a width $\sqrt{N} \ll N$, so that corrections can be considered negligible. In the end, we will see that in the determination of the macroscopic properties of boson stars, the results of the classical field and the exact N-state are very compatible. For the purposes of this work, we treat the two as mostly equivalent, except when qualitatively unique effects (e.g. decay) become important.

3.4. Semiclassical Boson Stars

One year after the original work of Kaup [123], a somewhat different approach was proposed by Ruffini and Bonazzola (RB) [125]. The RB method makes use of the fact that a scalar field can be expanded in creation and annihilation operators a and $a^\dagger$ labeled by energy and angular momentum quantum numbers n, ℓ, and ℓ_z,

$$\Phi(t, r, \theta, \varphi) = R_{n,\ell}(r)\, e^{-i\,\mu_n\, t}\, Y_{\ell,\ell_z}(\theta, \varphi)\, a_{n,\ell,\ell_z} + h.c. \tag{3.14}$$

where μ_n is the eigenenergy of level n, Y_{ℓ,ℓ_z} are spherical harmonics, and $R_{n,\ell}$ is a wavefunction describing the radial distribution. The commutators satisfy

$$[a_{n,\ell,\ell_z}, a^\dagger_{n',\ell',\ell'_z}] = \delta_{nn'}\, \delta_{\ell\ell'}\, \delta_{\ell_z\ell'_z} \tag{3.15}$$

For a BEC, it is appropriate to include in this expansion only the lowest energy state $n = 0$ with zero angular momentum $\ell = \ell_z = 0$,

$$\Phi(t, r) = R(r)\, e^{-i\,\mu_0\, t}\, a_0 + h.c. \tag{3.16}$$

In the RB method, one evaluates the expectation value of the Einstein and Klein Gordon (EKG) equations, using N-particle states built from the ground state creation operator $a_0^\dagger$,

$$|N\rangle = \frac{(a_0^\dagger)^N}{\sqrt{N!}}\, |0\rangle. \tag{3.17}$$

The expectation values, applied to the non-interacting bosonic theory, turns out not to affect the equations of motion represented in eq. (3.9) with $\Lambda = 0$. As a result, RB found the same maximum mass as Kaup, eq. (3.10). This result was also derived by [135].

The power of the RB method becomes apparent when self-interactions are included. As will be detailed in Chapter 4, if a boson star is accurately described by a zero-temperature condensate, then the expectation values on the state $|N\rangle$ resum higher-order diagrams in the N-to-N matrix element. As a result, compared to the classical field approach, the RB method, being semiclassical, has the advantage of containing leading order corrections to the self-interaction. We will discuss in greater detail the RB procedure as applied to the specific case of axion field theory, and the corrections to the self-interaction potential, in Chapter 4.

A second important difference between the semiclassical RB method and the classical method of Kaup is that the former is more generic from the standpoint of mixed states or particle number-changing processes. This is firstly because the generic expansion of eq. (3.14) contains contributions at all orders in n, ℓ, and ℓ_z, and can be separately included in investigations beyond the ground state. Further, the Kaup field is a classical field, a coherent state which has no definite particle number, whereas in the RB method, different contributions can be singled out. Matrix elements connecting states with different particle numbers can be considered in the RB framework, a central premise to the calculation of boson star decay; this will be investigated in detail in Chapter 5.

3.5. Nonrelativistic Limit for Boson Stars

In the case of weakly-bound boson stars (a very typical scenario)[7], one can expand the quantum field ϕ in terms of of a nonrelativistic wavefunction ψ. We can use an expansion of the form [136]

$$\phi(t,r) = \frac{1}{\sqrt{2\,m}}\left[e^{-i\,m\,t}\,\psi(t,r) + e^{i\,m\,t}\,\psi^*(t,r)\right]. \tag{3.18}$$

Such an expansion is useful in the low energy limit, where $m - \mu_0 \ll m$, because in operators containing higher powers of ϕ, one can neglect rapidly oscillating terms proportional to higher powers of $e^{\pm i\,m\,t}$. The wavefunction ψ is normalized to

$$\int d^3r |\psi(r)|^2 = N, \tag{3.19}$$

where N is the total number of particles in the condensate.

Consider, for example, the Lagrangian in eq. (3.5), and expand the field ϕ using eq. (3.18). Rapidly-oscillating terms involving higher orders in $e^{\pm i\,m\,t}$ can been dropped.

[7] This terminology is defined precisely in the discussion of Chapter 6. For now, "weakly bound" can be taken to mean *dilute*.

The second derivatives with respect to time are of $\mathcal{O}[(m-\mu_0)^2]$, and are thus negligible as well. In the end, one finds the effective low-energy Lagrangian for ψ to be [137]

$$\mathcal{L} = \frac{i}{2}(\dot{\psi}\,\psi^* - \psi\,\dot{\psi}^*) - \frac{1}{2\,m}\nabla\psi^*\cdot\nabla\psi + \frac{\lambda}{16\,m^2}(\psi^*\,\psi)^2. \tag{3.20}$$

For nonrelativistic fields, the momentum conjugate is $\pi = i\dot{\psi}^*$, so the first derivatives with respect to time reproduce the usual time dependence.

Gravity needs to be included in this framework as well; the gravitational interaction does not contribute significantly at the scale of individual particles, but becomes very important when considering heavy bound states. We can couple bosonic fields by hand to a Newtonian gravitational potential by including [137, 138]

$$V_{grav} = -G\,m^2\int d^3r'\frac{|\psi(r')|^2}{|\vec{r}-\vec{r}'|} \tag{3.21}$$

in the equation of motion. This potential satisfies the Poisson equation,

$$\nabla^2\,V_{grav} = 4\,\pi\,G\,m^2\,|\psi|^2, \tag{3.22}$$

and thus gives a good approximation to the gravitational interaction in the nonrelativistic limit.

Quantum corrections to ψ have been estimated by Guth et al. [137], and they are found to be very small for low-energy states; for the purposes of typical boson stars, we can safely neglect them. The Hamilton-Jacobi equations of motion generated by the Lagrangian in eq. (3.20), coupled to eq. (3.21), gives rise to the Gross-Pitäevskii (GP) equation [139–141]

$$i\,\dot{\psi} = \Big[-\frac{1}{2\,m}\nabla^2 + \frac{\lambda}{8\,m^2}|\psi|^2 - G\,m^2\int d^3r'\frac{|\psi(r')|^2}{|\vec{r}-\vec{r}'|}\Big]\psi. \tag{3.23}$$

Note also that it is sometimes advantageous to separate out the gravitational part of the GP equation by explicitly using eq. (3.22), giving the Gross-Pitäevskii + Poisson (GPP) system

$$\begin{aligned} i\,\dot{\psi} &= \Big[-\frac{1}{2m}\nabla^2 + \frac{\lambda}{8\,m^2}|\psi|^2 + V_{grav}\Big]\psi \\ \nabla^2\,V_{grav} &= 4\pi\,G\,m^2\,|\psi|^2. \end{aligned} \tag{3.24}$$

Solutions of the GPP equations for the wavefunction ψ, and self-consistently for the gravitational potential V_{grav}, correspond to gravitationally bound states of the original

boson fields, which are boson stars. In full generality, no analytic solutions exist, though some progress has been recently made in developing a quasi-analytic treatment which is applicable at arbitrary precision [142]. Here, we will briefly discuss a limited scenario in which exact solutions are possible, and then we will examine the full numerical solutions.

3.5.1. Thomas-Fermi Approximation

An example of an exactly soluble limit of the GPP system (3.24) in the context of boson stars was investigated by Boehmer and Harko in 2007 [143]. These authors make use of the Thomas-Fermi (TF) approximation to simplify the equations, a limit often used in condensed matter literature to analyze BEC states [20, 144]; the assumption is that the kinetic energy term $\sim \nabla^2 \psi$ is negligible compared to the gravitational potential V_{grav} or the self-interaction potential. Observe that this limit is only appropriate for condensates with an effective *repulsive* interaction; the TF approximation cannot give stable gravitationally bound configurations when the self-interaction is attractive. To see why, recall Figure 3.1 and the related discussion in Section 3.1 regarding attractive self-interactions: if the kinetic pressure is the only repulsive force (see Figure 3.1), its effect must be large enough balance that of the other two forces.

In the TF limit with a repulsive self-interaction, one can expand the wavefunction in the Madelung representation

$$\psi(t,r) = \sqrt{n(r)}\, e^{i\, S(t,r)}, \tag{3.25}$$

where $n(r) \equiv |\psi(r)|^2$ is the number density. In the limit of low velocities $v \equiv \nabla S/m$, we arrive at the following simplified GP equation:

$$\frac{\lambda}{2} \nabla\, n(r)^2 + n(r)\, \nabla\, V_{grav} = 0. \tag{3.26}$$

Using the dimensionless coordinate ξ and density θ, defined by $r = R_{TF}\, \xi$ and $n(r) = (\rho_c/m)\, \theta(\xi)$, we have

$$\frac{1}{\xi^2}\, \partial_\xi \Big[\xi^2\, \partial_\xi\, \theta(\xi) \Big] + \theta(\xi) = 0, \tag{3.27}$$

where R_{TF} is the radius of the condensate, and $\rho_c \equiv m\, n(0)$ is the central mass density. Eq. (3.27) is the Lane-Emden equation, used to describe a non-rotating polytrope of

index 1. The solution satisfying $\theta(0) = 1$ is

$$n_{TF}(r) = \frac{\rho_c}{m} \frac{\sin(\pi r/R_{TF})}{\pi r/R_{TF}}, \tag{3.28}$$

with

$$R_{TF} = \sqrt{\frac{\pi\lambda}{32}} \frac{M_P}{m^2} \tag{3.29}$$

the radius of the condensate.

The TF approximation is known to break down near the edge of a condensate [143]. Clearly the derivative of the wavefunction $\psi_{TF}(r) \sim \sqrt{\sin(\pi r/R_{TF})/(\pi r/R_{TF})}$ becomes very large as $r \to R_{TF}$. Further, at $r > R_{TF}$ the density function $n(r > R_{TF}) < 0$, so such an extrapolation clearly leads to nonsensical results. We will see in the next section that the exact wavefunction of a boson star typically decreases exponentially at large r, so it is likely that the TF solution can be matched onto an exponential representing this behavior at some $r < R_{TF}$. Note finally that given a particular model for the constituent bosons, the parameters λ and m are fixed, and thus, so is the radius in eq. (3.29); the TF approximation applied consistently gives rise to a fixed radius for boson stars. Again, this can be remedied by modifying the TF density function to account for boundary effects and nonzero kinetic energy.

The original Boehmer and Harko analysis was extended to include slowly rotating boson stars, which correspond to polytropes that are oblate spheroids [143]. Though rotating boson stars are important and interesting astrophysically, to the author's knowledge, no generic analysis of rotating boson stars has been performed, numerically or otherwise. Slowly-rotating solutions with attractive self-interactions were found numerically in [93], on the assumption that the rotation does not change the boson star shape in an important way. A more robust analysis of rotating boson stars is a topic for future work.

3.5.2. Numerical Methods

As we have pointed out, the TF approximation assumed by this analysis requires $\lambda > 0$, that is, repulsive self-interactions. For attractively interacting theories (e.g. axions, the focus of this work), a full solution of eq. (3.24) requires numerical methods. In [120], we analyzed the system by using a rescaling of the dimensionful quantities in the GPP

system (3.24)

$$\psi = \sqrt{\frac{m}{4\pi G}}\frac{1}{|\tilde{a}|}\tilde{\psi}, \qquad V - \mu = \frac{m}{|\tilde{a}|}\tilde{V}, \qquad r = \frac{\sqrt{|\tilde{a}|}}{m}\tilde{r}, \tag{3.30}$$

where $\tilde{a} = (\lambda M_P/m)^2/32\pi$ is a rescaled scattering length, and the dimensionless quantities on the RHS are denoted with a tilde. Note that $\mu < 0$ is the energy eigenvalue of the GP equation (3.23) for ψ, which can be identified with the chemical potential (the energy required to add one more boson to the system). In terms of these rescaled variables, the GPP equations (3.24) take the form

$$\begin{aligned}\left[-\frac{1}{2}\tilde{\nabla}^2 + \tilde{V} \pm |\tilde{\psi}|^2\right]\tilde{\psi} &= 0\\ \tilde{\nabla}^2\tilde{V} &= |\tilde{\psi}|^2,\end{aligned} \tag{3.31}$$

where repulsively interacting scenarios imply a "+" and attractive ones a "−", on the top line.

The attractive case is interesting to analyze numerically because it is not accessible from the standpoint of the TF approximation. Eqs. (3.31) are two second-order equations for $\tilde{V}(r)$ and $\tilde{\psi}(r)$, and thus require 4 boundary conditions. We require that the derivatives be flat at the origin, $\tilde{V}'(0) = 0$ and $\tilde{\psi}'(0) = 0$, and that $\tilde{\psi} \to 0$ exponentially as $\tilde{r} \to \infty$. Finally, since the physical gravitational potential V should vanish at $\tilde{r} \to \infty$, we identify $\tilde{V} \to -|\tilde{a}|\,\mu/m$ in the same limit. This allows us to determine the value of μ, the chemical potential. Because asymptotic boundary conditions are difficult to implement numerically, we use a method of *shooting*: we vary the central values $\tilde{\psi}(0)$ and $\tilde{V}(0)$ of the wavefunction and potential until the functions converge at some large $\tilde{r}$ to a prescribed level of precision. These resulting solutions are valid at this level of precision, and satisfy the required boundary conditions.

This numerical integration was originally performed in [126, 145]; using the scaling we presented above in eq. (3.30), I present here the similar results I have obtained using this method, which were reported in [120]. In the latter work, I derived the mass-radius relation shown in Figure 3.2, and pointed out the characteristics of a few integrated density profiles are shown in Figure 3.3. Note that contrary to the TF result, attractive boson stars do not have compact support on a finite radius R; their density decreases exponentially at large radial distances. In these circumstances, the "size" of the star is taken to be R_{99}, defined as the radius inside which .99 of the mass of the boson star is contained. The variables in these Figures are rescaled using eq. (3.30). In dimensionful

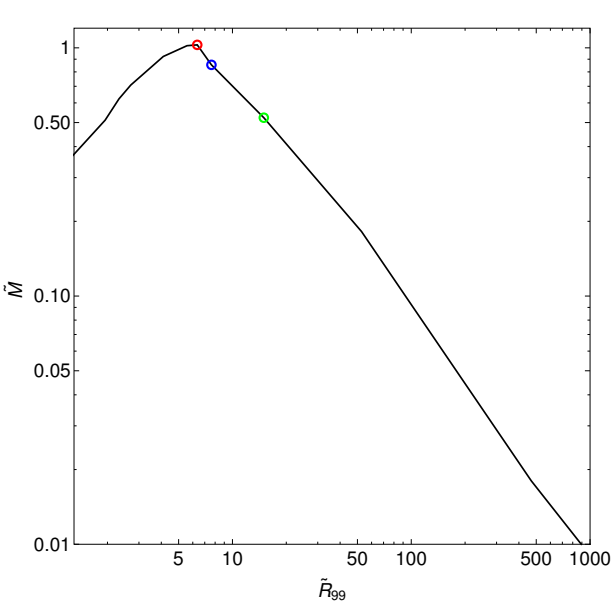

Figure 3.2.: The mass-radius relation for a boson star with attractive interactions. The three circles correspond to the density profiles in Figure 3.3. The dimensionless variables in the plot are defined in terms of the dimensionful ones as $\tilde{M} = \sqrt{|\tilde{a}|}\frac{m\,M}{M_P{}^2}$ and $\tilde{R}_{99} = \frac{m\,R_{99}}{\sqrt{|\tilde{a}|}}$. Figure reproduced from [120].

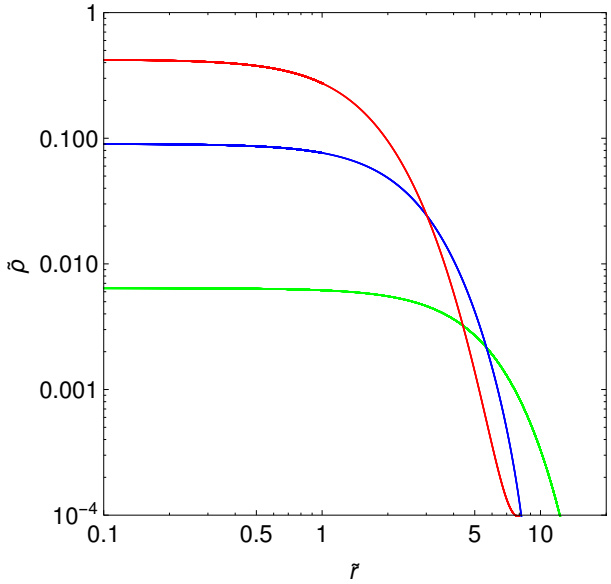

Figure 3.3.: Three examples of density profiles in the case of attractive interactions. The red profile corresponds to the profile of the maximum mass equilibrium, while the blue and green are taken on the stable branch of equilibria. The dimensionless variables in the plot are defined in terms of the dimensionful ones as $\tilde{\rho} = \frac{|\lambda|}{m^4}\,\rho$ and $\tilde{r} = \frac{m\,r}{\sqrt{|\tilde{a}|}}$. Figure reproduced from [120].

units, we can see that the maximum mass of attractive boson stars is

$$M_{max}^{att} \simeq \sqrt{32\,\pi}\,\frac{M_P}{|\lambda|}. \tag{3.32}$$

It is also interesting that the scaling of the radius, $R_{99} \sim \sqrt{|\lambda|}\,M_P/m^2$, is the same as in the repulsive TF case, given in eq. (3.29).

Given a solution to the GPP system of equations, we can compute the total energy using the GP energy functional [126],

$$E_B[\psi] = \int d^3r \left[\frac{|\vec{\nabla}\psi|^2}{2m} + \frac{1}{2}\,V_{grav}|\psi|^2 + \frac{\lambda}{16\,m^2}|\psi|^4\right]. \tag{3.33}$$

The variation of this energy at fixed N recovers the GP equation (3.24), with a Lagrange multiplier that is the eigenenergy μ. Thus μ and E_B are *not* the same. Whereas μ, identified as the chemical potential, is the energy required to add one more boson to the

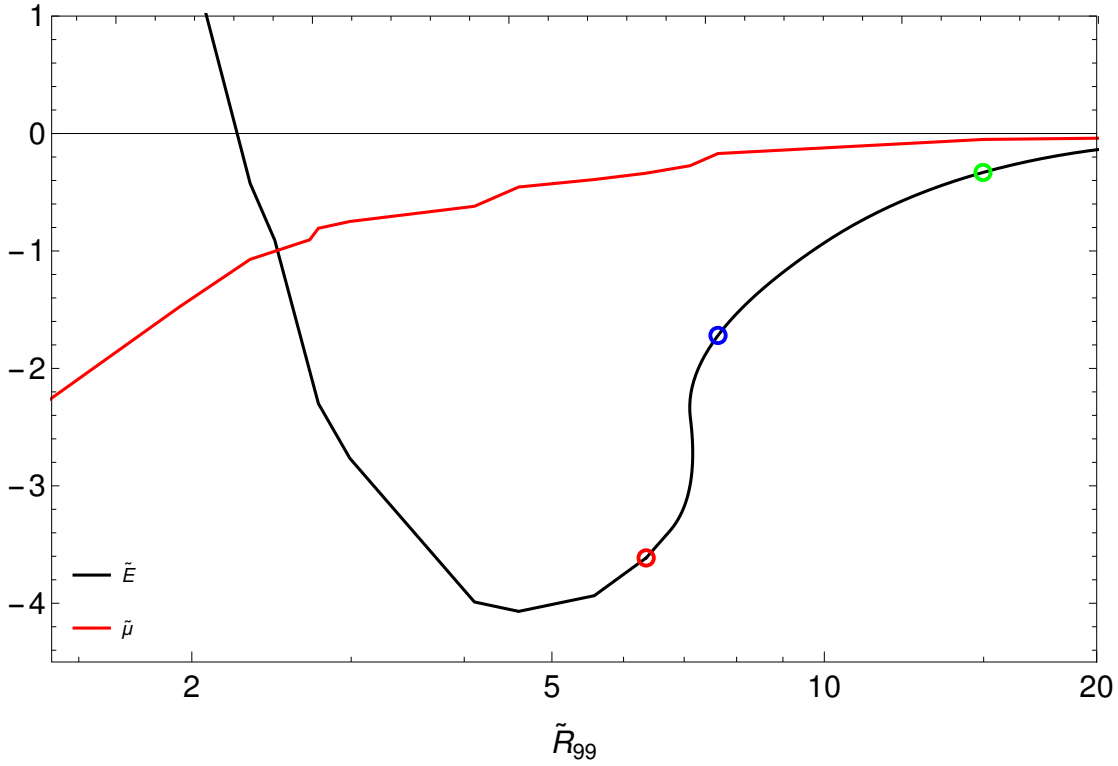

Figure 3.4.: The rescaled binding energy $\tilde{E} = |\tilde{a}|\,\frac{E_B}{m}$ (black curve) and the rescaled chemical potential $\tilde{\mu} = |\tilde{a}|\,\frac{\mu}{m}$ (red curve) as a function of the rescaled radius $\tilde{R}_{99} = \frac{m\ R_{99}}{\sqrt{|\tilde{a}|}}$. The three circles correspond to the density profiles in Figure 3.3.

system, $E_B[\psi]$ is the total Nonrelativistic energy, identified with the binding energy of the boson star state (which will be < 0 for a bound state). We find that the solutions at small R_{99}, to the left of the maximum mass in Figure 3.2, have lower binding energies than states on the right branch which have equal number of bosons N, as illustrated in Figure 3.4. While μ is a monotonically increasing function at increasing R_{99}, the binding energy E_B has a maximum magnitude very near the position of the maximum mass. The upshot of all of this is that states on the left, small R branch are *unstable*. We will encounter this fact in a slightly different context in the next section.

Numerical integration, while precise, can be inefficient, and the results can be difficult or impossible to generalize (for example, to different forms for the self-interaction potential). It is advantageous therefore to develop intuitions using approximate analytic methods. One procedure for accomplishing this is described in the next subsection.

3.5.3. Variational Method

There is a way to extract approximate analytic results in the nonrelativistic limit without numerical integration. The procedure makes use of the energy functional given in eq. (3.33). Rather than integrating to find the wavefunction ψ, we can use an approximate ansatz for ψ; this allows us to perform the integration analytically up to the size R of the boson star state. An extremum of the resulting energy as a function of R corresponds to a stable or metastable boson star. In this method, one can easily derive the scaling relationships among different dimensionful parameters. This method is sometimes used for condensed matter systems as well, where the condensate is trapped by a harmonic potential rather than a gravitational interaction [20, 146, 147]. The application of the method in the context of boson stars was first done in [126], whose analysis we follow closely here. Given a reasonable ansatz, this method can also be easily generalized to interactions beyond the standard $|\psi|^4$, a fact that we will make use of in the later chapters.

Consider, for example, a Gaussian ansatz for the wavefunction

$$\psi(r) = \frac{\sqrt{N}}{\pi^{3/4}\,\sigma^{3/2}}\, e^{-r^2/2\sigma^2} \tag{3.34}$$

where N is the number of particles. Note that σ could be considered the "size" of the condensate, although the wavefunction, in truth, extends to $r \to \infty$. We will adopt the convention that while σ represents the variational parameter, the radius of the condensate will be the conventional R_{99}.[8] Using this ansatz, the energy in eq. (3.33) is [126]

$$\begin{aligned} E_B(\sigma) &= \frac{3}{4}\frac{N}{m\,\sigma^2} - \frac{G\,m^2\,N^2}{\sqrt{2\pi}\,\sigma} + \frac{\lambda\,N^2}{\sqrt{2\pi}\,32\,m^2\,\sigma^3} \\ &= \frac{A\,N}{\sigma^2} - \frac{B\,N^2}{\sigma} + \frac{C\,N^2}{\sigma^3}, \end{aligned} \tag{3.35}$$

where in the second line we defined the coefficients

$$A = \frac{3}{4\,m}, \qquad B = \frac{G\,m^2}{\sqrt{2\pi}}, \qquad C = \frac{\lambda}{\sqrt{2\pi}\,32\,\pi\,m^2}. \tag{3.36}$$

Note that the form of the energy in eq. (3.35) does not depend on the choice of ansatz, but the value of the coefficients A, B, and C does.

The variational method is incredibly versatile, and in various limits, can be used to reproduce the scaling relations found using more precise methods. Macroscopic

[8] For the Gaussian ansatz, the two parameters are related roughly as $R_{99} \simeq 2.5\,\sigma$.

properties for stable configurations of the condensate can be extracted by minimizing this energy with respect to the parameter σ. In the case of the energy in eq. (3.35) above, we find extrema at the values

$$\sigma_{\pm} = \frac{A}{B\,N}\left[1 \pm \sqrt{1 + \frac{3\,B\,C\,N^2}{A^2}}\right]. \tag{3.37}$$

Which extrema correspond to stable configurations depends on the sign of C, that is, on the sign of λ and the nature of the self-interaction.

If the self-interaction coupling $\lambda = 0$, then $C = 0$, and the extrema are at $\sigma_- = 0$ and $\sigma_+ = 2\,A/B\,N$; this means that the only extremum with size > 0 is σ_+, which is an energy minimum. Changing from A and B back to physical parameters, the parameter σ has a value at the energy minimum of

$$\sigma_+^{NI} = \sqrt{\frac{\pi}{2}}\,\frac{3\,{M_P}^2}{m^3\,N}. \tag{3.38}$$

Recall that this is not the same as R_{99}, which we take to be the size of the boson star; the two are related via

$$R_{99} \approx 2.5\,\sigma_+^{NI} \approx 9.4\,(m^3\,G\,N)^{-1}. \tag{3.39}$$

We can compare this to precise numerical estimations of the radius [148], which give the results $R_{99} \approx 9.9\,(m^3\,G\,N)^{-1}$. The agreement in this case is stellar, within a few percent.

In the repulsive case, $C \propto \lambda > 0$, and again, the physical extremum with size > 0 is σ_+. To compare to previous results, consider the TF limit of the energy in eq. (3.33), where we must drop the kinetic energy term (if you like, setting $A = 0$). Then we find

$$\sigma_+^{TF} = \sqrt{\frac{3\,\lambda}{32\,\pi}}\,\frac{M_P}{m^2}, \tag{3.40}$$

which implies

$$R_{99} \approx 2.5\,\sigma_+^{TF} \approx .432\,\sqrt{\lambda}\,\frac{M_P}{m^2}. \tag{3.41}$$

Comparing to the exact result in eq. (3.29), we see that the scaling $\sqrt{\lambda}\,M_P/m^2$ is reproduced exactly, and numerical coefficient is $\mathcal{O}(10\%)$ different from the analytic result of eq. (3.29).

In both the non-interacting and repulsive interaction cases, the variational method is not sensitive to the existence of a maximum mass. Indeed, even numerical solutions of

the GPP system in eq. (3.24) are insensitive to it in these cases. This seems to imply that the boundary between gravitationally stable and unstable equilibria is, at least in these cases, a relativistic effect; this was pointed out for non-interacting theories by [125]. For attractive interactions, as we describe next, the maximum mass emerges naturally from a fully nonrelativistic analysis.

Consider finally the case of attractive self-interactions, $\lambda < 0$. In that case, either both extrema $\sigma_\pm > 0$, or both are complex numbers (no real extrema). In the former case, the nature of the extrema as maxima or minima could be easily determined by analyzing the second derivative. More to the point, however, observe that the total energy in eq. (3.35) $E_B \to -\infty$ as $\sigma \to 0$, and $E_B \to +\infty$ as $\sigma \to 0$. Given that there are two real critical points between these two limits, it is clear that the larger one, σ_+, is a local minimum of the energy, and σ_- is a local maximum.

The two extremal points $\sigma_\pm$ that we find for a given particle number N correspond precisely to the the numerical solutions in Section 3.5.2. The stable energy extremum, the large R branch illustrated in Figure 3.2, corresponds to the energy minimum $E_B(\sigma_+)$, whereas the unstable state, the small R branch of numerical solutions, corresponds to $E_B(\sigma_-)$. This was pointed out previously by other authors as well [126]. It must also be the case that the mass function $M(R)$ turns around at some extremum as well, as we found in the numerical case, which was illustrated in Figure 3.2.

We can see this behavior by considering the energy functional $E_B(\sigma)$ in eq. (3.35). When $C > 0$, a very large particle number $N > N_c \equiv A/\sqrt{3\,B\,C}$ would imply that the extrema $\sigma_\pm$ are complex; in that case, there are no real roots of the energy and no stable bound states. This gives rise to a maximum mass of

$$M_c = \frac{m\,A}{\sqrt{3\,B\,C}} = \sqrt{\frac{12}{|\lambda|}}\,\pi\,M_P. \tag{3.42}$$

This result was first derived by Chavanis [126], and it was also verified numerically by solving the nonrelativistic GP equation [120, 145]. Comparing to the exact result in eq. (3.32), we find that the difference in the numerical factor in the maximum mass is given by the ratio $\sqrt{32\pi}/\sqrt{12}\pi \approx .92$. We conclude that the variational method is appropriate in this regime as well.

We have assumed a particular (Gaussian) form for the wavefunction in this section. However, it is possible to perform a more general calculation of the variational energy using a generic ansatz for ψ, subject to only a few constraints. The physical results, as we have seen above, vary significantly across different self-interaction potentials, but

turn out not to depend very strongly on the choice of ansatz. A generic variational analysis is one of the cornerstones of Chapter 6.

3.6. Summary

Boson stars are gravitationally bound condensates of bosonic particles. The underlying theory is described by the particle mass m and its self-interaction potential $V(\phi)$. In this chapter, we took a common form for the self-interaction, $V(\phi) \propto \lambda \phi^4$, though the methods described could be applied to more exotic potentials. Boson stars are stabilized by a balance between the gravitational, kinetic pressure, and self-interaction forces, as described in Section 3.1 and illustrated in Figure 3.1.

It is generic in theories of boson stars that gravitational stability requires the total mass M be less than some critical value M_c. In this chapter, we described several of the results for maximum masses of boson stars originating in different theories, with repulsive, attractive, or no interactions. These results were compiled in [120], where the results were analyzed in the context of boson stars contributing to dark matter. The maximum mass of three classes of boson stars can be summarized:

$$M_c \simeq \begin{cases} .22 \sqrt{\frac{\lambda}{4\pi}} \frac{{M_P}^3}{m^2}, & \text{for } \lambda > 0 \text{ (repulsive interaction)} \\ .633 \frac{{M_P}^2}{m}, & \text{for } \lambda = 0 \text{ (non-interacting)} \\ \sqrt{\frac{32\pi}{|\lambda|}} M_P, & \text{for } \lambda < 0 \text{ (attractive interaction)} \end{cases} \tag{3.43}$$

This combines of the results of eqs. (3.10,3.13,3.32). For equal masses and moderate λ, it is clear that repulsive boson stars can have the largest masses, and attractive boson stars the smallest.

Before closing this chapter, we can add one more component to this story. If the bosons which constitute boson stars form an important component of some bosonic dark matter theory, then additional constraints can be imposed on possible bound states [120]. These constraints come in two categories. First, there exist strong upper bounds on the self-interaction strength of dark matter particles from observations of galaxy cluster collisions [36]. Second, there is a discrepancy between the results of numerical simulations of collisionless dark matter particles and observations of galaxy structure, which were reviewed in Chapter 1. It has been suggested that relatively strong self-interactions can solve these problems [42, 44, 55]. There is a finite range of self-interaction strengths which can simultaneously solve the small-scale problems

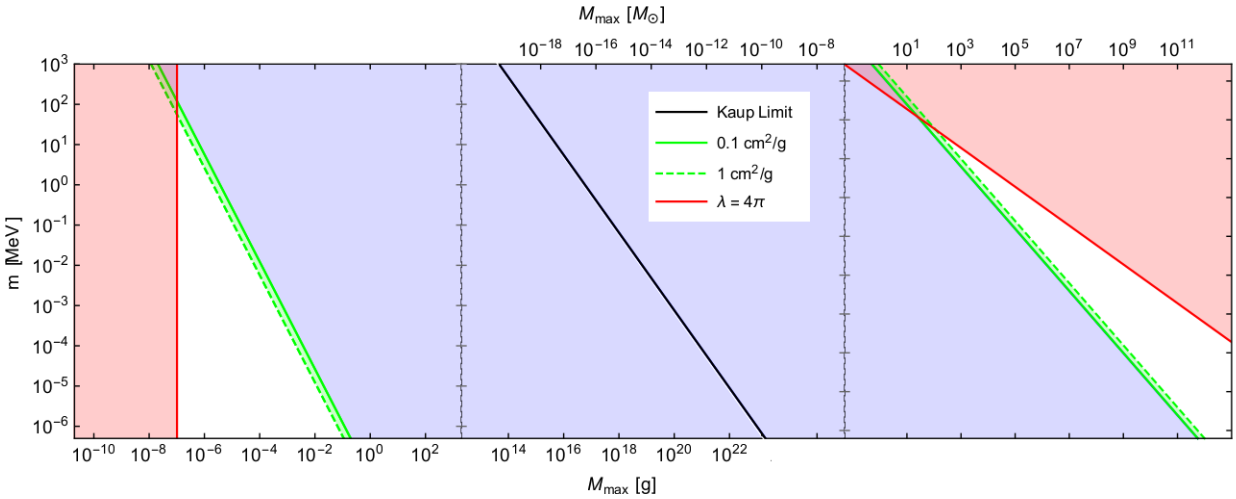

Figure 3.5.: The maximum mass of a boson star as a function of DM particle mass m. The green bands are the regions consistent with solving the small scale problems of collisionless DM. The blue region represents generic allowed interaction strengths (with $\sigma_{SI}/m \lesssim 0.1$ cm^2/g) extending to the Kaup limit which is shown in black. The red shaded region corresponds to $\lambda \gtrsim 4\pi$. Note that the boson star mass is measured in grams on the bottom horizontal axis, and in solar masses $M_\odot$ on the top. Figure adapted from [120].

while remaining consistent with the experimental upper bounds [120]:

$$\left(\frac{m}{1\text{ MeV}}\right)^{3/2} < \frac{|\lambda|}{10^{-3}} < 3\left(\frac{m}{1\text{ MeV}}\right)^{3/2}. \tag{3.44}$$

Our work in [120] combines many of the above considerations in a single analysis. One of the important contributions of that work is to summarize the full parameter space of boson stars which can form as a component of dark matter halo, as in Figure 3.5. The bounds in eq. (3.44) represent an upper bound on the interaction strength for repulsive and attractive interactions simultaneously, and the parameter range in which they are satisfied is illustrated by the green bands. On the other hand, there is also a large region of parameter space (represented in blue) in which boson stars are stable, satisfy astrophysical bounds, but the self-interactions are not sufficiently strong to solve the "cusp-core" and other problems; these theories are still viable if these problems have other solutions, e.g. through baryonic physics [149, 150]. One final important constraint is that of perturbativity of the underlying field theory: if $\lambda \gtrsim 4\pi$, then the basic perturbative analysis of eq. (3.5) breaks down (illustrated in red). With the exception of much larger or smaller constituent masses m, the entire space of allowed masses of dark matter boson stars is represented in Figure 3.5. This represents a vast parameter space, covering many orders of magnitude in dark matter mass m.

In light of the large space of allowed boson star theories, we will specialize to the particular case of axions in the chapters that follow. The experimental constraints on

axions, outlined in Chapter 2, constrain significantly the parameter space we consider; the typical QCD axion we will consider has a mass 10^{-6} eV $\lesssim m \lesssim 10^{-2}$ eV (a few orders of magnitude below the masses shown in Figure 3.5). Axions also have a peculiar self-interaction potential: it's leading term is attractive and $\propto \phi^4$ (as we considered here), but higher-order terms can be relevant. This will require a generalization of some of the methods presented above. We will begin to analyze these points in the next chapter.

Chapter 4.

Axion Stars in the Infrared Limit

"Look up at the stars and not down at your feet. Try to make sense of what you see, and wonder about what makes the universe exist. Be curious."
— Stephen Hawking

The motivation and consequences of axions as an extension to the SM were reviewed in Chapter 2. Because axions are light scalar particles, they can form condensates as described in Chapter 3. Using a semiclassical approach, in this chapter we will determine the full spectrum of weakly-bound axion stars; we also determine the mass and radius of gravitationally stable configurations as a function of the binding energy in the axion star. This chapter is primarily based on our work in [151].

4.1. Ruffini-Bonazzola Method for Axion Stars

Axions, and ALPs more generally, are versatile and ubiquitous among bosonic particles. The original proposal for these light scalars was in the context of solving the Strong *CP* Problem in QCD, and later, such particles were also found to be prime candidates for the constituents of dark matter, as we explained in Chapter 2. More generic ALPs emerge in numerous theories of physics beyond the SM, and have applications in many realms of physics (see Section 2.4).

Starting with the seminal works of Kaup [123] and Ruffini and Bonazzola [125], a large amount of literature has emerged surrounding the idea of gravitationally-bound scalar condensates; some of this was summarized in Chapter 3. Both Kaup and RB considered non-interacting bosons in their original works, and while their methods differed, the physical parameters defined by their solutions agreed with one another.

Further, they each determined the maximum mass of non-interacting condensates, which was inversely related to the particle mass m.

In the case of the axion, there are relevant self-interactions, and the leading such interaction is attractive. The RB method was extended to the case of axions first in [152, 153]; a more robust analysis was performed later in our work [151], which is summarized here. The basic components of the method, as presented in the original RB work, were explained in Section 3.4; below we review the relevant features in order to apply them to axion field theory.

Recall that the first step in the RB method is to expand the scalar field in creation and annihilation operators having definite energy and angular momentum quantum numbers; in the condensed state, one keeps only the ground state contributions. We thus expand the axion field $\mathcal{A}$ as

$$\mathcal{A}(t,r) = R(r)\left[e^{-i\,\mu_0\,t}\,a_0 + e^{i\,\mu_0\,t}\,a_0^\dagger\right] \tag{4.1}$$

where μ_0 is the eigenenergy of a single axion, and a_0 ($a_0^\dagger$) is the annihilation (creation) operator of the ground state axion, satisfying $[a_0, a_0^\dagger] = 1$ as in eq. (3.15). To a very good approximation, every axion in the condensate is in the ground state, which is described by a single spherically-symmetric wavefunction $R(r)$.

The second step of the RB procedure is to build up an N-particle ground state $|N\rangle$.[1] This simply amounts to applying the creation operator to the vacuum state N times, as in eq. (3.17). By using this state to take expectation values of the equations of motion, which are the Einstein and Klein-Gordon equations, we effectively include leading quantum corrections to the self-interaction. This will involve expectation values, for example, of the form

$$\begin{aligned}\langle N|\mathcal{A}^2|N\rangle &= 2\,N\,R(r)^2\\ \langle N-1|\mathcal{A}|N\rangle &= \sqrt{N}\,R(r)\,e^{-i\,\mu_0\,t},\end{aligned} \tag{4.2}$$

as well as several others. A detailed calculation of the expectation value for the full axion potential is found in Appendix A.

[1] Of course, the axion is a real scalar field, and so no symmetry protects axion stars from number-changing interactions. As we will explain in Chapter 5, the decay rate of axion stars through such interactions is negligible in typical scenarios, particularly for very weakly-bound axions, and thus to a good approximation we can define a conserved particle number N. Scenarios where the decay rates are relevant will be investigated in later chapters.

The interactions of an axion can be described by the instanton potential of eq. (2.18), reproduced here:

$$V(\mathcal{A}) = m^2 f^2 \left[1 - \cos\left(\frac{\mathcal{A}}{f}\right)\right], \tag{4.3}$$

where m and f are the mass and decay constant of the axion, respectively. To include the coupling to gravity, we write a general spherically symmetric gravitational metric as

$$ds^2 = -B(r)\, dt^2 + A(r)\, dr^2 + r^2\, d\Omega^2, \tag{4.4}$$

where $A(r)$ and $B(r)$ represent the deviations from a flat metric. We evaluate the expectation values of the tt and rr Einstein equations in eq. (1.1), and of the KG equation in eq. (1.2), which are

$$\begin{aligned} \langle N|G_\mu{}^\nu|N\rangle &= 8\,\pi\, G\, \langle N|T_\mu{}^\nu|N\rangle \\ \langle N-1|\left[\mathcal{D}\,\mathcal{A} - V'(\mathcal{A})\right]|N\rangle &= 0. \end{aligned} \tag{4.5}$$

The resulting equations of motion take the form

$$\begin{aligned} \frac{A'}{A^2\, r} + \frac{A-1}{A\, r^2} &= \frac{8\,\pi\, f^2}{{M_P}^2}\left[\frac{{\mu_0}^2\, N\, R^2}{B\, f^2} + \frac{N\, R'^2}{A\, f^2} + m^2\,[1 - J_0\left(\frac{2\sqrt{N}\, R}{f}\right)]\right], \\ \frac{B'}{A\, B\, r} - \frac{A-1}{A\, r^2} &= \frac{8\,\pi\, f^2}{{M_P}^2}\left[\frac{{\mu_0}^2\, N\, R^2}{B\, f^2} + \frac{N\, R'^2}{A\, f^2} - m^2\,[1 - J_0\left(\frac{2\sqrt{N}\, R}{f}\right)]\right], \\ \sqrt{N}\, R'' + \sqrt{N}\left(\frac{2}{r} + \frac{B'}{2\, B} - \frac{A'}{2\, A}\right) R' + A\left[\frac{\sqrt{N}\,{\mu_0}^2}{B} R - f\, m^2\, J_1\left(\frac{2\sqrt{N}\, R}{f}\right)\right] &= 0. \end{aligned} \tag{4.6}$$

Just as described in Section 3.3, the other nontrivial Einstein equations ($\theta\theta$ and $\varphi\varphi$) are equivalent to the KG equation above through a Bianchi identity. In the next section, we will make use of the physical limitations of the theory to expand and simplify these equations.

4.2. Double Expansion of Equations of Motion

The EKG equations of motion (4.6) form a closed set of equations, which can be solved for the axion wavefunction $R(r)$ and the two components of the metric tensor $A(r)$ and $B(r)$. However, these equations are complex and difficult to solve directly. By making use of certain physical limits, we can simplify them immensely.

Firstly, note that the RB method is semiclassical, with the procedure of taking expectation values of the equations of motion modifying the coefficients of the self-interaction terms. However, the axion wavefunction is coupled to a classical gravitational background. In the presence of sufficiently large metric deviations, there can be important back-reaction effects between the classical gravitational background and the quantum corrections to the self-interaction potential. This implies that we must work in the limit of *weak gravity*: the metric perturbations away from flatness should be small.

In the Einstein equations (4.6), the dimensionless parameter that controls the strength of the gravitational interaction is

$$\delta \equiv \frac{8\,\pi\,f^2}{{M_P}^2}. \tag{4.7}$$

In the limit $\delta \to 0$, the first two equations of (4.6) reduce to the vacuum Einstein equations. Note further that $\delta \ll 1$ holds in nearly any theory of axions, and in particular, holds tremendously well in QCD: for a typical QCD value $f = 6 \times 10^{11}$ GeV, $\delta = \mathcal{O}(10^{-14})$. Thus, we expand the metric functions

$$A = 1 + \delta\, a, \qquad B = 1 + \delta\, b, \tag{4.8}$$

where $a, b = \mathcal{O}(1)$, and safely neglect terms beyond the leading order in δ.

Expanding EKG equations (4.6) in powers of δ and truncating at leading order, we find

$$\begin{aligned}
a' &= -\frac{a}{z} + z\left[\frac{1}{4}{\epsilon_\mu}^2\, Z^2 + \frac{1}{4}Z'^2 + 1 - J_0(Z)\right], \\
b' &= \frac{a}{z} + z\left[\frac{1}{4}{\epsilon_\mu}^2\, Z^2 + \frac{1}{4}Z'^2 - 1 + J_0(Z)\right], \\
Z'' &= \left[-\frac{2}{z} + \frac{\delta}{2}(a' - b')\right] Z' - {\epsilon_\mu}^2(1 + \delta\, a - \delta\, b)\, Z + 2\,(1 + \delta\, a)\, J_1(Z),
\end{aligned} \tag{4.9}$$

where we have introduced the dimensionless eigenenergy $\epsilon_\mu \equiv \mu_0/m$, coordinate $z = m\,r$, and wavefunction $Z(z) = 2\sqrt{N}\,R(r)/f$. The coordinate z measures distances in units of the Compton wavelength of the axion, which (for example) is approximately $1/m \sim few$ cm for $m \sim 10^{-5}$ eV. For macroscopic states like axion stars, this is not an appropriate distance scale; a second small parameter, described below, that allows us to do a further rescaling.

Now, for weakly bound axion stars, we can systematically expand the equations (4.9) in powers of a parameter

$$\Delta \equiv \sqrt{1 - \frac{{\mu_0}^2}{m^2}}, \tag{4.10}$$

after rescaling the wavefunction $Z(z)$ and the coordinate z with powers of Δ corresponding to their engineering dimension. That is, we define a new coordinate $x = \Delta z$ and wavefunction $Y(x) = Z(z)/\Delta$. In the language of QFT, this expansion in Δ will require keeping only those operators which are relevant or marginal, while neglecting irrelevant operators. Keeping leading order in Δ is tantamount to the infrared (low-energy) limit of the theory. Note that when $\Delta \ll 1$, an axion star state (referred to as a "dilute axion star") is very weakly bound. For the purposes of this chapter, we will focus on these dilute states. There has recently been interest in solutions which have $\Delta = \mathcal{O}(1)$, so called "dense axion stars" [154], which can have very large binding energies. We postpone discussion of these more exotic dense states for Chapter 6.

Consider then the expansion of the axion potential

$$\begin{aligned} 1 - J_0(Z) &= \frac{1}{4}[Z^2 - \frac{1}{16}Z^4 + \frac{1}{576}Z^6 + ...] \\ &= \frac{1}{4}[\Delta^2 Y^2 - \frac{1}{16}\Delta^4 Y^4 + \frac{1}{576}\Delta^6 Y^6 + ...] \end{aligned} \tag{4.11}$$

It is easy to see that our systematic expansion in Δ provides justification to drop higher-order corrections to the self-interaction potential; higher-order terms in the expansion of $Z(z)$ will be suppressed by high powers of $\Delta \ll 1$. The eqs. (4.9), now to leading order in both δ and Δ, simplify to

$$\begin{aligned} a'(x) &= \frac{x}{2} Y(x)^2 - \frac{a(x)}{x}, \\ b'(x) &= \frac{a(x)}{x}, \\ Y''(x) &= -\frac{2}{x}Y'(x) - \frac{1}{8} Y(x)^3 + [1 + \kappa\, b(x)]\, Y(x). \end{aligned} \tag{4.12}$$

The single parameter remaining in these equations is

$$\kappa \equiv \frac{\delta}{\Delta^2}, \tag{4.13}$$

rather than δ or Δ separately. Note that since $b(x)$ is proportional to the Newtonian gravitational potential, $\kappa \sim G$ is the effective coupling of the field $Y(x)$ to gravity.

Leading order corrections to eqs. (4.12) are of $\mathcal{O}(\delta)$ and $\mathcal{O}(\delta\kappa)$. The requirement that these contributions be negligible, along with $\Delta \ll 1$, restricts the consistency of the double expansion to values of the parameter κ in the range

$$\delta \ll \kappa \ll \frac{1}{\delta}. \tag{4.14}$$

This can be an incredibly wide range: for QCD axions, $\delta \sim 10^{-14}$, so that we can consistently evaluate solutions over the range $10^{-14} \ll \kappa \ll 10^{14}$!

4.3. Numerical Methods and Physical Quantities

Even in the simplified form, the system of equations (4.12) have no exact solutions. We employ a shooting method to integrate these equations to calculate $Y(x)$, $a(x)$, and $b(x)$. Relativity requires $a(0) = 1$, but the values of $Y(0)$ and $b(0)$ are a priori arbitrary. The asymptotic boundary conditions are that $Y(x)$, $a(x)$, and $b(x)$ tend to zero at $x \to \infty$. It turns out that as $x \to \infty$, $Y(x)$ vanishes exponentially, while $a(x)$ and $b(x)$ have Newtonian asymptotics; the latter is difficult to implement in numerical calculations. However, notice from (4.12) that

$$a(x) + b(x) = -\frac{1}{2}\int_x^\infty x'\, Y(x')^2\, dx', \tag{4.15}$$

which asymptotically, will vanish exponentially (because $Y(x)$ does). We therefore impose the requirement that $\lim_{x\to\infty} a(x) + b(x) = 0$ be satisfied exponentially for valid numerical solutions.

The basic procedure for implementation of the shooting method is:

- fix a value of κ;
- at each κ, vary $Y(0)$ and $b(0)$ until $Y(x)$ and $a(x) + b(x)$ both vanish exponentially at large distances.

For given axion parameters m and f, the solutions can be parameterized by the given value of κ, or equivalently by Δ, or by $Y(0)$ (this third choice, to use the central density of the axion wavefunction as the free parameter, was used by [153]).

We have solved the system of equations (4.12) over a wide range of the parameter κ. Before detailing the numerical solutions, consider the calculation of the physical quantities. The most important parameters describing axion stars are the total mass M, the radius inside which 99% of the matter contained in the star is concentrated R_{99},

and the number of axions in the star N. These can essentially be determined by two functions [125, 135]: the energy momentum tensor

$$T_{\mu\nu} = \frac{2}{\sqrt{|g|}} \frac{\partial \mathcal{L}}{\partial g^{\mu\nu}}, \tag{4.16}$$

where our Lagrangian $\mathcal{L}$ is essentially that of eq. (3.5) and applied to axions; and the current 4-vector

$$J^{\mu} = i \left[\left(\frac{\partial \mathcal{L}}{\partial(\partial_{\mu}\mathcal{A}^{*})} \right) \mathcal{A}^{*} - \left(\frac{\partial \mathcal{L}}{\partial(\partial_{\mu}\mathcal{A})} \right) \mathcal{A} \right]. \tag{4.17}$$

We denote the gravitational metric by $g^{\mu\nu}$, and its determinant by $|g| = \det g$.

In fact, we have already determined the relevant components of $T_{\mu\nu}$: T_{tt} and T_{rr} are proportional to the RHS of the first and second equations in (4.6), respectively. It is also worth noting that, because axions are real scalars, the current vector J^{μ} defined in eq. (4.17) is not exactly conserved. This will be important when we define the particle number N below.

The mass of the star is given in leading order of the infrared limit ($\Delta \to 0$) by

$$M = \int d^3r \sqrt{|g|} \, \langle N|T_{00}|N\rangle \approx \frac{f^2}{m\,\Delta} U(\infty) = \frac{f^2}{m} \sqrt{\frac{\kappa}{\delta}} \, U(\infty). \tag{4.18}$$

where

$$U(y) = 2\,\pi \int_0^y Y(x)^2 \, x^2 \, dx. \tag{4.19}$$

Corrections to M are of $\mathcal{O}(\delta)$ and $\mathcal{O}(\Delta^2)$, and will be discussed shortly. Next, using the standard definition for the radius of a boson star, we define x_{99} as

$$\frac{U(x_{99})}{U(\infty)} \equiv 0.99. \tag{4.20}$$

Then restoring the appropriate scaling parameters, the radius of the axion star is

$$R_{99} = \frac{x_{99}}{m\,\Delta} = \sqrt{\frac{\kappa}{\delta}} \frac{x_{99}}{m}. \tag{4.21}$$

Particle number N is not a good quantum number, because axions are Hermitian scalars; however, to a good approximation, we can define an effective particle number which will be approximately conserved.[2] In this way way, we could define the number

[2] A more thorough discussion of non-conservation is presented in Chapter 5.

of particles in an axion star is determined by the (approximate) conservation of the 0 component of J^μ in eq. (4.17) [125, 135]

$$\langle N|J^0|N\rangle = \frac{2\,\mu_0\,N\,R(r)^2}{B(r)}, \tag{4.22}$$

which implies, at leading order in the infrared limit,

$$N = \int d^3r\,\sqrt{|g|}\,\langle N|J^0|N\rangle \approx \frac{f^2}{m^2}\sqrt{\frac{\kappa}{\delta}}\,U(\infty). \tag{4.23}$$

This argument is not precisely correct, so for completeness we outline an alternative derivation below.

Recall that the conjugate momentum for a scalar field Φ, using the mode expansion of eq. (3.14), can be written as

$$\Pi = D_t\,\Phi = \frac{1}{B}\left[-i\,\mu_n\,R_n(\vec{r})\,e^{-i\,\mu_n\,t}\,a_n + i\,\mu_n\,R_n^\dagger(\vec{r})\,e^{i\,\mu_n\,t}\,a_n^\dagger\right], \tag{4.24}$$

which is implicitly summed over n. D_t is a covariant time derivative which gives rise to the metric function B in the denominator, and we have ignored angular momentum modes above $\ell = 0$. The equal-time commutator of Φ and Π is

$$\left[\Phi(\vec{r}),\Pi(\vec{r}')\right] = \frac{2}{B}\,R_n^\dagger(\vec{r})\,R_n(\vec{r}'). \tag{4.25}$$

The requirement that the commutator be canonically normalized, $[\Phi,\Pi] = \delta^3(\vec{r}-\vec{r}')$, is equivalent to a completeness relation on the R_n functions:

$$\sum_n \frac{2}{B}\,\mu_n\,R_n^\dagger(\vec{r})\,R_n(\vec{r}') = \delta^3(\vec{r}-\vec{r}'). \tag{4.26}$$

Given that the R_n functions form a complete set, we can write down a related normalization condition,

$$\int \frac{2}{B}\,\mu_n\,R_n^\dagger(\vec{r})\,R_n(\vec{r})\,\sqrt{|g|}\,d^3r = 1. \tag{4.27}$$

Now specializing to the case $n = 0$ for the BEC and identifying $R_0(r)$ here with the axion star wavefunction $R(r)$, we find the same expression we had in eq. (4.23) using the approximate conservation of the current vector J^μ. The definition for N outlined in these last few paragraphs was used previously in [135].

Comparing with eq. (4.18), eq. (4.23) expression satisfies $N = M/m$, appropriate at leading order; however, that implies that the energy per particle is equal to the particle

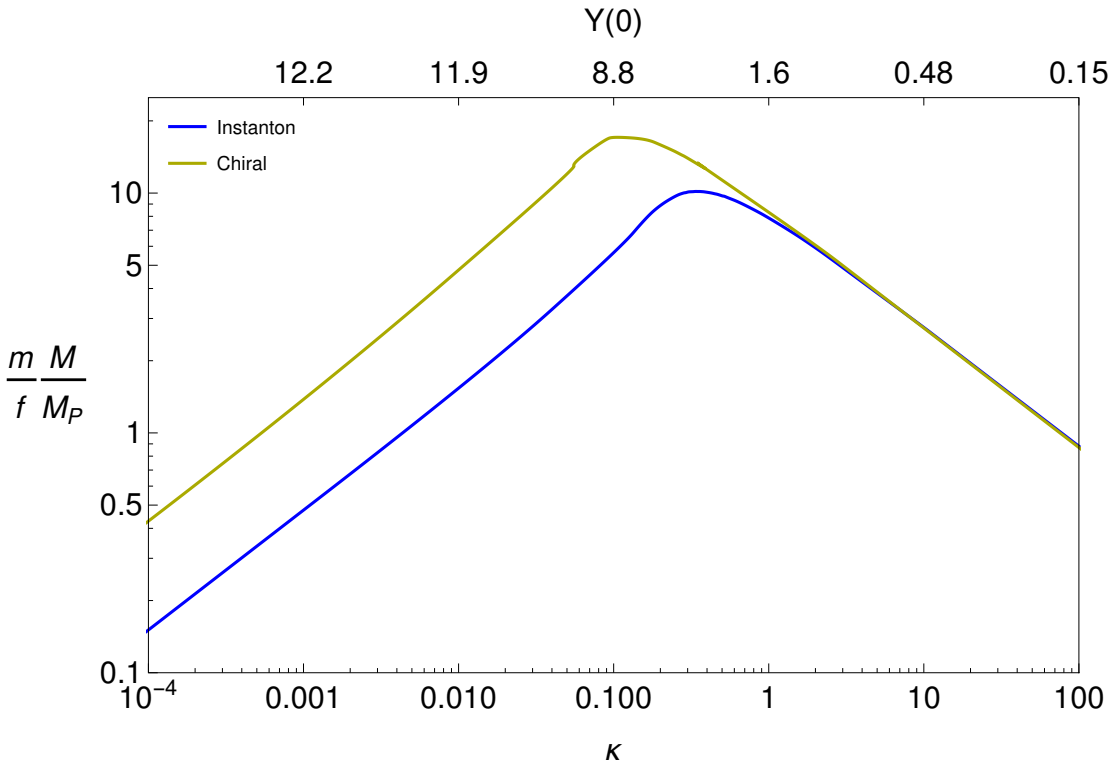

Figure 4.1.: The mass spectrum for axion stars using the instanton potential of eq. (2.18) (blue curve) and the chiral potential of eq. (2.15) (yellow curve), as functions of the parameter κ (bottom horizontal axis) and of $Y(0)$ (top horizontal axis). The masses on the vertical axis have been rescaled by the quantity $M_P\, f/m$.

mass, i.e. there is no binding energy. This is not the case in truth: it a consequence of the fact that the binding energy is a small correction to the mass, not accessible at leading order. In Appendix B, we calculate the corrections to both M and N at leading order in δ and Δ^2 which, in the region $\kappa = \mathcal{O}(1)$, are of the same order. The binding energy can be written as

$$E_B \equiv M - m\, N, \tag{4.28}$$

which will satisfy $E_B < 0$ for a bound solution. We will discuss these results in the next section as well.

We will see shortly that, in the most interesting range of solutions, $\kappa = \mathcal{O}(1)$. Then, analyzing the scaling with dimensionful parameters in eq. (4.21) and (4.18), we observe that

$$M \sim \frac{M_P\, f}{m}, \qquad R_{99} \sim \frac{M_P}{f\, m}. \tag{4.29}$$

This scaling is useful to keep in mind, and will occasionally be used in the coming chapters to describe "typical" axion star configurations.

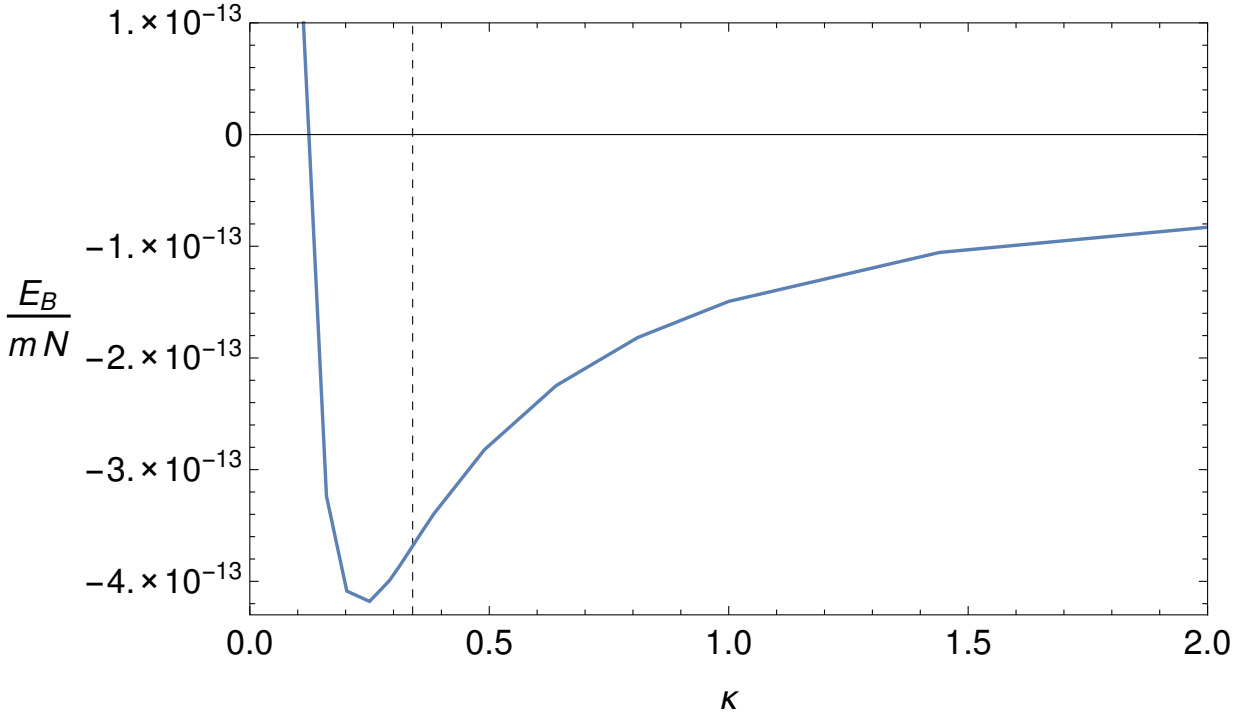

Figure 4.2.: The rescaled binding energy per particle, defined by $E_B = M - m\,N$, calculated at leading order in δ and Δ^2 in Appendix B. The position of the maximum mass, at $\kappa = .34$, is illustrated by a dashed, vertical line. To set the numerical scale we have fixed the QCD parameters $m = 10^{-5}$ eV and $f = 6 \times 10^{11}$ GeV.

4.4. Results

In this section, we present our results for the solutions of the EKG system (4.12). The blue curve in Figure 4.1 shows the mass spectrum of axion stars as a function of both the gravitational coupling κ and the central density $Y(0)$ for the axion instanton potential we have analyzed so far in this chapter (the yellow curve will be explained shortly). Observe that the critical value

$$M_c \approx 10.2\,\frac{M_P\,f}{m}, \tag{4.30}$$

the maximum mass, marks the boundary for gravitational stability. The two branches of solutions correspond directly to those found in Section 3.5.2 in the case of attractive interactions.

As described in the previous section, the binding energy defined in eq. (4.28) appears in $\mathcal{O}(\delta, \Delta^2)$ corrections to M and N, which I have derived and present in Appendix B. In Figure 4.2, we illustrate the resulting dependence of this binding energy on the parameter κ. Note hat the binding energy has a magnitude which is maximized near $\kappa \approx .25$, which is slightly below the position of the maximum mass at $\kappa = .34$. States at $\kappa \lesssim .25$ have binding energies whose magnitudes are rapidly decreasing as κ

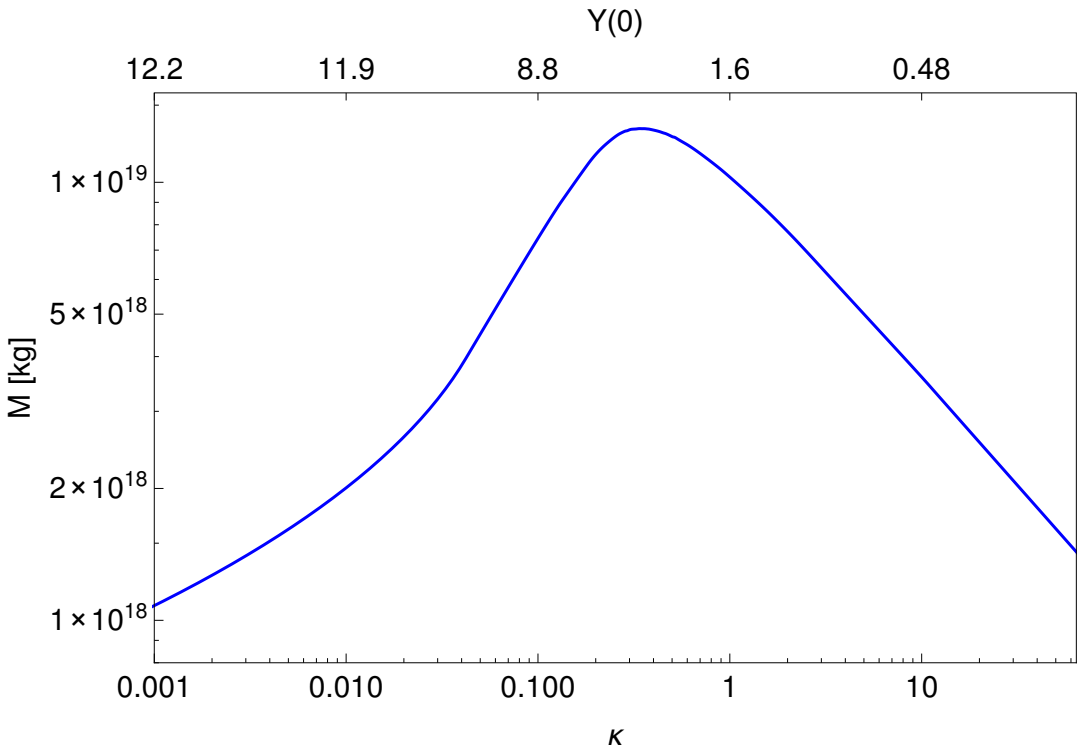

Figure 4.3.: The mass spectrum of weakly bound axion stars as a function of κ (bottom horizontal axis) and of $Y(0)$ (top horizontal axis), for the parameter choices $m = 10^{-5}$ eV and $f = 6 \times 10^{11}$ GeV. The maximum mass is located roughly at $\kappa \approx .34$. Figure reproduced and updated from [151].

decreases, and at $\kappa \lesssim .11$, the binding energy is *positive*. Such states are unbound, as it is energetically favorable to send their constituent particles to infinity. This is evidence that the small-κ branch of solutions are unstable.

The existence of a maximum mass implies that for a given N, there exist two mass states M_1 and M_2 with equal N but different values of Δ and thus different total energy. One of these states (say, M_1) would exist on the left branch of the mass curve, and the other (M_2) on the right. The discussion of the binding energy above, and the results of Figure 4.2, suggest that the state M_1 on the left branch, having a larger value for the parameter Δ, will typically have a larger total mass. This higher-energy state corresponds to the unstable branch of solutions we found in Section 3.5.2. For clarity, we summarize the relative parameter values of states on the two branches of solutions in Table 4.1.

We show the mass, scaled by $M_P\, f/m$ as in eq. (4.29), in Figure 4.1. On the branch with $\kappa > .34$, the mass and radius are well fit by the functions

$$M(\kappa) \approx \frac{8.75}{\sqrt{\kappa}} \frac{M_P\, f}{m}, \qquad R_{99}(\kappa) \approx 1.15\, \sqrt{\kappa}\, \frac{M_P}{f\, m}. \tag{4.31}$$

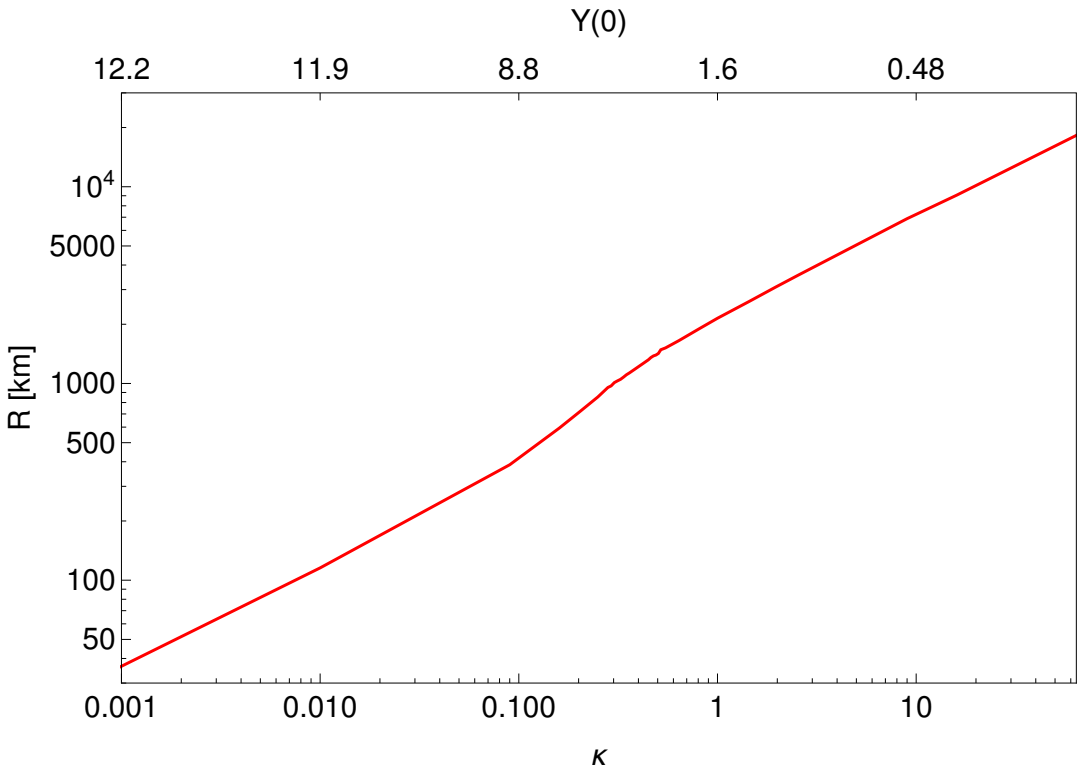

Figure 4.4.: The radii of weakly bound axion stars as a function of κ (bottom horizontal axis) and of $Y(0)$ (top horizontal axis), for the parameter choices $m = 10^{-5}$ eV and $f = 6 \times 10^{11}$ GeV.

	M	R_{99}	$M(R)$	κ	Δ	$Y(0)$	Stable?
Branch 1:	Larger	Smaller	$M \propto R$	Smaller	Larger	Larger	No
Branch 2:	Smaller	Larger	$M \propto R^{-1}$	Larger	Smaller	Smaller	Yes

Table 4.1.: Parameter comparison of the two branches of solutions for axion stars, evaluated at fixed N and δ. The parameters considered are: the total mass M, the radius R_{99}, the mass-radius relation $M(R)$, the effective gravitational coupling κ defined in eq. (4.13), the binding energy parameter Δ defined in eq. (4.10), and the central density $Y(0)$. We also note which branch is stable (last column).

We recover on this branch the approximate relation $M \propto 1/R_{99}$. The left branch, where $\kappa < .34$, has a slightly different relation:

$$M(\kappa) \approx 15.04 \sqrt{\kappa} \frac{M_P f}{m}, \qquad R_{99}(\kappa) \approx .55 \sqrt{\kappa} \frac{M_P}{f m}. \tag{4.32}$$

Note that on the left branch, both M and R_{99} are increasing functions of κ. We have already noted above that states with $\kappa \lesssim .25$ on this left branch correspond to energy *maxima*, and are unstable to collapse. As a result, we can set a lower bound on the

κ	M [kg]	R_{99} [km]	d [kg / m^3]	$\frac{E_B}{m\,N}$ [10^{-13}]
0.01	2.01×10^{18}	115	311	141
0.09	6.91×10^{18}	386	28.6	2.93
0.16	1.02×10^{19}	593	11.6	-3.24
0.25	1.27×10^{19}	854	4.85	-4.18
0.29	1.31×10^{19}	972	3.41	-3.99
0.34	1.33×10^{19}	1077	2.53	-3.71
0.38	1.32×10^{19}	1183	1.90	-3.39
0.64	1.20×10^{19}	1652	0.633	-2.25
1	1.03×10^{19}	2145	0.248	-1.49
4	5.56×10^{18}	4499	0.0146	$-.384$
16	2.85×10^{18}	9062	0.000913	$-.109$
100	1.15×10^{18}	22849	0.000023	$< 10^{-2}$

Table 4.2.: Macroscopic parameters describing a dilute axion star: mass M, radius R_{99}, average density d, and reduced binding energy per particle $E_B/m\,N$, as a function of $\kappa = \delta/\Delta^2$. To set the numerical scale we have fixed the QCD parameters $m = 10^{-5}$ eV and $f = 6 \times 10^{11}$ GeV.

radius of stable axion stars, which is

$$R_{min} \approx .85\,\frac{M_P}{f\,m}. \tag{4.33}$$

For the particular parameter choices $m = 10^{-5}$ eV and $f = 6 \times 10^{11}$ GeV, the mass and radius of gravitationally stable configurations are illustrated in Figures 4.3 and 4.4. While the radius is a monotonically increasing function of κ, the mass has a maximum of $M_c \approx 1.33 \times 10^{19}$ kg at $\kappa \approx .34$. In Table 4.2, we present the total mass M, radius R_{99}, average density $d = 3\,M/4\,\pi\,{R_{99}}^3$, and binding energy per particle $E_B/m\,N$ of the solutions for each value of κ considered. Observe that the average densities for axion stars, the fourth column in the table, are typically much less than the density of water, sometimes by many orders of magnitude.

As we have pointed out, states with $\kappa \lesssim .25$, or which exceed the maximum mass M_c, are unstable to collapse or to sending their constituent particles to infinity. If these unstable states do collapse, then it is appropriate to ask what the stable endpoint is of such collapse. We will examine collapsing axion stars in detail in Chapter 6.

4.5. The Chiral Potential

As described in Chapter 2, the instanton potential of eq. (2.18) does not take into account the effect of nonzero quark masses and nonperturbative QCD effects. The more precise potential to use would be the *chiral* one of eq. (2.15). We update the analysis in this section and comment on any changes.

In the double expansion of the EKG equations, all of the above derivations are still valid. Because the only relevant self-interaction in the infrared limit is the ϕ^4 term, only a single coefficient on the self-interaction part of the KG equation is modified; the third equation in (4.12) is changed to

$$\Upsilon''(x) = -\frac{2}{x}\Upsilon'(x) - .0428\,\Upsilon(x)^3 + [1 + \kappa\, b(x)]\,\Upsilon(x). \tag{4.34}$$

This change is akin to the modification of c_4 in Table 2.1 from the instanton case to the chiral one; the coefficient changes by roughly a factor of 3.

Redoing the numerical analysis above for the new potential, we find slight modifications of the results but no qualitative changes. The value of the maximum mass is $M_c \approx 12.8\, M_P\, f/m$ in the chiral case (compared to the instanton coefficient of 10.2), and it occurs at a value of $\kappa \approx .11$ (rather than $\kappa \approx .34$). We illustrate the change in the mass spectrum in Figure 4.1; the radius of the axion star is mostly unchanged, except for an $\mathcal{O}(1)$ modification in the range $.1 \lesssim \kappa \lesssim .4$, where the position of the maximum mass shifts.

4.6. Summary

Our work [151] builds on the seminal work of Ruffini and Bonazzola [125], a semiclassical method for investigating boson stars which was first applied to axions by [153]. By making use of the weak gravity ($\delta \ll 1$) and weak binding ($\Delta \ll 1$) limits, the equations of motion were made tractable, and a single dimensionless constant $\kappa = \delta/\Delta^2$ parameterized the solutions. Through simple relations, the solutions can also be parameterized by Δ or the central density $\Upsilon(0)$.

Solving the equations of motion over a wide range of κ, we found that while the radius is a monotonically decreasing function of the parameter Δ, the axion star mass has a maximum value M_c near $\kappa = .34$.[3] Gravitationally bound configurations of axions with masses greater than M_c are unstable and will collapse; this is investigated

[3]This value applies for the instanton potential. For the chiral potential, the maximum mass is at $\kappa = .11$

in greater detail in Chapter 6. In the allowed region $M < M_c$, there are two branches of solutions. The more weakly bound branch of solutions lie on an energy maximum, and are thus unstable either to collapse or to transition to a state on the more strongly bound branch, assuming a method for the dissipation of energy. The stable states, which have relatively larger radii, lie on the more strongly bound branch.

For QCD axions with $f = 6 \times 10^{11}$ GeV, the maximum mass was roughly $M_c \approx 1.3 \times 10^{19}$ kg,[4] though this method can be applied to other axion theories with vastly different input values for m and f. The scaling of the mass M and radius R_{99} with the dimensionful parameters of the underlying axion theory are given in eq. (4.29). For example, theories of axions with $m \sim 10^{-22}$ eV and $f \sim 10^{16}$ GeV, sometimes called Fuzzy Dark Matter models [112], can give rise to condensates of galactic scale [109–117]. The mass spectrum and stability properties of such condensates will be discussed in Chapter 5 in the context of axion star decay.

We have assumed in this chapter that an axion star has a well-defined particle number N. This is not strictly correct, as axions, being real scalars, have no quantum symmetry guaranteeing particle number conservation. We investigate the consequences of this fact in the next chapter.

[4] For the chiral potential, this value is $M_c \approx 1.7 \times 10^{19}$ kg.

Chapter 5.

The Lifetime of Axion Stars

"All things that have form eventually decay."
— Orochimaru

In Chapter 4, we derived the equations of motion describing axion stars in the weak gravity and weak binding limits, and solved them over a wide range of the one nontrivial parameter κ. The analysis assumed a well-defined particle number N, which is not strictly valid for the axion, as it is a real scalar field with no symmetry enforcing conservation of N. In this chapter, we investigate the consequences of non-conservation of particle number in an axion star. This chapter is primarily based on our work in [155, 156].

5.1. Symmetries and Conservation Laws

In quantum mechanics, Gell-Mann's famous totalitarian principle [157] is: "Everything not forbidden is compulsory." This principle, borrowed from T. H. White's "The Once and Future King", is a statement of the fact that any process in particle physics that is not directly in violation of a symmetry of the theory must occur, with some rate. The corresponding rate can be vanishingly small, but is only exactly zero when precluded by symmetry.

For example, the process of pion decay to a positron and a neutrino, $\pi^+ \to e^+ + \nu_e$, is allowed, but $\pi^+ \to e^- + \nu_e$ and $\pi^+ \to e^+ + \nu_\mu$ are not (the first violates the electromagnetic gauge symmetry, the second violates discrete lepton number symmetries) [158, 159]. There have been numerous cases in the history of particle physics where examination of symmetry principles have led to important discoveries. Pauli famously predicted the existence of the neutrino by the fact that its absence would

violate energy-momentum conservation in beta decay [160]; Gell-Mann predicted the existence of the Ω^- baryon using symmetries of the hadron sector [161, 162]. Clearly, symmetries occupy a very central role in modern day particle physics.

Of particular interest here is the notion of particle number conservation. As described in detail in Chapter 3, a complex scalar field Φ whose Lagrangian is a function of bilinears $(\Phi^\dagger \Phi)$ will possess a $U(1)$ symmetry that protects the field from particle number non-conserving interactions; that is to say, a complex scalar field has a conserved particle number N. However, no such symmetry exists for real scalar fields.

Axions, being real scalar fields, fall into this latter class. It is well known that free axions can decay to two photons [81–84]

$$a \to 2\,\gamma \tag{5.1}$$

as a result of the $a\,F\,\tilde{F}$ term in the Lagrangian of eq. (2.9). The rate for these decays is

$$\Gamma_a = \frac{(E/N)^2\,{\alpha_{em}}^2\,m^3}{64\,\pi^3\,f^2}, \tag{5.2}$$

where E/N is a model-dependent constant introduced in Chapter 2. In principle, this rate will be different for axions in a condensed state, because condensed axions can go off-shell. Nonetheless, eq. (5.2) implies an extremely long axion lifetime of 3×10^{41} years (for $m = 10^{-5}$ eV), leading previous authors to the conclusion that this decay process is unlikely to have cosmological significance [163].[1]

In the condensed axion star state, new decay channels become available. These include transitions where multiple condensed axions annihilate to form one or more highly energetic axions, which emerge from the axion star. We can represent these number-changing transitions by the process

$$A_N \to A_{N-n} + \sum_{s=0}^{\nu} a_{p_s} \tag{5.3}$$

where A_k represents an axion star with k axions, and a_p is an emitted axion of momentum p.[2] To be explicit, this process represents the annihilation of n *condensed* axions in an N-axion condensate to form $\nu < n$ *uncondensed* axions which are emitted. We could

[1] We plan to return to this question of condensed axion decay to photons in the near future.

[2] As we will see later, the emitted axions we will consider are not in momentum eigenstates, but their momentum is sharply peaked near a particular value.

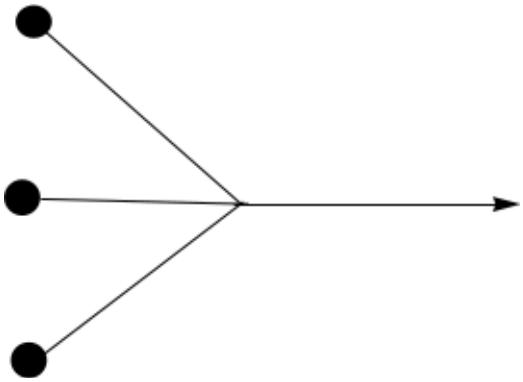

Figure 5.1.: A depiction of the process $3\,a_c \to a_p$ process taking place in an axion star. The filled blobs on the left side correspond to condensed axions a_c, while the arrow pointing to the right represents an outgoing scattering state axion a_p. Figure reproduced from [155].

also represent this process in a more the microscopic description,

$$n\,a_c \to \sum_{s=0}^{\nu} a_{p_s}. \tag{5.4}$$

The label c is used to distinguish the condensed states from scattering states.

The axion self-interaction potential, first introduced in Chapter 2 in eq. (2.18) (instanton) and (2.15) (chiral), contains only even powers of the axion field $\mathcal{A}$. As a result, number-changing interactions of the form (5.3) can only change axion number by an integer multiple of 2. The lowest-order process has $n = 3$ and $\nu = 1$, where a single high-energy axion is emitted,

$$3\,a_c \to a_p. \tag{5.5}$$

The diagram of Figure 5.1 depicts such a process. In spite of its apparent similarity, this depiction *is not a Feynman diagram*. In a Feynman diagram, the incoming and outgoing states are on shell, and in definite momentum states, whereas (as explained below) condensed axions in an axion star are not.

An axion star consists of axions with a definite energy $E = m + E_B/N$, where $E_B < 0$ is the binding energy of the axion star, defined in eq. (4.28). However, condensed axions have a momentum which is not fixed to a particular value. They participate in a wavefunction $R(r)$ which extends over a large radius $R_{99} \sim (m\,\Delta)^{-1}$, where Δ was defined in eq. (4.10); as a result, they have a momentum spread $\delta p \sim 1/R_{99} \sim m\,\Delta$. This momentum distribution is peaked at very low values, but is nonzero for all $0 \leq p < \infty$.

Energy and momentum conservation in the process of (5.5) requires that the three bound axions have sufficient momentum $p = \sqrt{9\,E^2 - m^2}$ to create a free axion, which

would not be possible for free axions at rest. But condensed axions are neither free nor at rest; their extended momentum distribution is what makes processes of this form possible. Now, observe that the probability that the three condensed particles obtain sufficient momentum decreases rapidly with the size of the condensate; nonetheless, *it is never exactly zero.* Because no symmetry precludes it, it must occur with some rate. The question of whether this decay process affects cosmology, due to the survival or non-survival of the condensate, is a question of numerical calculations and depends on the parameters of the axion theory, as well as the size and mass of the condensate. In the following sections, we will outline the calculation of this decay rate.

Before proceeding, we should note that the validity of our framework for calculating axion star decay was recently called into question [164, 165]. In particular, those authors questioned whether momentum could be conserved in the microscopic process (5.5). One version of this argument is based on the optical theorem: the scattering diagram

$$3\,a_c \to a \to 3\,a_c \tag{5.6}$$

has a propagator with no imaginary part (or so it is claimed), presumably because its denominator $E^2 - p^2 - m^2 \approx 8\,m^2 \neq 0$. If correct, this implies that the decay rate must vanish. On the contrary, however, this argument is based again on the premise that the momentum of the axions in the initial and final states is zero. We have seen that those particles are not in momentum eigenstates, and with a tiny probability they can produce sufficient momentum to allow the axion in the intermediate state to go on mass-shell. An explicit calculation of the imaginary part of this diagram can be found in the recent paper [166].

A second point made in [164, 165] is of a more macroscopic nature; they raise the question of how the three bound axions participating in the decay can transmit their momentum to the axion star as a whole. To that point, we will see below that the axion emitted in the decay process is in the form of a zero angular momentum spherical wave, which has equal probability to be emitted in any direction, and thus has a *vanishing average momentum*. So the average momentum in the process (5.5) is indeed conserved. We conclude that our calculation of the decay of axion stars, as presented below, respects energy and momentum conservation and thus rests on a stable foundation.

5.2. Decay Rates

We want to investigate the decay rate of axion stars through the process (5.5). As we have seen, it is possible for three bound axions to convert into a free axion, but only if

they can transfer a momentum of $p = \sqrt{9\,E^2 - m^2} = m\,\sqrt{9(E/m)^2 - 1}$. This is possible because the coordinate uncertainty of bound axions is $\delta x \sim R_{99} \sim (m\,\Delta)^{-1}$, implying that their momentum distribution is spread over a range of $\delta p \sim m\,\Delta$.

At strong binding, a condensed axion's energy is much smaller than its rest mass $E \ll m$, and it is easy to transfer sufficient momentum to the escaping axion. As a result, we may expect that the transition rate will be large for strongly bound axion stars; in truth, the method presented here applies only in the weak binding limit.[3] As the binding energy decreases from these very large values, it becomes increasingly difficult to transfer sufficient momentum to the created free axion. At a particular value of Δ, the transition rate becomes so small that the axion star survives from the big bang until the present time. A priori, we do not know whether this transition occurs in the weak or strong binding regimes.

In the original Ruffini-Bonazzola method [125], and in our application of it to axion stars [151] presented in Chapter 4, the axion field was expanded in bound states only. To quantify the calculation of the transition rate of bound to emitted particles, we propose to modify the axion field to include a term [155]

$$\phi_s(t,r) = \int d^3p\, a(\vec{p})\, e^{i\,\vec{p}\cdot\vec{r} - i\,\mu_p\,t}, \tag{5.7}$$

where μ_p is the eigenenergy of the scattering state axion labeled by momentum p, to represent axions in scattering states; that is, we expand the axion field as

$$\mathcal{A}(t,r) = R(r)\,e^{-i\,\mu_0\,t}\,a_0 + R(r)\,e^{i\,\mu_0\,t}\,a_0^\dagger + \phi_s(t,r) + \phi_s^\dagger(t,r) \tag{5.8}$$

where $[a(\vec{p}), a^\dagger(\vec{p}\,')] = (2\pi)^3\,2\,\mu_p\,\delta^3(\vec{p} - \vec{p}\,')$. The creation operators define states labeled by momentum $\vec{p}$ as

$$|\vec{p}\rangle = a^\dagger(\vec{p})\,|0\rangle \tag{5.9}$$

The first two terms in eq. (5.8) represent the usual contribution of the bound states, as in the original expansion of eq. (3.14) or eq. (4.1), whereas the last two terms represent the addition of scattering states. The combination of these different contributions form a complete set of states representing the axion field.

Note that the bound and scattering states we have written in eq. (5.8) are not strictly orthogonal. However, the bound states have a wavefunction which is sharply peaked at zero momentum (with width $\sim m\,\Delta$). On the other hand, the momentum of the

[3] The investigation of strongly bound condensates is made more complicated by higher-order quantum corrections to the field expansion, and possible backreaction in the gravitational metric if gravity becomes strong. This is a topic for future work.

emitted axion in the leading-order process is $p = m\sqrt{9(E/m)^2 - 1} \approx \sqrt{8}\,m$ in the weak binding $E \approx m$ limit; that is, its momentum is sharply peaked at a very large value. Thus, the overlap of these states is considered to be negligible in what follows.

In leading order, the transition rate is obtained from the matrix element of the interaction potential

$$\begin{aligned}\mathcal{M}_3 &= \int dt\, d^3r\, \langle N|V(\mathcal{A})|N-3,\vec{p}\rangle \\ &= m^2 f^2 \langle N|\left[1-\cos\left(\frac{\mathcal{A}}{f}\right)\right]|N-3,\vec{p}\rangle,\end{aligned} \tag{5.10}$$

where we have used the simplified instanton potential for axions of eq. (2.18). Here, $\langle N|$ represents an initial state of N bound axions, while $|N-3,\vec{p}\rangle$ represents the final state of $N-3$ bound axions and a single scattering state axion with momentum $\vec{p}$. Using the expansion of eq. (5.8) and the method for calculating expectation values outlined in Appendix A, we find at $N \gg 1$ that

$$\mathcal{M}_3 = -i\,m^2 f \int dt\, d^3r\, J_3\left(\frac{2\sqrt{N}\,R(r)}{f}\right)\ \langle 0|\phi_s(t,r)|\vec{p}\rangle. \tag{5.11}$$

Using eqs. (5.9) and (5.7), the transition element of the scattering state $\langle 0|\phi_s(t,r)|\vec{p}\rangle = \exp\left[i\,(\vec{p}\cdot\vec{r} - \mu_p\, t)\right]$. Thus the matrix element evaluates to

$$\mathcal{M}_3 = -i\,4\,\pi^2\,\frac{f}{p}\,\delta(3\,\mu_0 - \mu_p)\,I_3(p), \tag{5.12}$$

where

$$I_3(p) = m^2 \int_{-\infty}^{\infty} dr\, r\, \sin(p\,r)\, J_3\left(\frac{2\sqrt{N}\,R(r)}{f}\right) \tag{5.13}$$

is a dimensionless integral. In defining $I_3(p)$, we extended the integration region to $-\infty < r < \infty$ by analytically continuing $R(r)$ as an even function to $r < 0$.

As in Chapter 4, it is advantageous in the weak binding limit (where $\Delta \ll 1$) to use the rescaled wavefunction $Y(x) = 2\sqrt{N}\,R(r)/f\,\Delta$ and coordinate $x = \Delta\, m\, r$. We also define a dimensionless momentum $k = p/m$ for the emitted particle. In that case, the integral I_3 can be expanded in powers of Δ,

$$\begin{aligned}I_3(p) &= \Delta^{-2}\int_{-\infty}^{\infty} dx\, x\, \sin\left(\frac{k\,x}{\Delta}\right)\, J_3\left[\Delta\, Y(x)\right] \\ &\approx \frac{\Delta}{48}\int_{-\infty}^{\infty} dx\, x\, \sin\left(\frac{k\,x}{\Delta}\right)\, Y(x)^3.\end{aligned} \tag{5.14}$$

For a known solution for the wavefunction $Y(x)$, if Δ is moderately large, then the integral I_3 can be done numerically by brute force. However, at fixed κ and $\Delta \ll 1$, the factor $\sin(k\,x/\Delta)$ undergoes fast oscillations, resulting in extensive cancellations in the integral. In this range of Δ, this makes direct numerical calculation of I_3 difficult.

The problem becomes significantly more tractable when we examine the singularity structure of the solutions to the equations of motion (4.12). Solutions $Y(x)$ of these equations are real analytic functions on $-\infty < x < \infty$, and as a result, they can be analytically continued into the complex plane of x. Consider first the region of parameter space where $\kappa \ll 1$; in that region, gravity effectively decouples from the KG equation, resulting in a single equation describing the axion wavefunction

$$Y''(x) = -\frac{2}{x}\,Y'(x) + Y(x) - \frac{1}{8}\,Y(x)^3. \tag{5.15}$$

An analysis of the singularity structure of $Y(x)$ satisfying eq. (5.15), and the resulting computation of I_3, is presented in Appendix C. The result is

$$I_3 = i\,\frac{32\,\pi\,y_I}{3\,\Delta}\exp\left(-\frac{\sqrt{8}\,y_I}{\Delta}\right). \tag{5.16}$$

The value $y_I \approx 0.603156$ is obtained by analyzing the Taylor series around $x = 0$ and the numerically integrated form of the wave function $Y(x)$.

Of course, as we pointed out in Chapter 4, solutions with $\kappa \ll 1$ lie on the unstable branch of axion star configurations. The more interesting physical region has $\kappa \gtrsim .25$. However, the expression derived for I_3 can be carried over approximately into this latter range, because the term which couples $Y(x)$ to the gravitational potential $b(x)$ contributes a subleading correction to the singularity. Neglecting this contribution allows us to use the expression of eq. (5.16) in the range $\kappa = \mathcal{O}(1)$ as well.

Integrating over the relevant phase space, the total transition rate per unit time is

$$\begin{aligned}\Gamma_3 &= \frac{1}{T}\int \frac{d^3p}{(2\,\pi)^3\,2\,\mu_p}|\mathcal{M}_3|^2 \\ &= \frac{f^2}{2}\int \frac{d^3p}{p^2\,\mu_p}\,\delta(3\,\mu_0 - \mu_p)\;|I_3(k)|^2\,,\end{aligned} \tag{5.17}$$

where in the square of $\mathcal{M}_3$ we used the identity $|\delta(3\,\mu_0 - \mu_p)|^2 = (T/2\pi)\,\delta(3\,\mu_0 - \mu_p)$, and where T is the duration of the transition. The dimensionless momentum $k = p\,/\,m$

of the ejected axion is

$$k_3 = \frac{\sqrt{9\,E^2 - m^2}}{m} \approx \sqrt{8}, \tag{5.18}$$

approximately constant in the weak binding $E \approx m$ limit. Then using the delta function and (5.18) to integrate over three-momentum in (5.17), we obtain

$$\Gamma_3 = \frac{2\,\pi\,f^2}{m\,k_3}\,[I_3(k_3)]^2. \tag{5.19}$$

There are several possible higher-order contributions to the decay rate: terms of the form (5.3) for which $n > 3$ condensed axions annihilate at once; terms with $\mu > 1$ emitted axions; or both. In the first case, where a single axion is emitted, there must be an odd number of condensed axions in the initial state $n = 2\,\ell + 1$. Then the decay rate of eq. (5.19) has a simple generalization

$$\Gamma_{2\,\ell+1} = \frac{2\,\pi\,f^2}{m\,k_{2\,n+1}}\,[I_{2\,\ell+1}(k_{2\,\ell+1})]^2, \tag{5.20}$$

where

$$I_j(k) = \frac{1}{\Delta^2}\int_{-\infty}^{\infty} dx\,x\,\sin\left(\frac{k_j\,x}{\Delta}\right)\,J_j[\Delta\,Y(x)] \tag{5.21}$$

and

$$k_{2\,\ell+1} = \sqrt{4\,\ell\,(\ell+1) - [(2\,\ell+1)\,\Delta]^2}. \tag{5.22}$$

In the $\Delta \ll 1$ limit, the expansion of the Bessel function $J_{2\ell+1}$ in eq. (5.21) has a leading term proportional to $\Delta^{2\ell+1}$. Clearly, terms higher-order in ℓ will be suppressed by extra factors of Δ^2 and can be safely neglected.

The only other leading-order, local corrections are the ones in which two or more free axions are emitted at a single vertex, $\nu > 1$. Detailed discussion of the transition rate generated by these processes are provided in Appendix A. The most significant difference, compared to the transition rate calculated above, is an additional factor of $(m^2\,/\,f^2)^{\nu-1}$, which for $\nu > 1$ renders the production rate of several free axions in a single process overwhelmingly small. For QCD axions, the factor $m^2\,/\,f^2 \sim 10^{-50}$, and it is similarly small in all conceivable physical theories. Therefore, we also disregard these processes for the purpose of calculating the lifetime of axion stars in what follows.

We should also point out alternative methods for calculating decay of bosonic condensates. The methods are sometimes characterized as either "classical" [155, 166]

or "quantum" [164,167]. The classical decay calculation, of which the presentation here is an example, finds the decay rate as a *global* property of the whole condensate; the result thus depends on the overall size of the condensate or the tail of the momentum distribution. The quantum decay calculation, on the other hand, depends only on local properties and can be performed essentially in the standard method of QFT, using Feynman diagrams and effective field theories.

The advantage of the classical method is that it is sensitive to transitions originating in off-shell axions in the initial state. On the other hand, there are some allowed Feynman diagrams, those containing internal lines, which do not appear in the classical framework, as in Figure 1 of [164]. Because the quantum method is not sensitive to off-shell annihilations, processes like (5.5) are only accessible in the classical method, so we are confident that the calculation performed here is robust. For the purposes of this work, we will ignore other decay modes.

Nonetheless, it should be noted that the status of higher order modes, like $4\,a_c \to 2\,a_p$, is less clear. In [167], and more recently in [164], the authors found that the sum of three relevant diagrams for this process in the quantum picture cancel exactly, when using the instanton potential for axions. The rate we calculate here, in Appendix A, is nonzero, but uses the classical method which is only sensitive to the contact interaction diagram. We leave further discussion of the relation between classical and quantum decay of axion condensates to future work, but acknowledge that the literature is somewhat confused at this moment in time.

5.2.1. Spherical Waves (Alternative Derivation)

In our original work on the decay of axion stars [155], we used the plane wave expansion of eq. (5.7). However, the spherical symmetry of the ground state system led to the projection of only a zero angular momentum outgoing state; this state has (approximately) fixed magnitude of momentum, but equal probability to go in any direction. This is identical to an isotropic *spherical wave*, with zero average momentum. This section follows our derivation in [156].

With this in mind, we could have started with a field expansion in spherical waves from the outset. That is, we could have used

$$\phi_s(t,r) = \frac{1}{2\,\pi^2}\sum_{\ell=0}^{\infty}\sum_{\ell_z=-\ell}^{\ell} Y_{\ell,\ell_z}(\hat{r})\int_0^{\infty}\frac{dp\,p}{2\,\mu_p}\,j_\ell(p\,r)\,e^{-i\,\mu_p\,t}a_{\ell,\ell_z}(p), \tag{5.23}$$

where $j_\ell(p\,r)$ is a spherical Bessel function, and we use the "hat"ˆto denote a unit vector $\hat{r} = \vec{r}/|\vec{r}|$. The spherical wave annihilation operators satisfy the commutation relation

$$\left[a_{\ell,\ell_z}(p), a^\dagger_{\ell',\ell'_z}(p')\right] = (2\pi)^3\, 2\,\mu_p\,\delta(p-p')\,\delta_{\ell,\ell'}\,\delta_{\ell_z,\ell'_z}. \tag{5.24}$$

Using this set of operators as a basis, the states labeled by p, ℓ, and ℓ_z are simply

$$|p\ell\ell_z\rangle = a^\dagger_{\ell,\ell_z}(p)\,|0\rangle. \tag{5.25}$$

This choice for the complete set of scattering states is completely equivalent to the set of plane waves in the previous section. Note that the annihilation operators in the two bases are related as

$$a_{\ell,\ell_z}(p) = i^\ell\, p \int d\Omega_p\, Y^*_{\ell,\ell_z}(\hat{p})\, a(\vec{p}), \tag{5.26}$$

which can also be inverted,

$$a(\vec{p}) = \frac{1}{p}\sum_{\ell=0}^{\infty}\sum_{\ell_z=-\ell}^{\ell} i^{-\ell}\, Y_{\ell,\ell_z}(\hat{p})\, a_{\ell,\ell_z}(p). \tag{5.27}$$

Then the states of eq. (5.7) and eq. (5.23) are *precisely equal*. One can be derived from the other by using the expansion of the exponential in spherical harmonics,

$$e^{i\,\vec{p}\cdot\vec{r}} = 4\pi \sum_{\ell=0}^{\infty}\sum_{\ell_z=-\ell}^{\ell} i^\ell\, j_\ell(p\,r)\, Y^*_{\ell,\ell_z}(\hat{p})\, Y_{\ell,\ell_z}(\hat{r}). \tag{5.28}$$

Evaluating $\phi_s(t,r)$ in eq. (5.7) using the annihilation operators defined in eq. (5.27), one obtains the expression in eq. (5.26).

Rather than the expression in eq. (5.11), the matrix element in this basis has the form

$$\begin{aligned}\mathcal{M}_3^{sph} &= -i\,m^2\,f \int dt\, d^3r\, J_3\left(\frac{2\sqrt{N}\,R(r)}{f}\right)\ \langle 0|\phi_s(t,r)|\vec{p}\rangle \\ &= -i\,m^2\,f \int dt\, d^3r\, J_3\left(\frac{2\sqrt{N}\,R(r)}{f}\right)\ \sqrt{4\pi}\, j_0(p\,r)\, e^{-i\,\mu_p\,t}\end{aligned} \tag{5.29}$$

Although this matrix element is different when using the spherical waves, the decay rate is calculated using a different integration over phase space, and the final answer is

the same as in eq. (5.17):

$$\begin{aligned}\Gamma_3 &= \frac{1}{T}\int \frac{1}{(2\pi)^3}\frac{dp}{2\,\mu_p}|\mathcal{M}_3^{sph}|^2 \\ &= \frac{f^2}{2}\int \frac{d^3p}{p^2\,\mu_p}\,\delta(3\,\mu_0-\mu_p)\;|I_3(k)|^2\,.\end{aligned} \tag{5.30}$$

This alternative derivation in terms of spherical waves gives a good intuitive idea of how the process (5.5) proceeds. The outgoing state, having zero angular momentum and (approximately) fixed momentum magnitude $p \approx \sqrt{8}\,m$, is emitted with equal probability in every direction from the axion star. This basis is also easily generalizable to the case of nonzero rotation, where a rotating axion star would be coupled to nonzero angular momentum modes $\ell, \ell_z \neq 0$. Based on the approximate calculation of [93], the expectation is that rotating axion stars can achieve larger masses than their static counterparts. A full analysis of rotating condensates is beyond the scope of this work; we hope to return to this topic in a future publication.

5.3. Constraints

Repeated occurrences of the process (5.5) can lead to a nonzero decay rate for an axion star, and thus a nontrivial lifetime. Suppose, for example, that axion stars are produced early in the universe (say, during minicluster collapse as described in Section 2.3); then a comparison of the axion star lifetime with the age of the universe $\tau_U = 13.82 \times 10^9$ years will tell us whether axion stars could exist in the present day. Taking this as our measure, we can set constraints on axion stars as a component of DM halos.

The average lifetime for an axion star to lose three axions through the process (5.5) is $\tau_3 = 1/\Gamma_3$. Then the total lifetime of a decaying axion star can be computed using

$$\frac{d\,\tau}{d\,N} \approx m\,\frac{d\,\tau}{d\,M} \approx -\frac{1}{\tau_3}, \tag{5.31}$$

that is, for an axion star of mass M,

$$\tau \approx \frac{1}{3\,m}\int_0^M \frac{d\,M'}{\Gamma_3} = \frac{k_3}{6\,\pi\,f^2}\int_0^M \frac{d\,M'}{|I_3|^2}. \tag{5.32}$$

Now, in the form of eq. (5.16), I_3 is a function of Δ and not of M. On the other hand, recall from Chapter 4 that on the relatively large-Δ branch of solutions (the left side of Figure 4.3), the mass and the parameter Δ were inversely related. Recasting eq. (4.32)

gives

$$M(\Delta) \approx y_M \frac{f^2}{m\,\Delta}, \tag{5.33}$$

with $y_M \approx 50.13$, so that the expression of eq. (5.32) is an exponential in M. We shall discover shortly that the transition from stable to unstable axion stars occurs on this more strongly bound branch.

Finally, note that on this same branch of solutions, a decaying axion star losing its mass through decay will have a continually increasing value of Δ. Since the integrand $1/|I_3|^2$ is a very rapidly increasing function of M, the lifetime is dominated by the contributions near the upper bound of the integral; the decay rate increases as the axion star loses mass. Thus we can cut this integral off at an arbitrary lower limit. Performing the integration, we arrive at the final result

$$\tau(M) \approx \frac{3\,{y_M}^3\,f^4}{4096\,\pi\,y_I^3\,m^3\,M^2} \exp\left(\frac{4\sqrt{2}\,y_I\,m\,M}{f^2\,y_M}\right). \tag{5.34}$$

Using eq. (5.33), this is equivalent to

$$\tau(\Delta) \approx \frac{3\,y_M\,\Delta^2}{4096\,\pi\,{y_I}^3\,m} \exp\left(\frac{4\sqrt{2}\,y_I}{\Delta}\right). \tag{5.35}$$

We find that almost irrespective of the value of m, the transition from stable to unstable axion stars occurs near $\Delta \sim .04 - .06$. As anticipated by our use of eq. (5.33), the transition to decay instability occurs on the branch of solutions with very small κ, where the mass-radius relation was $M \propto R$. In our original work, we focused on the regime of QCD axions, and set limits on the masses of axion stars by requiring $\tau(\Delta) > \tau_U$, to see which states could survive from the early universe until today. The result of this analysis is presented in Figure 5.2: the upper bound (red line) is the maximum mass derived in Chapter 4, whereas the lower bound (green line) is the minimum mass for the condensate to be stable against decay.

Note that once one fixes the product $m\,f$, the maximal mass scales with m^{-2}, while the minimal mass scales approximately with m^{-3}. This is easy to see in (5.33): the maximum mass is a curve of constant $\kappa \simeq .34$, while the minimum is a curve of (approximately) constant $\Delta \simeq .04 - .06$.

However, the transition to decay instability occurs on the branch of solutions which were *already gravitationally unstable*; we analyzed these solutions in detail in Chapter 4. This is of interest for several reasons. First, this implies that the gravitationally stable

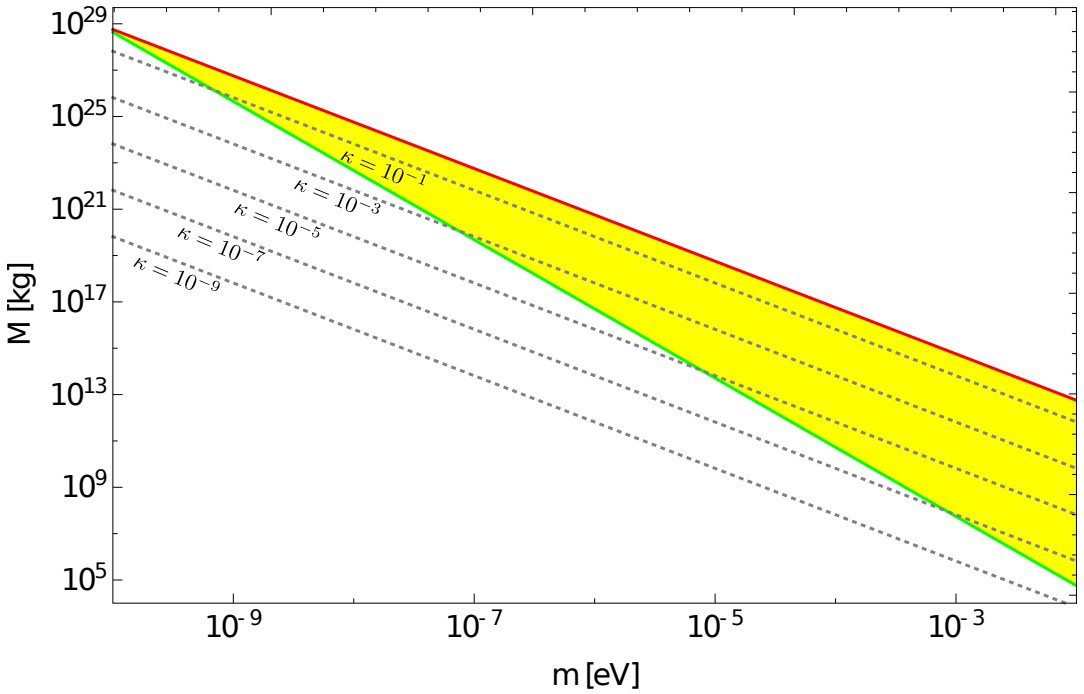

Figure 5.2.: Upper (maximum mass derived in Chapter 4, red line) and lower (stability against axion emission, green line) bounds for the masses of axion stars on the $M \propto R$ branch of axion stars, as functions of the axion mass in QCD. The dotted lines correspond to different values of the κ, which parametrizes the effective coupling to gravity. Figure reproduced and updated from [155].

solutions on the large-κ, very small-Δ branch are all *stable against decay* with very long lifetimes. This is important if axion stars are to be long-lived enough to contribute to DM.

Second, we can extend this analysis to ALPs which are not described by QCD-like parameters. In particular, there has recently been a great amount of interest in ALPs with very tiny masses $m \sim 10^{-22}$, as theories of this type can give rise to condensates of galactic scale. Typically, these theories also require very large decay constants f as well. In the context of DM, these theories are known by the name "Fuzzy Dark Matter" (FDM) [112], and have been written about extensively [109–117]. Axion condensates in these models correspond to solitonic cores of DM halos, surrounded by a virialized distribution of free axions contained within a de Broglie wavelength.

Applying the formulas of Chapter 4, we can calculate the masses of axion condensates in FDM models as we did for QCD axions; these curves, as functions of Δ, are given in Figure 5.3, for different choices of the decay constant f. Recall that states on the large-Δ branch are not gravitationally stable, as they correspond to maxima of the total energy. For the FDM mass $m = 10^{-22}$ eV, the transition to decay instability occurs

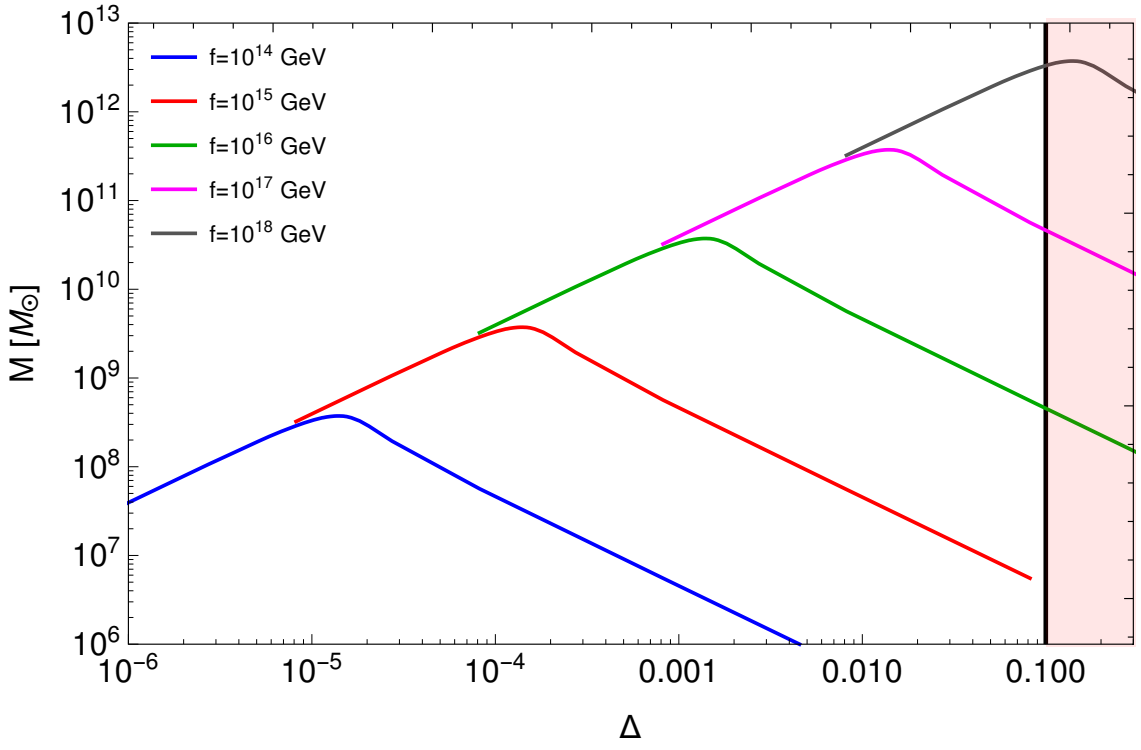

Figure 5.3.: The allowed masses for condensates of axion particles in FDM, as a function of the parameter Δ; these condensates constitute the cores of FDM halos. Axion condensates in the shaded region are unstable to decay to relativistic axions with a very short lifetime. Here we have used the model parameters $m = 10^{-22}$ eV, and f in the range between 10^{14} and 10^{18} GeV; increasing the particle mass m merely shifts these curves down proportionally to $1/m$.

at $\Delta \approx .1$, represented by the red shaded region.[4] As in our QCD calculation, for most values of f, this transition occurs on the gravitationally unstable branch. However, at $f \sim 10^{18}$ GeV, the transition occurs instead on the stable, smaller-Δ branch. This provides constraints on models with decay constants f in this range.

There is a third reason that this decay calculation is interesting. Observe once more that τ is a one-to-one function of Δ in the relevant parameter space. This means that, to the extent that we can calculate Δ, we can determine the decay rate, even in extreme scenarios in which equilibrium solutions of the EKG equations are not accessible. In particular, we will use this fact to determine the properties of collapsing axion stars in Chapter 6.

[4] This is, of course, very close to the edge of the method's consistency, as we have assumed $\Delta \ll 1$. The corrections to the decay rate appearing at next-to-leading order in Δ will begin to be relevant close to this transition.

5.4. Summary

We have examined the decay of axion stars through number-changing transitions. Because axions are real scalars, and because condensed axions are not in momentum eigenstates, these number-changing transitions can occur without violating any discrete or continuous symmetry. We have explained in detail, for example, how the decay process of eq. (5.3) conserves energy and (average) momentum.

The leading-order transition taking place in an axion star is of the form (5.5). We have shown that transitions with $n > 3$ condensed axions annihilating in a single interaction have matrix elements suppressed by higher powers of $\Delta \ll 1$, and that emission of $\nu > 1$ axions in the final state leads to suppression by higher powers of $m^2/f^2 \ll 1$. For our purposes, it is safe to neglect these contributions.

The decay rate for (5.5) is a one-to-one function of Δ. We found that axion stars with $\Delta \gtrsim .04 - .06$ have lifetimes shorter than the age of the universe, and so could not survive from the early universe to the present day. For QCD axion parameters, this transition occurs on the branch of states which are gravitationally unstable, indicating that gravitationally stable axion stars also have long lifetimes in terms of decay. For ultralight axions, the bounds from stability against decay can be competitive with those from gravitational stability, as we observe in Figure 5.3.

We should also point out that that if a substantial fraction of dark matter is composed of weakly bound axion stars, then the ratio of dark matter to luminous matter becomes a function of time. This is due to the fact that axions emitted from axion stars are highly relativistic, and they escape from galaxies and from galaxy clusters. Thus, by comparing the rotation curves of galaxies of different ages one should be able to put an upper limit on the contribution of weakly bound axion stars to dark matter.

In the next chapter, we will consider the final state of gravitationally unstable axion stars, those with $M > M_c$, which will turn out to depend on the decay rates we have calculated here as well.

Chapter 6.

Collapse of Axion Stars

"Modern science says: 'The sun is the past, the earth is the present, the moon is the future.' From an incandescent mass we have originated, and into a frozen mass we shall turn. Merciless is the law of nature, and rapidly and irresistibly we are drawn to our doom."

— Nikola Tesla

In Chapter 4, we calculated the masses for weakly bound axion stars, and found a maximum allowed for gravitational stability. Axion stars exceeding this bound are unstable to collapse, as are states with smaller radii than those at the maximum. In this chapter, we analyze the collapse process and determine the final state of the collapsing star. This chapter is primarily based on our work in [168] and [169].

6.1. Setup

As we have seen starting in Chapter 3, the mass spectrum of stable boson star states depends crucially on its self-interaction potential. Recall, for example, the instanton self-interaction potential for axions, eq. (2.18); its $1-\cos(\mathcal{A}/f)$ form gives rise to an infinite sum of coupling terms, with increasing powers of the axion field $\mathcal{A}$. For weakly bound axion stars, we argued in Chapter 4 that only the leading self-interaction is relevant; higher-order terms are suppressed by $\mathcal{A}/f \ll 1$ when the field density is small (or equivalently, by higher powers of the (small) binding energy parameter Δ, defined in eq. (4.10)).

However, we have now also seen in Chapter 5 that increasing axion star densities lead to increasingly large binding energies. When Δ becomes not so small, higher-order terms in the expansion of the potential will become relevant. Now in this regime, to

use the full RB method as we did in Chapter 4, we would need to solve numerically the EKG system of equations anew every time an additional self-interaction term became relevant. A generic analysis of the spectrum of states, in particular in the limit of using the full series of self-interaction terms, would be extraordinarily difficult.

Due to the complexity of the problem, it is advantageous to make use of the analytic power of the *variational method*, outlined in Section 3.5.3. Recall that this method requires working in the nonrelativistic regime, using a substitution of the axion field $\mathcal{A}$ with a low-energy wavefunction ψ, defined by eq. (3.18). The extrema of the total energy will correspond to stable or metastable states, which are axion stars. This procedure sacrifices the numerical precision of the RB method, but the advantage is that we retain strong analytical control throughout all stages of the calculation. As we have argued previously, the variational method gives good order of magnitude estimates of the relevant physical quantities, which will be sufficient for our purposes.

We follow precisely the procedure for taking the nonrelativistic limit outlined in Section 3.5 for the substitution of $\mathcal{A}$ for ψ. One difference to note is that in this case, the axion self-interaction potential $V(\mathcal{A})$ contains terms higher-order in the wavefunction than ψ^4. In particular, we will take $V(\mathcal{A})$ to be either the instanton potential of eq. (2.18), or the chiral potential of eq. (2.15). We will begin in a generic way, and specialize to one of these specific cases only later.

The dynamical Lagrangian for the axion field has the form

$$\mathcal{L} = \frac{1}{2}\left(\partial_\mu \mathcal{A}\right)^2 - V(\mathcal{A}). \tag{6.1}$$

As we observed in Chapter 3, in the nonrelativistic limit, the mass term in the Lagrangian (proportional to $\mathcal{A}^2$) is canceled by one of the two-derivative terms. We will absorb this mass term into an effective low-energy potential for the wavefunction ψ,

$$W(\psi) = V(\mathcal{A}) - \frac{m^2}{2}\mathcal{A}^2. \tag{6.2}$$

The total energy in the nonrelativistic limit is

$$E[\psi] = \int d^3r \left[\frac{|\nabla\psi|^2}{2m} + \frac{1}{2}V_{grav}\,|\psi|^2 + W(\psi)\right]. \tag{6.3}$$

If we were to take $W(\psi) = \lambda\,|\psi|^4/16\,m^2$, then this expression is identical to eq. (3.33) we derived in Section 3.5.2.

The variational method requires some ansatz for the wavefunction ψ in order to evaluate the integral in eq. (6.3). However, a significant amount of progress can be

made under very general assumptions. Using the basic scaling relations of eq. (4.29) (appropriate for dilute axion stars), we begin by defining a dimensionless radius ρ and particle number n by

$$R = \frac{1}{m}\frac{\rho}{\sqrt{\delta}} \qquad N = \frac{f^2}{m^2}\frac{n}{\sqrt{\delta}}, \tag{6.4}$$

where $\delta = 8\,\pi\,f^2/M_p^2$ was defined in eq. (4.7). We will take

$$\psi(r) = \sqrt{m}\,f\,\zeta\,F\left(\frac{r}{R}\right) \equiv \sqrt{m}\,f\,\zeta\,F\left(\xi\right) \tag{6.5}$$

for our ansatz, with $\xi \equiv r/R$; without loss of generality, we can choose $F(0) = 1$. The dimensionless constant ζ is fixed by the normalization requirement that $\int \psi^*\psi\, d^3r = N$, which implies

$$\zeta \equiv \sqrt{\frac{\delta\, n}{C_2\,\rho^3}}. \tag{6.6}$$

We will further require that the function $F(\xi) \to 0$ as $\xi \to \infty$, and that it is a monotonically decreasing function.[1] Using this generalized ansatz, we can evaluate the energy $E(\rho)$ of eq. (6.3), and define a rescaled energy per particle $e(\rho)$ as

$$e(\rho) \equiv \frac{E(\rho)}{m\,N\,\delta} = \frac{D_2}{2\,C_2}\frac{1}{\rho^2} - \frac{B_4}{2\,C_2{}^2}\frac{n}{\rho} - \frac{n}{\rho^3}\,v(\rho), \tag{6.7}$$

where

$$v(\rho) = 4\,\pi\,\frac{\rho^6}{n^2\,\delta^2}\int d\xi\,\xi^2\,\frac{W(\psi)}{m^2\,f^2} \tag{6.8}$$

is a rescaled parameter defining the self-interactions, and where we defined the functions

$$B_4 = (4\,\pi)^2\int d\xi\,\xi\,F(\xi)^2\int_0^\xi d\eta\,\eta^2\,F(\eta)^2 \tag{6.9}$$

$$C_k = 4\,\pi\int d\xi\,\xi^2\,F(\xi)^k \tag{6.10}$$

$$D_2 = 4\,\pi\int d\xi\,\xi^2\,F'(\xi)^2. \tag{6.11}$$

For a given ansatz, the functions B_4, C_k, and D_2 are numerical constants.

[1] This latter requirement could be relaxed. A rotating axion star, for example, would have a node at $\xi = 0$ and thus its wavefunction has an extremum.

The coefficient functions of eq. (6.9–6.11) could be easily generalized to account for corrections from special or general relativity. Corrections to the kinetic energy, which would emerge from special relativity, are proportional to higher powers of the momentum p, giving coefficients analogous to D_2, but with higher powers of the derivative $F'(\xi)$. Similarly, general relativistic corrections would appear as higher order contributions analogous to B_4. We have estimated the leading corrections to these terms and they are negligible in the range of parameters we consider here.

Specializing now to the case of the instanton potential, we can derive an explicit form for the self-interaction parameter $v(\rho)$ in eq. (6.8); this was the case considered in our original work on the topic [168]. The chiral potential [169], which is somewhat more complicated, will be treated separately in Section 6.5.

To evaluate eq. (6.2), note that the expansion in the axion field contains only even powers of $\mathcal{A}$. The nth term is proportional to the factor

$$\mathcal{A}^{2n} = \frac{{}^{2n}C_n}{(2m)^n}(\psi^*\,\psi)^n + \mathcal{O}(e^{\pm i\,m\,t}), \tag{6.12}$$

where ${}^{2n}C_n$ are binomial coefficients.[2] Dropping the rapidly oscillating pieces, we obtain

$$\begin{aligned} W(\psi) &= m^2\,f^2\left[1-\cos\left(\frac{\mathcal{A}}{f}\right)\right] - \frac{m^2}{2}\,\mathcal{A}^2 \\ &\to m^2\,f^2\left[1-\sum_{n=0}^{\infty}\frac{{}^{2n}C_n\,(-1)^n}{(2n)!}\left(\frac{\psi^*\,\psi}{2mf^2}\right)^n\right] - \frac{m}{2}\,\psi^*\,\psi \\ &= m^2\,f^2\left[1-\frac{\psi^*\,\psi}{2mf^2}-\sum_{n=0}^{\infty}\frac{(-1)^n}{(n!)^2}\left(\frac{\psi^*\,\psi}{2mf^2}\right)^n\right] \\ &= m^2\,f^2\left[1-\frac{\psi^*\,\psi}{2mf^2}-J_0\left(\sqrt{\frac{2\psi^*\,\psi}{mf^2}}\right)\right] \end{aligned} \tag{6.13}$$

where $J_0(x)$ is a Bessel function of the first kind.[3] Inserting the generic ansatz of eq. (6.5) for ψ, this implies that the rescaled self-interaction parameter v for the instanton potential has the form

$$\begin{aligned} v_I(\rho) &= 4\,\pi\,\frac{\rho^6}{n^2\,\delta^2}\int d\xi\,\xi^2\left[1-\frac{\zeta^2}{2}F(\xi)^2 - J_0\left(\sqrt{2}\,\zeta\,F(\xi)\right)\right] \\ &= \sum_{k=0}^{\infty}\left(-\frac{1}{2\,C_2}\right)^{k+2}\frac{C_{2\,k+4}}{[(k+2)!]^2}\left(\frac{n\,\delta}{\rho^3}\right)^k. \end{aligned} \tag{6.14}$$

[2] Not to be confused with C_k, the integrals defined in eq. (6.10).

[3] The J_0 dependence of the axion self-interaction potential was pointed out in [151] and later in [154,170]

In this form, it is clear that interactions higher-order in ψ give rise to terms in the variational energy which are proportional to higher powers of $n\,\delta/\rho^3$. We can define a truncated energy by only evaluating the sum up to some maximum $k_{max} = K$:

$$e_K(\rho) = \frac{D_2}{2\,C_2}\frac{1}{\rho^2} - \frac{B_4}{2\,C_2{}^2}\frac{n}{\rho} - \frac{n}{\rho^3}\sum_{k=0}^{K}\left(-\frac{1}{2\,C_2}\right)^{k+2}\frac{C_{2\,k+4}}{[(k+2)!]^2}\left(\frac{n\,\delta}{\rho^3}\right)^k. \tag{6.15}$$

Clearly, then, $\lim_{K\to\infty} e_K(\rho) = e(\rho)$ recovers the expression in eq. (6.7).

6.2. Spectrum of Axion Star States

What is typically done is to truncate the expansion of the energy of eq. (6.15) at $K = 0$, leaving only the leading attractive self-interaction of axions. This is equivalent to leading order of δ, which is $\delta = \mathcal{O}(10^{-14}) \ll 1$ in QCD (for $f = 6\times10^{11}$ GeV and $m = 10^{-5}$ eV) [80]; in that case, the self-interaction term in eq. (6.14) reduces to

$$v_I(\rho)\Big|_{\delta=0} = \frac{C_4}{16\,C_2{}^2}. \tag{6.16}$$

As we will explain below, truncating at this order implies that the potential appears unbounded from below as the axion star size decreases, $R \to 0$.

Even so, there can exist local energy minima, corresponding to metastable states which are dilute and weakly bound. These dilute states are well described by the leading order energy $e_0(\rho)$, and have been studied in great detail previously [126, 137, 145, 151]. The extrema of $e_0(\rho)$ with respect to ρ determine the radii of metastable minima and maxima of the binding energy; these occur at the rescaled radii

$$\rho_\pm = \frac{C_2\,D_2}{B_4\,n}\left[1 \pm \sqrt{1 - \frac{3}{8}\frac{B_4\,C_4}{C_2{}^2\,D_2{}^2}n^2}\right]. \tag{6.17}$$

This is a generalization of the analysis of the attractive interactions case we considered in Section 3.5.3 to an arbitrary ansatz. As we explained there, the larger radius extremum ρ_+ is a local minimum of the energy, whereas the smaller radius one ρ_- is an energy maximum. We can also see that there exists a critical rescaled particle number

$$n_c = \sqrt{\frac{8}{3}}\frac{C_2\,D_2}{\sqrt{B_4\,C_4}}. \tag{6.18}$$

For $n < n_c$, there exists a metastable minimum of the energy. An axion star state with a radius ρ_+ is what we will call a *dilute axion star*, and we will see shortly that they

correspond to rescaled radii which are $\rho = \mathcal{O}(1)$. These are the states on the stable branch of solutions in Chapter 4, using the semiclassical RB method. The unstable branch of solutions correspond to states with radii ρ_-, which are energy maxima.

If a stable, dilute axion star accretes too much mass $M > m\,N_c$, or suffers a large radial perturbation, it will become unstable, and begin to collapse. In the absence of any additional self-interaction terms, the final state will be a black hole, as no stable state exists between the dilute radius R_+ and the Schwarzschild radius R_S. A full description of this process can be found in [171], who used a Gaussian ansatz for the wavefunction and calculated the time for collapse to a black hole, which was on the order of an hour.

However, as ρ decreases, the truncation of the self-interaction becomes inappropriate. The next to leading order self-interaction term is of $\mathcal{O}(n\,\delta/\rho^3)$, and is *repulsive*; the next term after that is attractive; and so on (observe the alternating sign in the expansion of eq. (6.14)). At very small radii, where many such terms contribute, it is unclear a priori whether the net result can be a repulsive self-interaction with sufficient strength to stabilize the collapsing star. With this in mind, we will examine the energy functional, including higher-order interactions, and determine whether the endpoint of collapse can lie at a radius greater than the Schwarzschild radius of the axion star. Such a result would be evidence that axion stars stabilize before they collapse to black holes.

In order to make the calculation a bit more concrete concrete, we now further specialize to the case of a specific ansatz. Following [126, 168, 171], we use a Gaussian function of the form

$$\psi(r) = \frac{\sqrt{N}}{\pi^{3/4}\sigma^{3/2}} e^{-r^2/2\sigma^2}, \tag{6.19}$$

which corresponds to eq. (6.5) with $F(\xi) = e^{-\xi^2/2}$. The coefficient functions of eq. (6.9–6.11) evaluate to

$$B_4 = \sqrt{2\pi^5}, \qquad C_k = 2\sqrt{\frac{2\pi^3}{k^3}}, \qquad D_2 = \frac{3\pi^{3/2}}{2}, \tag{6.20}$$

giving a truncated energy of

$$e_K(\rho) = \frac{3}{4}\frac{1}{\rho^2} - \frac{1}{\sqrt{2\pi}}\frac{n}{\rho} - \frac{1}{2\,\delta}\sum_{k=0}^{K} \frac{(-1)^k}{[(k+2)!]^2\,(k+2)^{3/2}} \left(\frac{n\,\delta}{2\pi^{3/2}\rho^3}\right)^{k+1}, \tag{6.21}$$

in the case of the Gaussian ansatz.

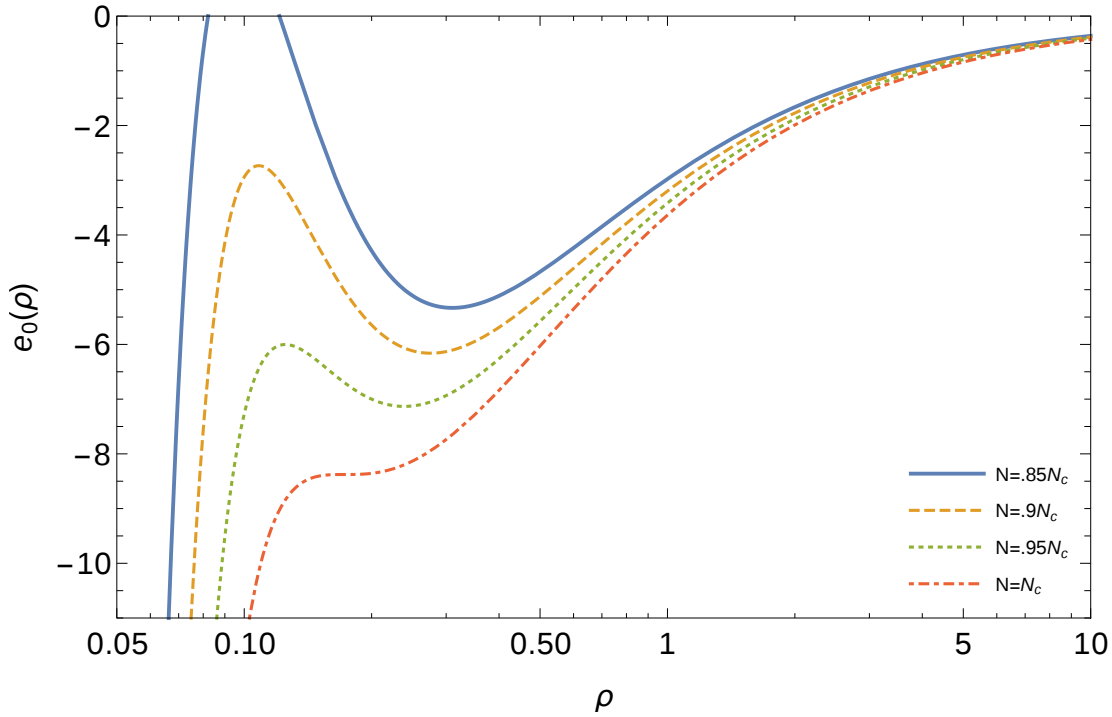

Figure 6.1.: The truncated energy $e_0(\rho)$ near the position of the dilute minimum ρ_+ for different choices of particle number: $N = .85N_c$, $N = .9N_c$, $N = .95N_c$, and $N = N_c$. Note that the local minimum at ρ_+, represented in the plot, disappears at $N = N_c$. Including additional terms in $e_K(\rho)$ for $K > 0$ makes a negligible difference in this range of ρ. Figure reproduced from [168].

Dilute axion stars, which are well-described by the leading order expansion $e_0(\rho)$, have energy extrema at

$$\rho_\pm = \sqrt{\frac{3}{32\pi}}\frac{n_c}{n}\left[1 \pm \sqrt{1 - \frac{n^2}{{n_c}^2}}\right]. \tag{6.22}$$

These energy extrema are real-valued only up to a critical particle number $n_c \approx 2\pi\sqrt{3}$. We illustrate the energy functional for a dilute axion star in Figure 6.1. One striking feature in this figure is that ρ_+ and ρ_- merge to a point at $N = N_c$. It is also worth noting that that the energy maximum, occurring at ρ_-, has higher total energy than the minimum at ρ_+; thus the former state, being unstable, could relax to the latter (given some mechanism for the dissipation of energy), or collapse towards $\rho \to 0$, depending on its initial perturbations. At sufficiently small values of N, in fact, this energy maximum shifts above the horizontal axis; this corresponds to a state with positive energy which is unstable to sending its constituent axion particles to infinity.

Converting to physical units using eq. (6.4), we find that the maximum mass of a dilute axion star is approximately $M_c = f^2\, n_c / m\sqrt{\delta} \sim 10^{18}$ kg, within an order of magnitude of the exact numerical result reported in Section 4.4. The state with this

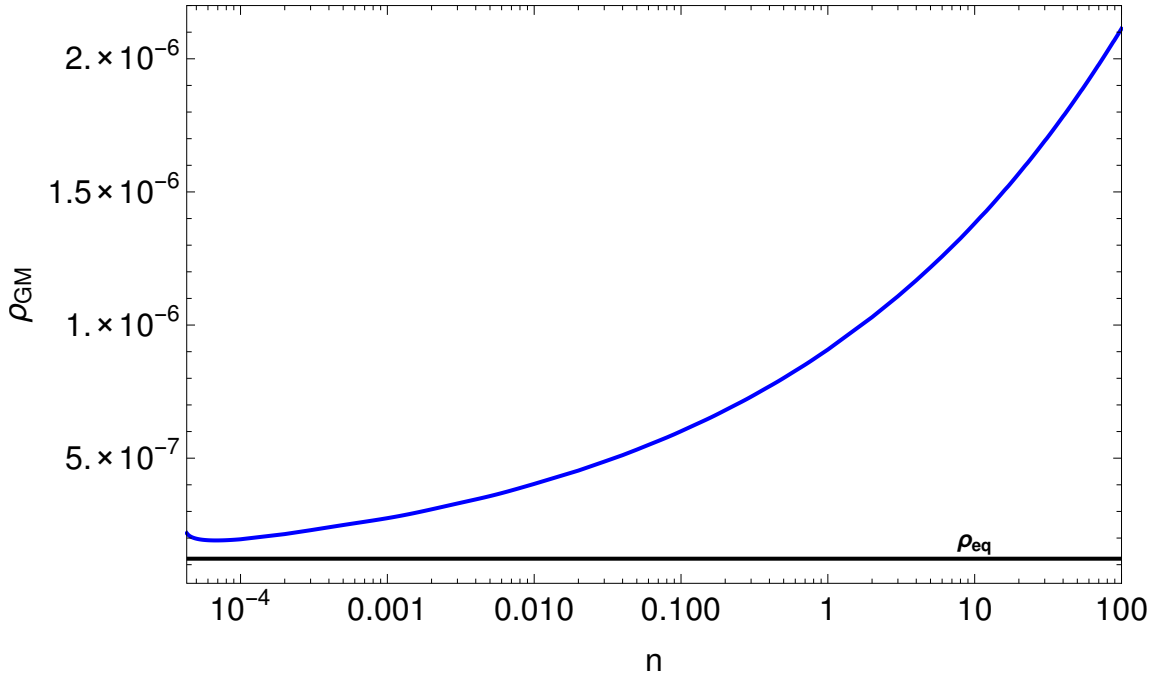

Figure 6.2.: The position ρ_{GM} of the global minimum of the rescaled energy in eq. (6.7), as a function of the reduced particle number n. The global minimum always lies at a radius $\rho_{GM} > \rho_{eq}$, the position at which the kinetic energy $\sim 1/\rho^2$ becomes dominant, which is depicted by the horizontal black line. Figure reproduced from [168].

maximum mass would have a radius $R_{99} \approx 500$ km, also in good agreement with previous estimates. We take this to be further evidence of the efficacy of this method. At masses $M > M_c$, the dilute $\rho = \mathcal{O}(1)$ extrema disappear.

At smaller values of ρ, higher-order self-interactions become relevant. We show in Appendix D, using the full integral form of the self-interaction (the top line of eq. (6.14)), that in the limit $\rho \to 0$ the self-interaction energy *is bounded*. More to the point, this implies that the total energy is *bounded from below*, and always has a global minimum occurring at a small radius $\rho \ll 1$. States which exist at this global minimum, having very small radii, are called "dense axion stars" [154]. If stable, these dense states can give rise to novel astrophysical detection signatures [172].

Because the full axion star energy is bounded from below, there exists a global minimum of the energy at a radius ρ_{GM}. We calculated numerically the position of this global energy minimum, using the integral representation of the self-interaction term in eq. (6.14); the result is represented by the blue line in Figure 6.2. The physical radii of dense axion stars with $N \sim N_c$ is of order $R_{GM} = \rho_{GM}/m\sqrt{\delta} \sim few$ meters.

The existence of these dense axion star states cannot be determined when using the leading truncation of the energy $e_0(\rho)$. In fact, truncation of the energy in eq. (6.21) at

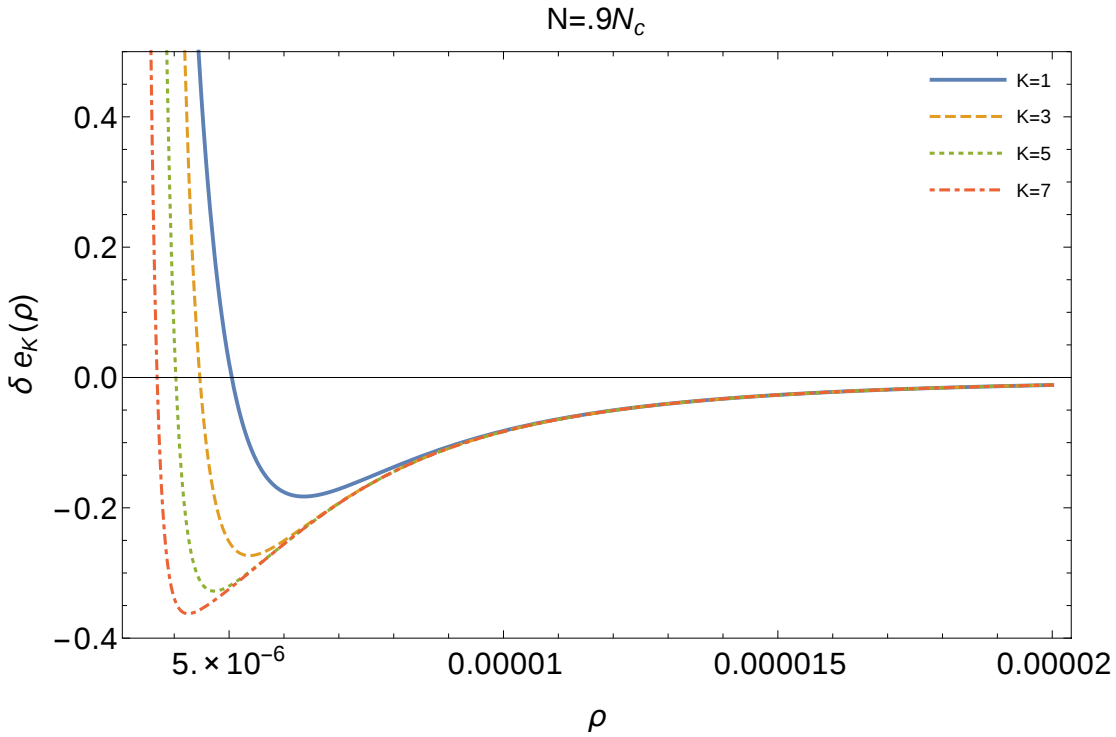

Figure 6.3.: The energy $e_K(\rho)$ multiplied by the small parameter δ for $N = .9\, N_c$ at increasing odd orders in K: $K = 1$, $K = 3$, $K = 5$, and $K = 7$. The existence of a dense global energy minimum is preserved at each order, but shifts to smaller radii as K increases. The repulsive kinetic term $\sim 1/\rho^2$ dominates the total energy at $\rho = \rho_{eq} \sim 10^{-7}$. Figure reproduced from [168].

any even order $K = 0, 2, 4, ...$ leads similarly to an unbounded functional and no global minimum. We thus emphasize that when considering dense states, it is important to truncate on a repulsive term in the energy expansion, $K = 1, 3, 5, ...$ The simplest case is

$$e_1(\rho) = \frac{3}{4}\frac{1}{\rho^2} - \frac{1}{\sqrt{2\pi}}\frac{n}{\rho} - \frac{1}{32\pi\sqrt{2\pi}}\frac{n}{\rho^3} + \frac{\delta}{864\pi^3\sqrt{3}}\frac{n^2}{\rho^6}. \tag{6.23}$$

In this case, the energy *is* bounded from below and has a minimum at a very small radius $\rho = \rho_D$. At these small values of ρ, the energy is well approximated by the self-interaction terms only (gravity and kinetic energy are negligible), and we find the analytic expression

$$\rho_D \approx \sqrt{\frac{2}{\pi}}\left(\frac{n\,\delta}{3^{7/2}}\right)^{1/3} \tag{6.24}$$

is a good approximation for the position of the global minimum. At $n = n_c$, $\rho_D \approx 7 \times 10^{-6}$, corresponding to $R_{99} \sim 7$ meters. Comparing with the global minimum of the full energy in Figure 6.2, we find a difference of only about a factor of $3 - 4$ near this value of $n \sim n_c$, a reasonable order of magnitude agreement. This justifies our

truncation of the energy at the leading repulsive term, i.e. $e_1(\rho)$, in this analysis. The difference between ρ_D and ρ_{GM} does become large if n increases far above n_c.

In Figure 6.3, we illustrate the effect of truncating at increasingly higher orders in the self-interaction potential. Each curve shows the energy truncated on an odd value of K (that is, a repulsive term in the potential), because it is only these truncated energies that possess a global minimum and can approximate the true energy minimum at ρ_{GM}, shown in Figure 6.2. We observe that, as subsequent higher orders in odd K, the shift in the energy minimum becomes smaller, and in the limit $K \to \infty$, the minima of $e_K(\rho)$ converge to the true minimum ρ_{GM}. For the particular value of $N = .9\, N_c$ illustrated, the series converges to $\rho_{GM} \approx 7 \times 10^{-7}$.

For the Gaussian ansatz, we have shown further [168] that the self-interaction energy approaches a finite constant in the limit $\rho \to 0$, implying that the kinetic energy (proportional to $1/\rho^2$) dominates in this limit; the gravitational interaction (proportional to $1/\rho$) gives a subleading contribution. This allowed us to estimate the radius at which the self-interaction and kinetic energy terms in eq. (6.7) were of roughly equal magnitude, which occurs when

$$\frac{3}{4}\frac{\delta}{\rho^2} \sim \frac{1}{2}. \tag{6.25}$$

Numerically, using QCD axion parameters, this occurs at $\rho_{eq} \sim 10^{-7}$, or a radius of $R_{eq} \sim 5$ cm. This value ρ_{eq} is represented by the solid black line in Figure 6.2. Note that the position of the global minimum is always at $\rho_{GM} > \rho_{eq}$.

Note also that the value $R_{eq} \sim 5$ cm is of the same order as the axion reduced Compton wavelength, $\lambda_c \sim 1/m \sim 2$ cm. It should be noted that on length scales of $\mathcal{O}(\lambda_c)$, neglecting higher powers of $e^{\pm i m t}$ in the expansion of eq. (3.18) would fail, as special relativistic corrections to the kinetic energy could be large. Of course, weakly bound stars have radii much larger than this, and as we describe below, even collapsing stars are well described by the nonrelativistic approximation until the last moments of collapse. The leading correction to the kinetic energy, which is proportional to p^4, has an expectation value which is down by a factor of $\delta/\rho^2 \ll 1$ compared to the leading-order term. We will thus postpone any further consideration of these relativistic corrections to the energy, which will be addressed in a future publication.

We observed in Figure 6.2 that the global minimum of the energy always occurs at a radius larger than ρ_{eq}, where the kinetic energy becomes dominant. Further, consider that the Schwarzschild radius $R_S = 2\,M/{M_P}^2$ is, after the usual rescaling of eq. (6.4),

$$\rho_S = 2\,n\,\delta. \tag{6.26}$$

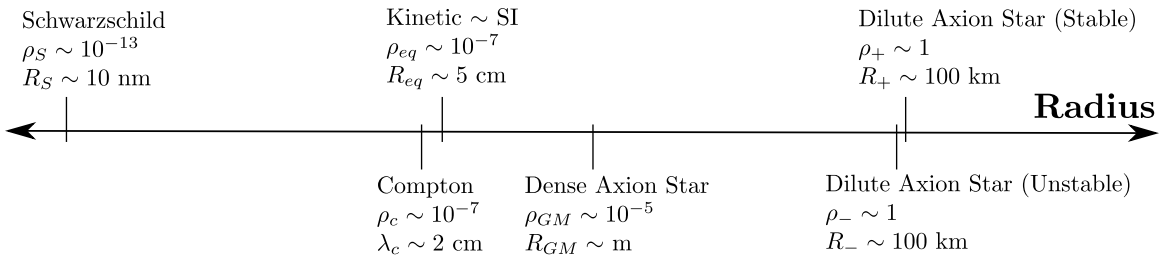

Figure 6.4.: The relevant distance scales in the analysis of axion stars, in terms of the dimensionless radius ρ and the dimensionful one R. From left to right, the scales are: the Schwarzschild radius of an axion star; the Compton wavelength of a single axion; the radius at which the kinetic energy of an axion star is approximately equal to its self-interaction energy; the radius of a dense axion star; and the radius of a dilute axion star (both the unstable and stable radius). To set the numerical scale, we fix the parameter choices $m = 10^{-5}$ eV and $f = 6 \times 10^{11}$ GeV (appropriate for QCD), and consider bound states with $N \sim N_c$.

For QCD parameters, $\rho_S \sim 10^{-13} \ll \rho_{GM}$ as well. This means that the global minimum of the axion star energy always occurs at a radius much larger than the corresponding Schwarzschild radius, implying that QCD axion stars *cannot form black holes*; they are stabilized in a dense state with radius $\rho_{GM} \gg \rho_S$. Note that this conclusion can be modified somewhat in more exotic axion theories with large decay constants f, as with those considered in [173].

There are thus a number of relevant distance scales to consider when analyzing axion stars, which span many orders of magnitude. We represent this spectrum pictorially in Figure 6.4. Most importantly, we note that $\rho_S \ll \rho_{GM}$ (a dense axion star is much larger than a black hole), and that $\rho_{GM} \ll \rho_+$ (a dilute axion star is much larger than a dense one).

In [168], we also analyzed explicitly the results for an ansatz of the form

$$\psi(r) = \sqrt{\frac{4\,\pi\,N}{(2\pi^2 - 15)R^3}} \cos^2\left(\frac{\pi\,r}{2\,R}\right) \qquad (r < R). \tag{6.27}$$

The results are qualitatively similar to those of the Gaussian ansatz, with $\mathcal{O}(1)$ changes to numerical quantities. For some analyses, this ansatz is somewhat more attractive than the Gaussian one in eq. (6.19), because it has compact support on a finite radius R. This choice of ansatz will be used in Chapter 7 when we analyze axion star collisions in an astrophysical setting.

6.3. Collapse Process

As we have pointed out, dilute axion stars are only gravitationally stable up to some maximum mass M_c; if a stable state continues to accrete mass, it will begin to collapse. However, we can now conclude that the endpoint of this collapse will not be a black hole state; the dense radius ρ_{GM}, which is a global minimum of the energy, is always much larger than the corresponding Schwarzschild radius. Thus, collapsing dilute axion stars are stabilized at a radius ρ_{GM}, and could form dense axion stars. We analyze this collapse classically in this section, and consider the effect of axion star decay in the next.

The collapse of dark matter halos consisting of condensed scalar particles was examined by [174], using a time-dependent formalism that originated in [20], and was utilized more recently by [126, 175]. The application of this method to an axion star, at leading-order in the self-interaction potential, was recently performed by [171]; it was in this latter work that it was shown that collapsing boson stars with attractive self-interactions form black holes. In [168], we used a similar analysis, taking into account higher-order terms in the self-interaction potential.

Classical collapse is described by the dynamical equation

$$E_{tot} = \alpha \frac{M}{2} \dot{R}(t)^2 - E(R) \tag{6.28}$$

where $\alpha = 3/4$ for the Gaussian ansatz, $E(R)$ is given by eq. (6.7) and E_{tot} is a constant. $R(t)$ is the size of the condensate, which varies with time during collapse. Integrating this equation, we can calculate the collapse time from a size $R(t=0) = R_0$ to some other size $R(t)$,

$$\begin{aligned} t &= \sqrt{\frac{\alpha\, M}{2}} \int_{R(t)}^{R_0} \frac{dR}{\sqrt{E(R_0) - E(R)}} \\ &= \frac{{M_P}^2}{m f^2} \sqrt{\frac{\alpha}{2}} \int_{\rho(t)}^{\rho_0} \frac{d\rho}{\sqrt{e(\rho_0) - e(\rho)}}, \end{aligned} \tag{6.29}$$

where in the second equality we have rescaled the dimensionful quantities using eq. (6.4).

We wish to investigate the effect of self-interactions in the axion potential on the collapse process. From our previous considerations, we feel it appropriate to include the first *two* terms in the self-interaction potential, which is to say, we use $e_1(\rho)$ to approximate the full energy. In that case, the global energy minimum ρ_D approximates

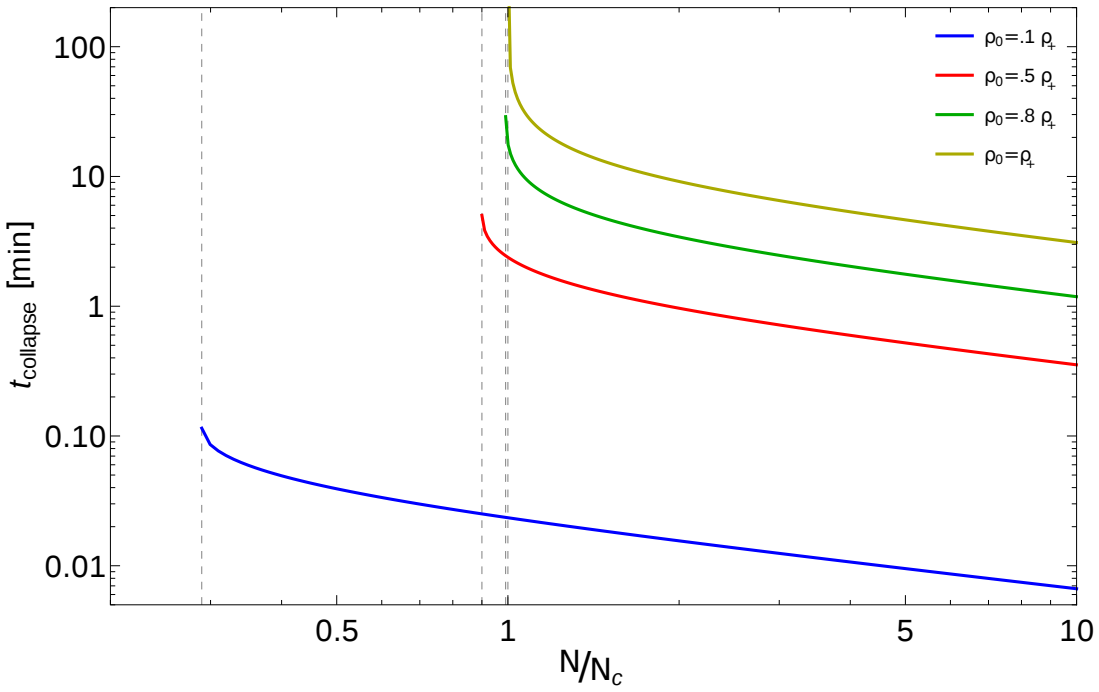

Figure 6.5.: Collapse time for an axion star as a function of n/n_c, for different choices of starting radius ρ_0: $\rho_0 = .1\rho_+$, $\rho_0 = .5\rho_+$, $\rho_0 = .8\rho_+$, and $\rho_0 = \rho_+$. At $N < N_c$, condensates can still collapse if the starting radius $\rho_0 < \rho_+$. Figure reproduced from [168].

the true global minimum of the energy. Considering this radius as the endpoint of collapse, we integrate eq. (6.29) not to $\rho = 0$, but rather to $\rho = \rho_D$.

If the axion star has $n = n_c$ and begins its collapse at ρ_+, then of course at the collapse time is formally infinite, because the potential is precisely flat in that case. For that reason, we analyze the collapse time for values of n which are slightly larger than n_c. We also investigate the change in collapse time as the starting size ρ_0 deviates from ρ_*. This latter case could be of interest, say, if axion star collapse can be catalyzed by collisions with astrophysical sources. As we will see in Chapter 7, if collapse is catalyzed by astrophysical collisions, then even condensates with $N < N_c$ can collapse, provided that in the collision its radius is sufficiently reduced. These considerations are represented together in Figure 6.5.

We can also track the radius of the axion star as a function of time, throughout the collapse process; see the top panel of Figure 6.6. For a large portion of the total collapse time, the radius changes little, as the star rolls slowly down a shallow potential, but later collapses fast to the dense minimum of radius ρ_D. Typical collapse times are $\mathcal{O}(1-10)$ minutes for $N = few \times N_c$.

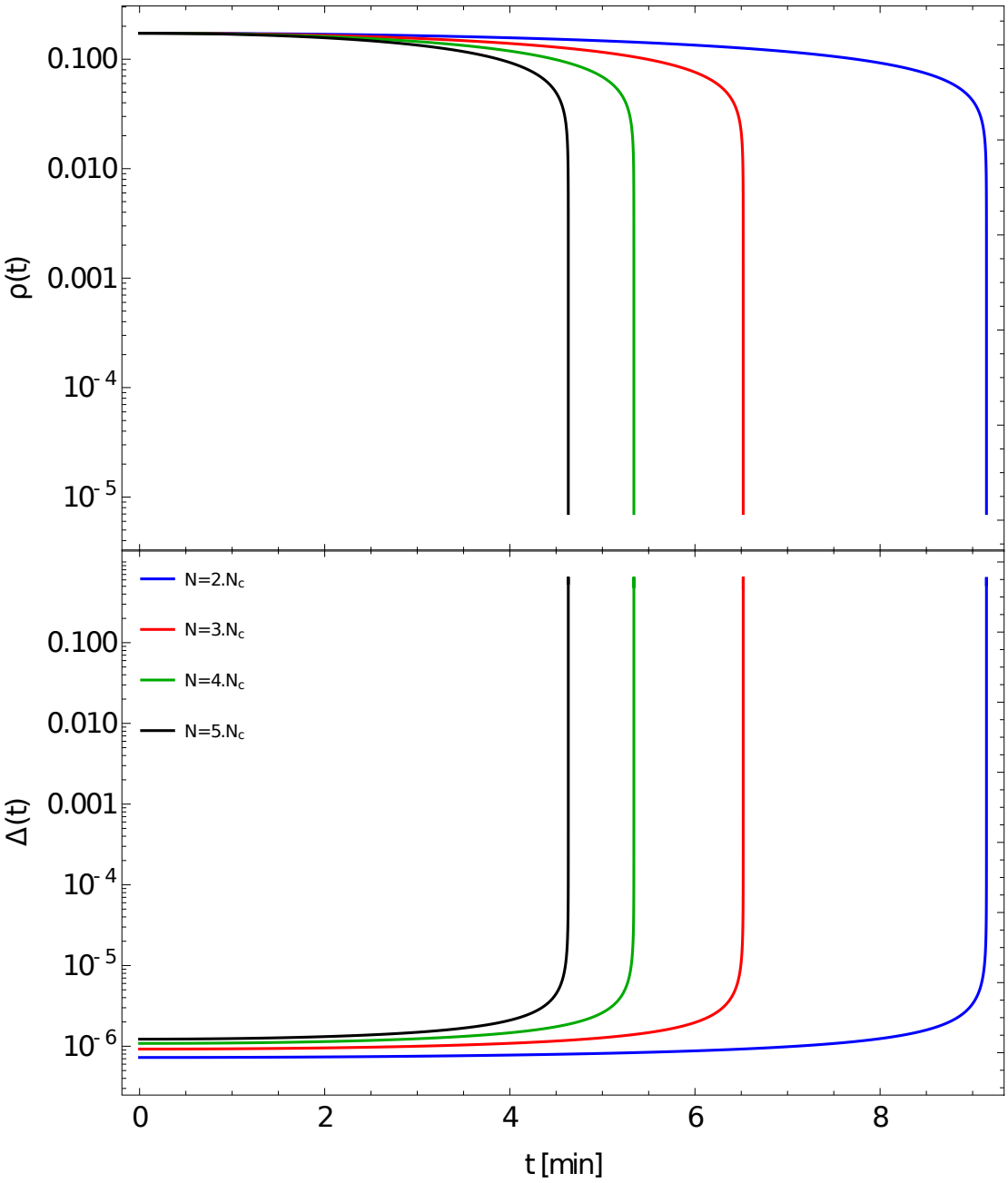

Figure 6.6.: Top: The dimensionless radius of a collapsing axion star using the approximate energy $E_1(\rho)$ as a function of time, for different choices of particle number N: $N = 2N_c$ (blue), $N = 3N_c$ (red), $N = 4N_c$ (green), and $N = 5N_c$ (black). Bottom: The parameter Δ as a function of time for the same choices of N. At large values $\Delta \gtrsim .05$, the decay rate through number changing interactions increases rapidly. Figure reproduced and updated from [168].

6.4. Emission of Relativistic Axions

To estimate the rate of decay of a collapsing axion star to relativistic particles, we need to compute the parameter Δ, which depends on the chemical potential μ (rather than the binding energy). In the variational method, we can calculate chemical potential

using

$$\mu(\rho) = \frac{3}{4}\frac{1}{\rho^2} - \frac{2}{\sqrt{2\pi}}\frac{n}{\rho} - \frac{1}{16\pi\sqrt{2\pi}}\frac{n}{\rho^3} + \frac{3\,\delta}{864\pi^3\sqrt{3}}\frac{n^2}{\rho^6}, \tag{6.30}$$

which is accurate at next-to-leading order in the self-interaction. This is very similar to the total energy in eq. (6.23), but the numerical factors on the interaction terms are changed.[4] Using $\Delta = \sqrt{1-\mu^2/m^2}$, defined in eq. (4.10), we can use eq. (6.30) to track Δ as a function of time during collapse.

In a simple classical collapse scenario, a dilute axion star would collapse into a dense one, and that would be the end of the story. However, we have seen in Chapter 5 that emission of relativistic axions from the condensate becomes increasingly probable as the density, and binding energy, of an axion star increases. This is precisely what happens during the collapse of an axion star. Recall that the rate of emission of relativistic particles through single-particle emission, calculated in Chapter 5, was

$$\Gamma = \frac{2\,\pi\,f^2}{\sqrt{8}\,m}\left[\frac{32\pi\,y_I}{3\Delta}\exp\left(-\frac{\sqrt{8}y_I}{\Delta}\right)\right]^2. \tag{6.31}$$

The decay rate depends only on Δ, which is a one-to-one function of ρ, and thus also of the collapse time t as defined in eq. (6.29). In the bottom panel of Figure 6.6, we plot the parameter Δ, defined in eq. (4.10), as a function of time during the collapse of an axion star. In the last moments of collapse, as its radius rapidly decreases, Δ increases rapidly. This implies that the decay rate rises rapidly as well.

We find that $\Delta \sim .05$ at $\rho \sim 10^{-4}$ (compared with $\rho_D \sim 10^{-5}$). In these last moments of collapse, the decay rate in eq. (6.31) becomes astronomically large; $\Gamma \sim 1$ emitted axion/sec at $\Delta \sim .0223$, and rises to $\Gamma \sim 10^{50}$ emitted axions/sec at $\Delta \sim .1$. We therefore are led to the conclusion that axion stars, as they collapse, emit many highly energetic free axions. Such an explosion, referred to as a Bosenova, has been observed experimentally by condensed matter physicists using cold atoms [29]. If dark matter consists of axion stars, then this decay process could deplete the total amount of dark matter in galaxy clusters. This effect is considered in a different context in [176].

In the months since our original work on this topic [168], a number of papers appeared which corroborated this basic picture. In the parameter space of QCD axions, Tkachev et al. performed a numerical simulation of collapsing axion condensates and concluded that $\mathcal{O}(40)\%$ of the initial mass in the condensate is converted to relativistic scalar radiation, after a series of alternating collapses and "bounces" [177]. A short time later, a second group performed a classical analysis in the regime of very large decay

[4] We described the differences in the derivation between E_B and μ in Section 3.5.2.

constants, $f \sim M_P$; they found that in this parameter range, some condensates can form black holes, while others exhibit a characteristic Bosenova effect similar to what we predicted [173]. They found a "triple point" in the plane of f and M, describing the stability of axion condensates. Extrapolating their analysis to the QCD range of f leads to a conclusion similar to ours, i.e. that black hole formation is not possible.

We emphasize again that the analysis of the decay process in [155] strictly applies only at weak binding, when $\Delta \ll 1$. This condition holds for the dilute initial state as well as throughout a large portion of the collapse process, but it is possible that some new dynamics take hold at truly strong binding $\Delta = \mathcal{O}(1)$, as for the dense global minimum of the energy where $\Delta \sim .56$. We have concluded that relativistic axion emission becomes important during collapse, but it is possible that a stable, strongly bound remnant remains.

6.5. The Chiral Potential

The analysis above (and our original work [168]) used the instanton potential V_I to analyze the axion self-interactions; however, as we have pointed out several times, the chiral potential V_C is more precise when considering QCD axions. While V_I is more tractable and lends itself more easily to an analytic expansion, it is in principle possible that our conclusions (the boundedness of the energy, the existence of a dense global energy minimum) would have been different if we had used V_C. In our follow-up work [169], we generalized our analysis to the chiral case, as explained below.

The potential we wish to consider has the form derived in Section 2.2, eq. (2.15) [80, 178]; for notational simplicity we will rescale it as

$$\frac{V_C(\mathcal{A})}{m^2 f^2} \equiv \mathcal{V} = \frac{1+z}{z}\left[1 + z - \sqrt{1 + z^2 + 2z\,\cos\left(\frac{\mathcal{A}}{f}\right)}\right]. \tag{6.32}$$

Using the particle data group [13] values of

$$\begin{aligned} m_u &= 2.15 \pm 0.15\ \text{MeV} \\ m_d &= 4.70 \pm 0.20\ \text{MeV}, \end{aligned} \tag{6.33}$$

we find that

$$z = \frac{m_u}{m_d} \simeq 0.457. \tag{6.34}$$

To recover the form of the instanton potential in eq. (2.18), one merely needs to take the $z \to 0$ limit, which gives $\mathcal{V} = 1 - \cos(\mathcal{A}/f)$. In this sense, the chiral potential is strictly more general than the instanton potential.

We will follow the procedure of [151] and write $\mathcal{A} = \mathcal{A}^+ + \mathcal{A}^-$, where $\mathcal{A}^+$ ($\mathcal{A}^-$) creates (annihilates) one axion in the ground state wavefunction. Expanding eq. (6.32) in a power series of the cosine, we have

$$\mathcal{V} = \frac{1+z}{z}\left[1+z-\sqrt{1+z^2}\sum_{j=0}^{\infty}\binom{\frac{1}{2}}{j}\left(\frac{2z}{1+z^2}\right)^j\left[\cos\left(\frac{\mathcal{A}^+ + \mathcal{A}^-}{f}\right)\right]^j\right]. \tag{6.35}$$

Now noting that in leading order of N, $\mathcal{A}^+$ and $\mathcal{A}^-$ commute, we have

$$\cos\left(\frac{\mathcal{A}^+ + \mathcal{A}^-}{f}\right) = \frac{1}{2}\left(e^{i\mathcal{A}^+/f}e^{i\mathcal{A}^-/f} + e^{-i\mathcal{A}^+/f}e^{-i\mathcal{A}^-/f}\right). \tag{6.36}$$

Then we can evaluate the jth power of the cosine,

$$\begin{aligned}\left[\cos\left(\frac{\mathcal{A}^+ + \mathcal{A}^-}{f}\right)\right]^j &= \frac{1}{2^j}\sum_{k=0}^{j}\binom{j}{k}e^{i(j-2k)\mathcal{A}^+/f}e^{i(j-2k)\mathcal{A}^-/f} \\ &\to \frac{1}{2^j}\sum_{k=0}^{j}\binom{j}{k}\sum_{m=0}^{\infty}(j-2k)^{2m}(-1)^m\frac{1}{(m!)^2}\left(\frac{\mathcal{A}^+\mathcal{A}^-}{f^2}\right)^m \\ &= \frac{1}{2^j}\sum_{k=0}^{j}\binom{j}{k}J_0\left[(j-2k)\left(\frac{2\sqrt{\mathcal{A}^+\mathcal{A}^-}}{f}\right)\right].\end{aligned} \tag{6.37}$$

where in the second step, we expanded the exponentials and kept only those terms with equal numbers of $\mathcal{A}^+$ and $\mathcal{A}^-$. Inserting this expression into eq. (6.35) gives the self-interaction energy density as follows:

$$\mathcal{V} = \frac{1+z}{z}\left\{1+z-\sqrt{1+z^2}\sum_{j=0}^{\infty}\binom{\frac{1}{2}}{j}\left(\frac{z}{1+z^2}\right)^j\sum_{k=0}^{j}\binom{j}{k}J_0\left[(j-2k)\left(\frac{2\sqrt{\mathcal{A}^+\mathcal{A}^-}}{f}\right)\right]\right\} \tag{6.38}$$

We require a correspondence with the results in the nonrelativistic Gross-Pitäevskii approach [168], given by the expansion of eq. (3.18). This is obtained by using

$$\frac{2\sqrt{\mathcal{A}^+\mathcal{A}^-}}{f} = \sqrt{\frac{2}{m}}\frac{\sqrt{\psi^*(r)\,\psi(r)}}{f} = \sqrt{2}\zeta\left|F\left(\frac{r}{R}\right)\right|, \tag{6.39}$$

and evaluating the self-interaction potential in terms of the rescaled wavefunction $F(\xi)$, as defined in eq. (6.5). The range of ξ is either finite such that we can choose $\xi_{\rm max} = 1$,

or it is infinite, in which case we choose $F(\xi) = \mathcal{O}(\xi^{-2})$, as $\xi \to \infty$. Then the rescaled self-interaction energy, defined in eq. (6.8), is

$$v_C = 4\,\pi\,\frac{\rho^6}{n^2\,\delta^2}\int d\xi\,\xi^2\,\frac{1+z}{z}\sqrt{1+z^2}\sum_{j=0}^{\infty}\binom{\frac{1}{2}}{j}\left(\frac{z}{1+z^2}\right)^j \times\sum_{k=0}^{j}\binom{j}{k}\left\{1-J_0\left[(j-2k)\sqrt{2}\,\zeta\,F(\xi)\right]-\frac{(j-2k)^2\,\zeta^2}{2}\,F(\xi)^2\right\}, \tag{6.40}$$

so that the expression in the energy functional (6.7) evaluates to

$$\begin{aligned}\frac{E_{SI}}{m\,N} &= -\frac{n\,\delta}{\rho^3}\,v_C \\ &= -\frac{1+z}{z}\sqrt{1+z^2}\sum_{j=0}^{\infty}\binom{\frac{1}{2}}{j}\left(\frac{z}{1+z^2}\right)^j\frac{4\,\pi}{\zeta^2\,C_2} \\ &\times\sum_{k=0}^{j}\binom{j}{k}\int_0^{\infty}d\xi\,\xi^2\left\{1-J_0\left[(j-2\,k)\,\sqrt{2}\,\zeta\,F(\xi)\right]-(j-2\,k)^2\frac{\zeta^2}{2}\,F(\xi)^2\right\}\end{aligned} \tag{6.41}$$

In order to perform the summations over j and k in eq. (6.41), we trade them for integrals, which are easier to estimate. First, we will perform the summation over k by using the standard integral representation for the Bessel function,

$$J_0[(j-2\,k)\,u] = \frac{1}{\pi}\int_0^{\pi} e^{i\,(j-2\,k)\,u\,\sin t}dt. \tag{6.42}$$

Substituting (6.42) into (6.41) we can perform the summation over k, yielding

$$\begin{aligned}\frac{E_{SI}}{m\,N} &= -\frac{1+z}{z}\sqrt{1+z^2}\sum_{j=0}^{\infty}\binom{\frac{1}{2}}{j}\left(\frac{2\,z}{1+z^2}\right)^j \\ &\times\frac{4\,\pi}{\zeta^2\,C_2}\int_0^{\infty}\left[1-\frac{1}{\pi}\int_0^{\pi}[\cos(\sqrt{2}\,\zeta\,F(\xi)\,\sin t)]^j\,dt - j\,\zeta^2\frac{F(\xi)^2}{2}\right]\xi^2\,d\xi.\end{aligned} \tag{6.43}$$

Now the summation over j can also be performed, to yield the following expression for the energy functional:

$$\frac{E_{SI}}{m\,N} = -\frac{4\,\pi}{\zeta^2\,C_2}\int_0^{\infty} I\left[\sqrt{2}\,\zeta\,F(\xi)\right]\,\xi^2\,d\xi + \frac{1}{2}, \tag{6.44}$$

where we have defined the integral

$$I(u) = \frac{1+z}{z\,\pi}\int_0^{\pi}\left[1+z-\sqrt{1+z^2+2\,z\,\cos(u\,\sin t)}\right]dt. \tag{6.45}$$

It is easy to see that the integrand of eq. (6.45) is bounded for all u and for all $t \in \{0, \pi\}$, and that it is monotonic, being minimized at $z \to 0$. But the $z \to 0$ limit of $I(u)$ is nothing but the rescaled instanton potential

$$\lim_{z\to 0} I(u) = 1 - J_0(u). \tag{6.46}$$

We conclude that the boundedness of the instanton potential implies the boundedness of the chiral potential. It thus suffices to show that the instanton self-interaction potential is bounded from below, and we have shown exactly this in Appendix D. The general conclusions of this chapter (the boundedness of the energy, the existence of a global energy minimum) are thus unchanged when considering the chiral potential.

6.6. Summary

In this chapter, we have analyzed the process of axion star collapse using a nonrelativistic method, following mostly our work in [168]. Dilute axion stars, examined in detail in Chapter 4, are well-described by a leading-order expansion of the axion self-interaction potential; they have rescaled radii of roughly $\rho_+ = \mathcal{O}(1)$, corresponding to physical radii of $R_+ \sim 100$ km. However, we have seen that higher-order interaction terms become increasingly relevant during collapse. When the rescaled radius of the axion star approaches very small values $\rho = \mathcal{O}(\delta^{1/3})$, the leading-order truncation of the potential breaks down.

By taking into account all orders in the expansion of the axion potential, we have shown that the total energy is always bounded from below, and thus it has a global minimum. The radius at which the energy is minimized is very small, $R_{GM} \sim few$ meters for typical QCD axion parameters, corresponding to a scaled radius of $\rho_{GM} \sim 10^{-6}$. This can be approximated by a *next-to-leading* order expansion of the energy, because such an expansion ends on a repulsive term, and thus has a global energy minimum; this minimum, occurring at $\rho = \rho_D$, can be used to approximate the true global minimum as ρ_{GM}. Because this dense state always exists at a radius much larger than the corresponding Schwarzschild radius, we concluded that QCD axion stars *cannot form black holes*. The dense states found here closely resemble those found by the authors of [154] using a different method.

Unstable dilute states can collapse. Given that they cannot form black holes, we analyzed the collapse process from the dilute radius $\rho \sim \rho_+$ to the approximate dense state which has $\rho \sim \rho_D$. We found that collapse takes place over a timespan of the order of a few minutes to an hour, depending on the exact parameters used.

During collapse, the rate for the decay process we analyzed in Chapter 5 becomes increasingly large; as a result, we concluded that during collapse towards the dense state, a large number of relativistic axions are emitted from the axion star. This conclusion, that collapsing axion stars exhibit a Bosenova behavior in the last moments of collapse, has been since corroborated by other authors using different methods [173, 177].

Finally, we have extended the analysis of [168] to the case of the chiral potential [169], which takes into account nonperturbative effects in the axion self-interaction potential. We proved analytically, using a generic ansatz for the wavefunction, that the chiral potential is bounded below by the instanton potential, and thus the global energy minimum of the latter is an absolute lower bound for the former. We concluded that our general conclusions are unchanged when using the chiral potential.

We have supposed in this chapter that collapse might be triggered by gravitational instability, that states with masses $M > M_c$ could form (possibly by accretion of free axions onto existing condensates) and would subsequently collapse. In the next chapter, we examine a very different mechanism for the stimulation of axion star collapses: astrophysical collisions.

Chapter 7.

Collisions of Dark Matter Axion Stars

"Look deeper through the telescope and do not be afraid when the stars collide towards the darkness, because sometimes the most beautiful things begin in chaos."

— Robert M. Drake

In the last few chapters, we analyzed the macroscopic properties, stability, and collapse process of axion stars. We have found that axion stars can exist in stable, dilute configurations, and as a result, they could reasonably contribute to dark matter. In this chapter, we examine some of the consequences of this hypothesis; in particular, we investigate the frequency of collisions between axion stars and other astrophysical bodies, and determine which axion stars would survive such collisions. This chapter is primarily based on our work in [179].

7.1. Axion Stars as Dark Matter

Beginning in Chapter 2, we have pointed out that axion particles make very good dark matter candidates. In particular, QCD axions are naturally produced cold in the early universe, in approximately the right abundance to account for the observed "missing mass" in galaxies. Other ALPs, coming from different models beyond the SM, can be produced via a similar mechanism as well.

When QCD axions form, the axion field can have large density fluctuations with sizes of Hubble scales; these are called "axion miniclusters" [89, 90]. Such states are not stable and will eventually collapse, fragment, and form a mixture between a dilute background of free axions, and condensed axions in the form of stable axion stars. The spectrum of masses of the axion stars in the final state remains an open question;

however, as we have observed in Chapter 4, there is a maximum mass (and minimum radius) allowed for these states to be gravitationally stable.

Further, it is not currently known what fraction of axions produced in the early universe should be in axion stars today. At the one extreme, it is possible that all axions in miniclusters formed axion stars in the early universe; in that case, it is still possible that some fraction of these stars has been since converted to either free cold axions (e.g. if axion stars can be ripped apart by tidal forces in the galaxy [180]), or to relativistic particles (e.g. via the decay process described in Chapter 5). At the other extreme, it is possible that miniclusters collapse without forming stable gravitationally bound condensates, but axion stars might still form later in the universe (e.g. through late-time gravitational thermalization [181] or accretion inside of ordinary stars, similar to the mechanism of [182–184]). The primordial mass spectrum of axion stars will also change relative to the present-day distribution if existing axion stars can grow in mass by accreting free axions. Clearly, this question is many-faceted and its answer is not well understood.

Nonetheless, given that axions typically have very low energy and they *can* form stable bound states, in the absence of a detailed study of formation, we take the view that they sometimes *do*. This means that a typical axion dark matter halo will contain some fraction of its mass in the form of axion stars. These axion stars will be distributed throughout the galaxy, and as compact objects, they will have typical virial speeds of the order $v \sim 10^{-3}$.

As a result, these axion stars will occasionally participate in collisions. These collisions can occur between two axion stars; or between one axion star and another astrophysical object, like an ordinary star or a neutron star, or even the earth. One might expect that such collisions would not lead to any observable effect, as axions do not interact strongly with the nuclear or electromagnetic forces. However, at the very least, axion star collisions will modify their energy functional, and it is at least possible that this could lead otherwise stable axion stars to become unstable to collapse. We will see that the frequency of collisions, as well as the parameter space for stability and the possible detectable signatures, will depend heavily on which object an axion star collides with.

In what follows, we will consider collisions of three types, occurring between an axion star and: (a) another axion star; (b) an ordinary star; and (c) a neutron star. For notational simplicity (and to avoid confusion about different types of "stars"), we will use the abbreviation ASt to denote an axion star, OSt to denote an ordinary star, and NSt to denote a neutron star.

7.2. General Framework

For two populations of astrophysical objects, the first being ASts and the other labeled by i, the general expression for the collision rate is

$$\Gamma_i = \frac{1}{S}\int d^3r\, n_{AS}(\vec{r})\, n_i(\vec{r})\langle\sigma\, v\rangle_i \tag{7.1}$$

where $n(\vec{r})$ denotes the number density of some population of astrophysical objects, σ_i is the cross section for a collision, and v is the relative velocity between the objects. The "symmetry factor" $S = 2$ if the colliding objects are of the same type, and $S = 1$ otherwise. The expectation value

$$\langle\sigma\, v\rangle_i \equiv \int_0^{2\,v_{vir}} f_{MB}(v)\,\sigma_i\, v\, d^3v \tag{7.2}$$

is an average over velocities in the halo, for which we will use a Maxwell-Boltzmann distribution of velocities

$$f_{MB}(v) = f_0\, \exp\Big(-\frac{v^2}{v_{vir}^2}\Big). \tag{7.3}$$

The distribution is normalized so that $\int_0^{2v_{vir}} f_{MB}(v)\, d^3v = 1$, and v_{vir} is the virial velocity in the halo.

In the special case where either density distribution is trivial, that is, that the objects are distributed with constant density throughout the halo, eq. (7.1) simplifies greatly. In that case, $n_i(\vec{r}) = N_i/V_{gal}$ is constant, where N_i is the total number of objects i present and $V_{gal} = 4\pi R_{gal}^3/3$ is the volume of the galaxy.[1] Then the integration is trivial, and the rate for collisions of a species i with ASts in a dark matter halo is

$$\hat{\Gamma}_i = \frac{N_{AS}\, N_i\, \langle\sigma_i\, v\rangle}{\frac{4\pi}{3}R_{gal}^3}. \tag{7.4}$$

This expression is significantly simpler than eq. (7.1), and often gives a good order of magnitude estimate. But as we will see in later sections, the number density distributions of astrophysical objects are far from trivial, and as a result, eq. (7.4) sometimes vastly underestimates collision rates.

[1] In this work we will use data for the Milky Way to approximate the collision rates for "typical" galaxies. For this reason we set $R_{gal} \approx 10^5$ light-years, which is the radius of the Milky Way.

For the collision cross section, we will use

$$\sigma_i = \pi \left(R_i + R_{AS}\right)^2 \left(1 + \frac{2\,G\left(M_i + M_{AS}\right)}{v^2\left(R_i + R_{AS}\right)}\right), \tag{7.5}$$

with R_i the radius of the body which collides with the ASt, and M_i is its mass. This is the geometric cross section modified by an enhancement factor to account for classical capture through gravitational effects.

The number of ASts in the galaxy N_{AS} could be estimated, albeit on an extreme view of their preponderance, by assuming that the total mass $M_{DM} \approx 10^{12} M_\odot$ of the dark matter in the Milky Way consists of ASts with a fixed mass very close to the critical value $M_{AS} = M_c \approx 10^{19}$ kg.[2] ($M_\odot = 2 \times 10^{30}$ kg is a solar mass.) In truth, there are two prominent effects that would modify this estimate. First, as we explained in Section 7.1, dark matter may consist only partially of ASts, the rest potentially being in a dilute background of axions or some other dark particles; we represent this uncertainty in the total dark matter fraction by a multiplicative factor $0 \lesssim \mathcal{F}_{DM} \lesssim 1$, so that the total dark matter mass in ASts is $\mathcal{F}_{DM} M_{DM}$. Secondly, ASts likely have some spread in their mass distribution, and so some ASts will have masses smaller than the maximum M_c; we introduce a second factor $0 \lesssim \mathcal{F}_{AS} \lesssim 1$, so that the average mass of a single ASt is $\mathcal{F}_{AS} M_{AS}$. These competing effects can, of course, compensate each other in the calculation of N_{AS}. The total number of ASts in the Milky Way is

$$N_{AS} = \frac{\mathcal{F}_{DM} M_{DM}}{\mathcal{F}_{AS} M_{AS}} \approx \frac{\mathcal{F}_{DM} 10^{12} M_\odot}{\mathcal{F}_{AS} 10^{19}\text{kg}} = 2 \times 10^{23} \frac{\mathcal{F}_{DM}}{\mathcal{F}_{AS}}. \tag{7.6}$$

Once we have determined the rate of collisions of a given type, we wish to investigate how the ASt energy functional changes to determine whether some fraction of otherwise stable states would be caused to collapse. To do this, we will return again to the *variational method* of approximating the energy functional, which was introduced in Section 3.5.3 and used extensively in Chapter 6. In the latter, we performed significant portions of the analysis using a Gaussian function as an approximation of the axion star wavefunction. This choice is not so advantageous here, because a Gaussian wavefunction has no well-defined radius, and so it is somewhat difficult to determine precisely whether a collision has or has not taken place.

[2] This value of the critical mass corresponds to the QCD axion parameter choice $f = 6 \times 10^{11}$ GeV.

Instead, we will use here an ansatz of the form

$$\psi(r) = \begin{cases} \sqrt{\dfrac{4\,\pi\,N}{(2\pi^2-15)R^3}}\cos^2\left(\dfrac{\pi\,r}{2\,R}\right), & r \le R \\ 0, & r > R \end{cases} \tag{7.7}$$

Then, evaluating the total nonrelativistic energy given in eq. (6.7), we find

$$E_{AS}(\rho) = m\,N\,\delta\Big[\frac{A}{\rho^2} - \frac{B\,n}{\rho} - \frac{C\,n}{\rho^3} + \frac{D\,\delta\,n^2}{\rho^6}\Big], \tag{7.8}$$

where ρ and n are a rescaled radius and particle number (respectively) defined in eq. (6.4), and where the constants have the values

$$\begin{aligned} A &= \frac{\pi^2(2\pi^2-3)}{6(2\pi^2-15)} \approx 5.8 & B &= \frac{(3456\pi^4 - 13800\pi^2 - 166705)}{1440(2\pi^2-15)^2} \approx 1.0 \\ C &= \frac{35\pi(24\pi^2-205)}{2304(2\pi^2-15)^2} \approx .068 & D &= \frac{77\pi^2(600\pi^2-5369)}{691200(2\pi^2-15)^3} \approx .0057 \end{aligned} \tag{7.9}$$

for the cosine ansatz of eq. (7.7). Recall from Chapter 6 that the structure of eq. (7.8) is ansatz-independent, whereas the values of the coefficients A, B, C, D are not.

The four terms on the RHS of eq. (7.8) correspond to kinetic, self-gravitational, attractive interaction, and repulsive interaction energies, respectively. As emphasized in Chapter 6, when analyzing the collapse of a dilute axion star to a dense one, it is important to keep at least the first repulsive self-interaction term (here, $\propto 1/\rho^6$) in the expansion of the axion self-interaction, so that the total energy is bounded form below. Higher-order interaction terms neglected here are proportional to $(\delta/\rho^3)^k$ with $k > 2$, i.e. suppressed by high powers of $\delta \ll 1$.

Near $\rho = \mathcal{O}(1)$, there exists a local minimum of the energy as long as $N < N_c$, the critical value of the particle number. In this range, the energy is well-approximated by only the first three terms in eq. (7.8), and has a local minimum at a rescaled radius

$$\rho_+ = \frac{A}{B\,n}\Big[1 + \sqrt{1 - \frac{3\,B\,C}{A^2}n^2}\Big]. \tag{7.10}$$

This local minimum is illustrated in Figure 7.1 for two different values of n (the red and blue curves). One can easily read off the critical rescaled particle number $n_c = A/\sqrt{3\,B\,C}$; the energy of an ASt with effective particle number $n > n_c$ is also illustrated in Figure 7.1 (the black dashed curve).

At any rescaled particle number n, the global minimum of the energy in eq. (7.8) lies at a very small radius $\rho_D \ll 1$ [168]. At these small radii, the last two terms of eq.

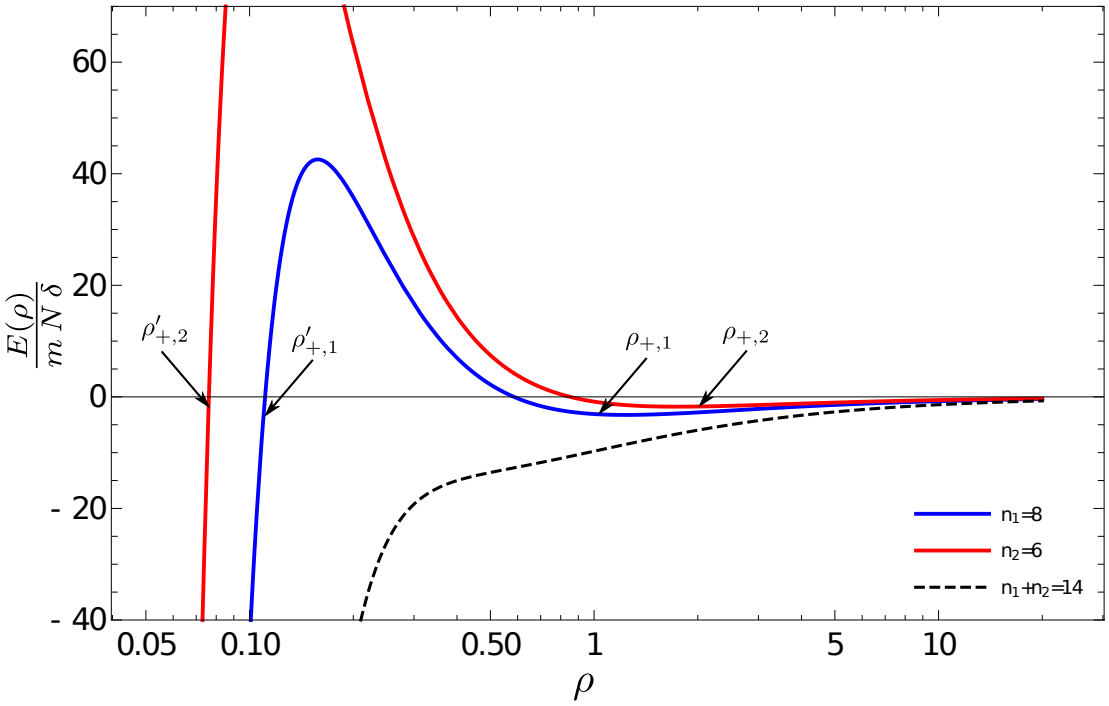

Figure 7.1.: The two solid lines denote the rescaled energy functionals of two stable ASts in the vicinity of ρ_+, which have $n_1 = 8$ (blue) and $n_2 = 6$ (red). The points labeled in the graph are: the local minimum of ASt 1 (2), $\rho_{+,1}$ ($\rho_{+,2}$), and the isoenergetic point on the left of the maximum of ASt 1 (2), $\rho'_{+,1}$ ($\rho'_{+,2}$). The black, dashed curve is the full energy of these two ASts occupying the same volume, which has no minimum in this range of ρ, because the effective particle number $n_{eff} = n_1 + n_2 > n_c$; thus, during such a collision, the ASts begin to collapse. Figure reproduced from [179].

(7.8) dominate and the energy minimum lies approximately at a rescaled radius of

$$\rho_D \approx \left(\frac{2\,D\,n\,\delta}{C}\right)^{1/3}. \tag{7.11}$$

For QCD axions with the cosine ansatz, $R_+ \approx 200$ km and $R_D \approx 7$ meters when $n \approx n_c \approx 12.6$. Note $n = n_c$ corresponds to the maximum mass of a dilute ASt, which we saw in Chapter 4 is $M_c \equiv m\,N_c \approx 10^{19}$ kg. An ASt with $n > n_c$ (as illustrated by the dashed line in Figure 7.1) possesses only a dense energy minimum at $\rho_D \ll 1$ (not pictured). An ASt in such a state is referred to as a *dense* ASt, and its stability is an open question.

In this chapter, we will consider only *dilute states*, rather than dense ones, as the initial configurations of the colliding ASt. This is because, first, the collision rates for dense ASts can be suppressed in some cases by the very small factor $(R_+/R_D)^2 \sim 10^{-10}$, as defined by eqs. (7.10) and (7.11), compared to dilute ASts; and second, because it is possible that otherwise stable dilute ASts can collapse as a result of collisions, making them additionally interesting.

There are various mechanisms for stimulating collapse from R_+ to R_D. For example, if ASts form against a dilute background of free axions, they could accrete such axions, thereby acquiring masses $M > M_c$ and triggering collapse; however, it is not clear how efficiently such accretion would occur. Instead, we will analyze in the coming sections whether in some cases collapse can be catalyzed by interactions between ASts and other astrophysical sources, including other ASts or OSts.

ASts collapsing from the dilute radius R_+ to the dense one R_D move quickly from small to large binding energies, as we saw in Chapter 6. When the binding energy becomes large, the rate of number-changing interactions in the ASt grows quickly, and so the ASt emits many relativistic axions as it collapses [155, 173, 177]. In the end, we will speculate about the observable effects of ASt decay, which could be stimulated by collisions and subsequent collapse.

Axions couple to photons through an effective dimension-5 operator, shown in eq. (2.9); this coupling allows decay of free or condensed axions through a process $a \to 2\gamma$, though this rate is believed to be small enough to be ignored on cosmological timescales [163]. However, during a collision with a NSt, strong magnetic fields can stimulate these interactions, leading to a burst of photons that could potentially be observable [185–188]. The idea that such collisions could be the origin of the observed (but unexplained) Fast Radio Bursts (FRBs) [189–192] appeared originally several years ago, and has been investigated as recently as this year [193]. Because of the unique detection signatures arising from these collisions, we will revisit the calculation of the collision rate of ASts with NSts as well.

7.3. Collisions Between Pairs of Axion Stars

7.3.1. Collision Rate

In this section we examine the case of two ASts colliding with each other. In that case, we use the radius $R_{AS} = 200$ km, which matches our approximate choice for $M_{AS} = 10^{19}$ kg (recall Figures 4.3 and 4.4). For a typical velocity $\bar{v} = 300$ km/s, the enhancement factor of the cross section, given in eq. (7.5), is

$$\frac{2\,G\,M_{AS}}{\bar{v}^2\,R_{AS}} \approx 10^{-7}. \tag{7.12}$$

Clearly this small correction in the ASt cross section is negligible in this case. We can approximate the rate by assuming a trivial number density distribution, as in eq. (7.4);

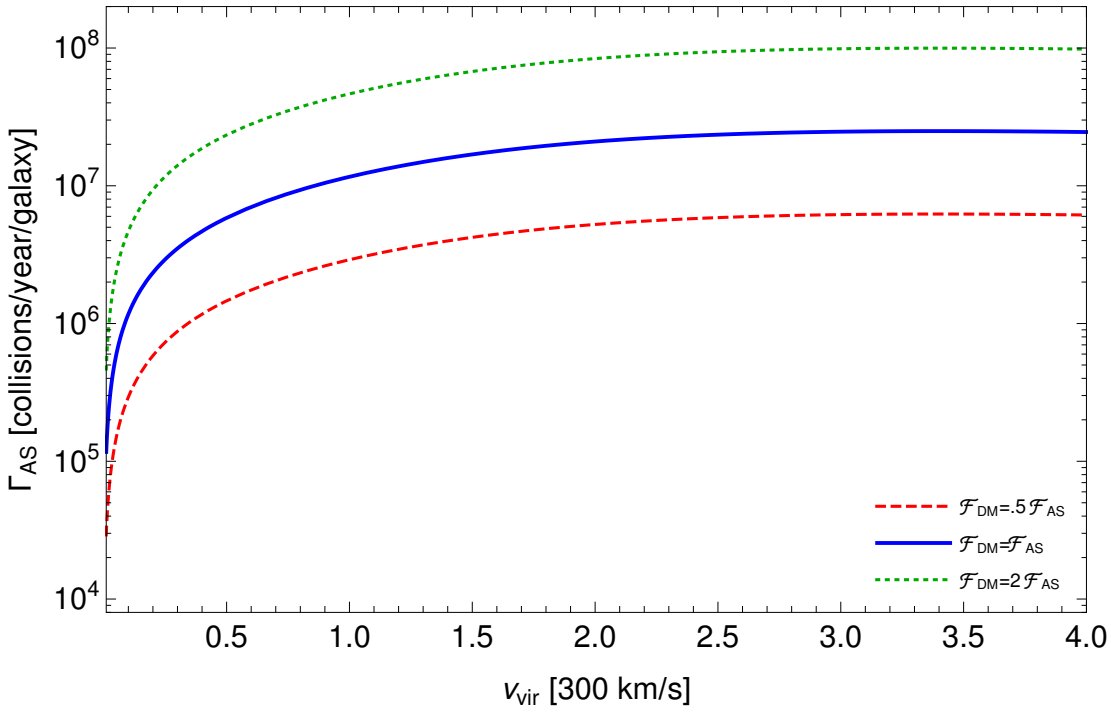

Figure 7.2.: The collision rate of two ASts as a function of $\eta = v_{vir}/(300\ \mathrm{km/s})$, evaluated at different values of $\mathcal{F}_{DM}/\mathcal{F}_{AS}$. Figure reproduced from [179].

this gives the result

$$\hat{\Gamma}_{AS} \approx 3 \times 10^7 \left(\frac{\mathcal{F}_{DM}}{\mathcal{F}_{AS}}\right)^2 \frac{\text{collisions}}{\text{year} \cdot \text{galaxy}}. \tag{7.13}$$

We can improve on this rough estimate by taking into account the number density distributions of ASts. If ASts are a component of dark matter, then it is reasonable to assume that they are distributed according to the Navarro-Frenk-White (NFW) profile [39,40], which was introduced in eq. (1.3). For clarity we reproduce it here:

$$\rho_{NFW}(r) = \frac{\rho_0}{\frac{r}{R_0}\left(1+\frac{r}{R_0}\right)^2}, \tag{7.14}$$

where ρ_0 and R_0 are scale mass density and radius for the halo. An analysis of this kind was recently performed by [194], who considered primordial black holes as dark matter. Taking the Milky Way as a sample galaxy, we use the values of ρ_0, R_0, and virial mass M_{vir} from [195]. These values are reported in Table 7.1. We will also take into account velocity dispersion by assuming the Maxwell-Boltzmann distribution of eq. (7.3), though the precise value of v_{vir} is somewhat uncertain. We introduce an $\mathcal{O}(1)$ factor η representing the deviation of v_{vir} from the value $\bar{v} = 300$ km/s used above.

That is,

$$v_{vir} = \eta\, \bar{v}, \tag{7.15}$$

so fixing the value of M_{vir} from [195], we have a virial radius of

$$R_{vir} = \frac{G\, M_{vir}}{\eta^2 \bar{v}^2} \approx \frac{2.22 \times 10^{18}\ \text{km}}{\eta^2}. \tag{7.16}$$

The velocity-averaged cross section is

$$\langle \sigma\, v \rangle_{AS} = \int_0^{2v_{vir}} f_{MB}(v)\, \sigma_{AS}\, v\, d^3v \approx 1.6 \times 10^8\, \eta \frac{\text{km}^3}{\text{sec}}, \tag{7.17}$$

implying a total rate for collisions

$$\begin{aligned} \Gamma_{AS} &= \frac{1}{2} \int_0^{R_{vir}} 4\pi r^2 \Big(\frac{\mathcal{F}_{DM} \rho_{NFW}(r)}{\mathcal{F}_{AS} M_{AS}} \Big)^2 \langle \sigma\, v \rangle_{AS}\, dr \\ &= \frac{2\pi \langle \sigma\, v \rangle_{AS}}{M_{AS}^2} \Big(\frac{\mathcal{F}_{DM}}{\mathcal{F}_{AS}} \Big)^2 \int_0^{R_{vir}} r^2 \rho_{NFW}(r)^2\, dr \\ &\approx 10^7\, \eta \Big(\frac{\mathcal{F}_{DM}}{\mathcal{F}_{AS}} \Big)^2 \Big[1 - \Big(\frac{\eta^2}{4.5 + \eta^2} \Big)^3 \Big] \frac{\text{collisions}}{\text{year} \cdot \text{galaxy}}. \end{aligned} \tag{7.18}$$

Note that the dependence on η in the last bracket comes from the uncertainty in R_{vir} in the upper bound of the integral; we can safely neglect this dependence except at $\eta \gtrsim 3$, a very unlikely range. Taking $\eta = 1$, we have

$$\Gamma_{AS}|_{\eta=1} = 10^7 \Big(\frac{\mathcal{F}_{DM}}{\mathcal{F}_{AS}} \Big)^2 \frac{\text{collisions}}{\text{year} \cdot \text{galaxy}}. \tag{7.19}$$

Thus in this case, the constant density approximation in eq. (7.4) gives a reasonable estimate, that of eq. (7.13). The full decay rate Γ_{AS} over a range of η, and for different values of $\mathcal{F}_{DM}/\mathcal{F}_{AS}$, is represented in Figure 7.2. The dependence on $\mathcal{F}_{DM}$ and $\mathcal{F}_{AS}$ implies that the true collision rate could easily be larger or smaller by a few orders of magnitude from the approximate value 10^7 collisions/year/galaxy.

7.3.2. Induced Collapse

During one of these collisions, the energy functional of eq. (7.8) changes for both ASts. In particular, if the two colliding ASts have particle numbers N_1 and N_2, then their

ρ_0 [$M_\odot$/kpc^3]	R_0 [kpc]
1.4×10^7	16
M_{vir} [$M_\odot$]	–
1.5×10^{12}	–

L_1 [pc]	L_2 [pc]	$L_\odot$ [kpc]	f
2600	3600	8	.12
H_1 [pc]	H_2 [pc]	$Z_\odot$ [pc]	–
300	900	25	–

$A_{0,r}$ [kpc^{-1}]	α	$A_{0,z}$ [kpc^{-1}]	$A_{2,z}$ [kpc^{-1}]	k_1	$k_2^<$	$k_2^>$
5×10^{-3}	1.83	1.8×10^{-5}	35.6×10^{-3}	13×10^{-3}	18.4×10^{-3}	.05
A	λ [kpc]	$A_{1,z}$ [kpc^{-1}]	–	b_1 [kpc]	$b_2^<$ [kpc]	$b_2^>$ [kpc]
95.6×10^{-3}	4.48	1.87	–	12.8×10^{-3}	.03	.65

Table 7.1.: Astrophysical parameters describing the Milky Way, which we use in the calculation of collision rates. The table on the top-left describes the dark matter halo using an NFW profile using data from [195]; the top-right table describes the distribution of stars using [196]; and the table along the bottom gives parameters describing the distribution of neutron stars using [197].

combined energy functional will take the form

$$E_{2AS}(\rho) = m\,(N_1+N_2)\,\delta\Big[\frac{A}{\rho^2} - \frac{B\,(n_1+n_2)}{\rho} - \frac{C\,(n_1+n_2)}{\rho^3} + \frac{D\,\delta\,(n_1+n_2)^2}{\rho^6}\Big]. \quad (7.20)$$

If the sum $n_1 + n_2 > n_c$, then both stars begin to collapse, as their combined energy no longer has a local minimum at $\rho = \mathcal{O}(1)$. An example of the change in the energy functional is illustrated in Figure 7.1: whereas the two separate ASts had energy minima at $\rho_{+,1}$ (blue curve) and $\rho_{+,2}$ (red curve), their combined energy function (black dashed curve) possesses no dilute minimum. While these two ASts overlap, they both begin to collapse.

If the two ASts have a mechanism for dissipating energy, they might become bound and merge together completely; in that case, if $N_1 + N_2 = N_c$, the collapse will have plenty of time to run its course, and will be described precisely by the analysis of Chapter 6. However, there is no guarantee that colliding ASts will merge; because they move with some relative velocity v_{rel}, they may occupy the same volume for only a finite time. Another way to say this is that, in light of the weak self-interactions of axions, it is possible that such objects would pass right through one another. Indeed, no mechanism is known for dissipating energy during the collision–with the exception of gravitational waves, but the corresponding rate of energy dissipation is negligibly small.[3]

[3]This is the case because the masses of QCD ASts are too small to have a significant gravitational wave output, but the situation could be different in some more generic axion theory which allows very heavy bound states. We plan to return to this point in a future work.

An important, related note is that our discussion here will ignores differences in phase for the colliding ASts; taking this into account in the future could increase the merger rate for condensates close to being in-phase, or lead to inelastic "bounces" when the condensates are out of phase [198]. For sufficiently large velocities, these effects are likely to be negligible, but could be relevant for ASts with low relative velocities. We hope to return to this point in the near future.

For the purposes of this work, we will assume that colliding ASts do not dissipate energy and become bound, and so the energy functional changes for only a finite time; we approximate this time by $t_{in} = 2(R_1 + R_2)/v_{rel}$, where R_1 and R_2 are radii of the two ASts. Nonetheless, collapse will begin when the stars occupy the same volume, as the energy functional changes as above. If the ASts overlap for a sufficiently long time, then when the stars separate, they will already be gravitationally unstable and will continue to collapse.

Under what conditions will an ASt participating in a collision continue to collapse after the collision has ended? A sufficient condition for this would be that prior to the end of the collision, its radius has decreased from ρ_+ to ρ'_+, identified as the point isoenergetic with ρ_+ on the left branch of the energy curve (illustrated in Figure 7.1). As we pointed out in Chapter 6 (c.f. eq. (6.29)), the collapse time from ρ_+ to some other point ρ_{end} is

$$t = \sqrt{\frac{\alpha\, M}{2}} \int_{R_{end}}^{R_+} \frac{dR}{\sqrt{E(R_+) - E(R)}}, \tag{7.21}$$

where the constant α takes the value

$$\alpha = \frac{3(315 - 50\pi^2 + 2\pi^4)}{5\pi^2(2\pi^2 - 15)} \approx .2 \tag{7.22}$$

for the cosine ansatz. Thus we will consider t_*, defined as the time to collapse from ρ_+ to ρ'_+ (i.e. using $R_{end} = R'_+$).

Full collapse from the dilute radius ρ_+ to the dense radius ρ_D was shown in Chapter 6 to last a time on the order of tens of minutes, or even a few hours, depending on the value of N/N_c. We find that collapse from ρ_+ to ρ'_+, catalyzed by collision of two nearly-critical ASts, takes nearly as long as a collapse all the way to ρ_D. This is easy to understand once one observes that the potential is shallow at the beginning of the collapse, near $\rho = \rho_+$, and becomes steeper towards the end (see Figure 7.1). Because collapses occur slowly, we conclude that colliding ASts only collapse if they move with a sufficiently low relative velocity, so that the two ASts occupy the same volume for a

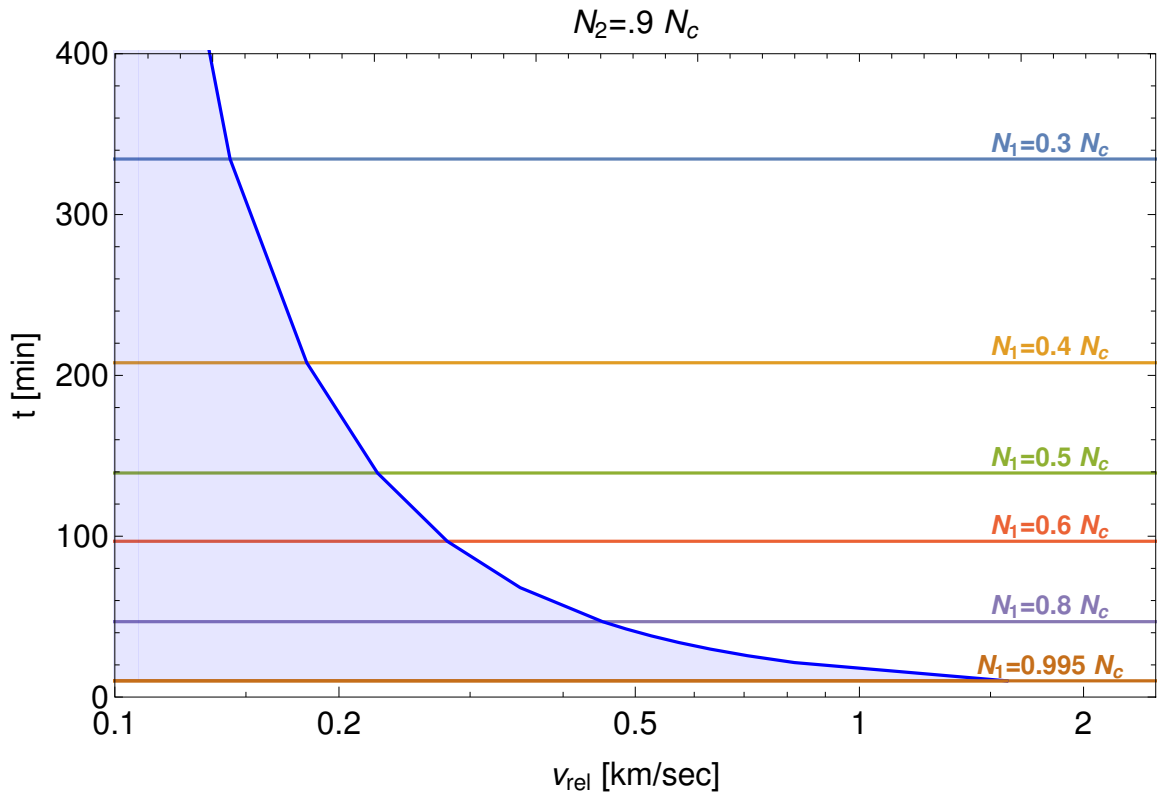

Figure 7.3.: The relevant timescales for the collision and possible collapse of two ASts. The horizontal lines are the required times t_* for an AST with N_1 particles to collapse from ρ_+ to ρ'_+, given that it collides with a second AST which has N_2 particles at a relative velocity v_{rel}. The blue curve represents the approximate time t_{in} that one AST spends traversing the other. If $t_{in} < t_*$ (the blue shaded region), then the AST collapses. Figure reproduced from [179].

long enough time interval. We investigate next how small v_{rel} must be for collapse to be induced.

In Figure 7.3, we compare the approximate collision time $t_{in} = 2(R_1 + R_2)/v_{rel}$ to the time t_* required for a star to collapse from ρ_+ to ρ'_+, defined in eq. (7.21), at different values of n. We observe that $v_{rel} \lesssim 1$ km is required for nearly any two ASts to collapse as a result of the collision process. For the Maxwell-Boltzmann distribution of velocities we have been assuming, as in eq. (7.3), the probability that two ASts have a relative velocity $v_{rel} \lesssim V$ is

$$P(v_{rel} \lesssim V) = \sqrt{\frac{2}{9\pi}}\left(\frac{V}{v_{vir}}\right)^3 + \mathcal{O}\left(\frac{V}{v_{vir}}\right)^5. \tag{7.23}$$

For $V = 1$ km/sec, this gives $P(v_{rel} < 1\ \text{km/sec}) \approx 10^{-8}$. This implies that while the collision rate in eq. (7.19) is high, the fact is that even on the extreme assumption that all ASts are very close to critical ($N \sim .9\, N_c$), the total rate of collapses induced by

collisions of two ASts is very small,

$$\Gamma_{collapse} \sim \Gamma_{AS} \times P(v_{rel} < 1\frac{\text{km}}{\text{sec}}) \approx .1 \left(\frac{\mathcal{F}_{DM}}{\mathcal{F}_{AS}}\right)^2 \frac{\text{collapses}}{\text{year} \cdot \text{galaxy}}. \tag{7.24}$$

The rate of induced collapses is even lower if some of the colliding ASts are less massive. We conclude that collapses induced by collisions between two ASts very likely have a negligible effect on the overall mass distribution of ASts, or more generally, of dark matter.

We also note in passing that if ASts collide but do not collapse fully from ρ_+ to ρ'_+ (e.g. a scenario outside of the shaded blue region of Figure 7.3), they will oscillate around their respective dilute minima after emerging from the collision. With no mechanism for damping, such oscillations would continue indefinitely.

7.4. Collisions Between Axion Stars and Ordinary Stars

7.4.1. Collision Rate

Consider next the case of an ASt colliding with an OSt, in which case $i = \odot$ in eq. (7.4), referring to stellar matter. We begin with the approximate number of stars in the Milky Way, $N_\odot = 10^{11}$. Taking the sun as a "typical" star, we use the radius $R_\odot = 7 \times 10^5$ km in the cross section, and we assume for now that stars also move at a virial velocity $\bar{v} \approx 300$ km/s. The resulting enhancement factor in the cross section (7.5) is

$$\frac{2\,G\,(M_\odot + M_{AS})}{\bar{v}^2\,(R_\odot + R_{AS})} \approx 4.25. \tag{7.25}$$

Combining the above parameters, the constant density estimate of the collision rate using eq. (7.4) is

$$\hat{\Gamma}_\odot \approx 400\,\frac{\mathcal{F}_{DM}}{\mathcal{F}_{AS}}\,\frac{\text{collisions}}{\text{year} \cdot \text{galaxy}}. \tag{7.26}$$

As in the previous section, we can improve on our estimation of the rate by allowing ASts to be distributed according to the NFW profile in eq. (7.14). For the distribution of stars, we use the phenomenological fit found in [196] assuming cylindrical symmetry; the authors used a double exponential to describe the disk and a power law for the baryonic halo component. Here we neglect the halo component, which constitutes a few percent correction and is thus negligible at the level of precision of this work. The

distribution is

$$n_\odot(\ell, z) = n_d(L_\odot, 0) \exp\left(\frac{L_\odot}{L_1}\right) \exp\left(-\frac{\ell}{L_1} - \frac{z + Z_\odot}{H_1}\right) + f\, n_d(L_\odot, 0) \exp\left(\frac{L_\odot}{L_2}\right) \exp\left(-\frac{\ell}{L_2} - \frac{z + Z_\odot}{H_2}\right). \tag{7.27}$$

Note that in this section we work in cylindrical coordinates, with $\ell = \sqrt{x^2 + y^2}$ the distance from the galactic center in the galactic plane, and z the height above the galactic plane.

The expression of eq. (7.27) for the stellar distribution depends on the fit parameters $L_{1,2}$, $H_{1,2}$, and f, as well as the position of the sun $(L_\odot, Z_\odot)$. We use the best fit values reported in [196] and ignore uncertainties; these values are reproduced in Table 7.1. The sample in that analysis contained only about 10^8 stars, whereas the total number in the Milky Way is understood to be closer to 10^{11}. To remedy this, we rescale the final parameter in the fit, the overall normalization $n_d(L_\odot, 0)$, by requiring the total number of stars to be

$$\int n_\odot\, d^3r = N_\odot = 10^{11}; \tag{7.28}$$

this implies

$$n_d(L_\odot, 0) \approx .15\text{pc}^{-3}. \tag{7.29}$$

The collision rate of ASts with OSts using eq. (7.1) is then[4]

$$\Gamma_\odot = 2 \int_0^{R_{vir}} dz \int_0^{R_{vir}} d\ell\, 2\pi\, \ell \left(\frac{\mathcal{F}_{DM} \rho_{NFW}(\sqrt{\ell^2 + z^2})}{\mathcal{F}_{AS} M_{AS}}\right) n_\odot(\ell, z) \langle \sigma\, v \rangle_\odot. \tag{7.30}$$

For simplicity, in this section we do not take into account the velocity dispersion of stars and use only the virial velocity v_{vir}. In that case, it is easy to compute

$$\langle \sigma\, v \rangle_\odot \approx \sigma_\odot\, v_{vir} = 2.4 \times 10^{15} \eta\, \frac{\text{km}^3}{\text{sec}}. \tag{7.31}$$

Performing the integrals over ℓ and z gives the result[5]

$$\Gamma_\odot = 3000\, \eta\, \frac{\mathcal{F}_{DM}}{\mathcal{F}_{AS}} \frac{\text{collisions}}{\text{year} \cdot \text{galaxy}}. \tag{7.32}$$

[4] We assume also a $z \leftrightarrow -z$ symmetry, allowing us to integrate only on $z \in \{0, R_{vir}\}$ and multiply by 2.

[5] In this expression, we have neglected the uncertainty of R_{vir}, represented by additional factors of η, in the integration bounds; in Section 7.3, we found the resulting dependence on η to be negligible. This approximation would not be appropriate if $\eta \gg 1$.

Comparing the more precise result of eq. (7.32) to the approximation in eq. (7.26), we see that in this case, taking the ASt and stellar distributions into account increases the rate by nearly an order of magnitude. This likely reflects the fact that the distribution of OSts in the Milky Way is very far from a constant density; OSts are packed very densely into the galactic disk, and the density is peaked strongly at low z. Collisions occur with a much higher frequency near the galactic center, where the density of both ASts and OSts is very large; this fact is not captured by the constant-density approximation.

Finally, note that the estimate in eq. (7.32) is likely an underestimate of the total collision rate of ASts with OSts. This is because in the estimate of the cross section, we took the sun as a "typical" star, which is likely a reasonable approximation for the $\mathcal{O}(10^{11})$ stars contained in our sample. However, many stars have radii R_s much larger than $R_\odot$ of the sun, and the cross sections for those stars is enhanced by a factor of order $(R_s/R_\odot)^2 \gg 1$. We have also ignored smaller stars, like red dwarfs, but their contribution to the collision rate is likely to be a small correction.

7.4.2. Induced Collapse

To determine the effect of a collision in this case, observe that as an ASt passes through an OSt, there will be an additional contribution to its gravitational energy due to the stellar potential $V_s(r)$. To estimate this contribution, consider first an ASt at rest at a point concentric with that of an OSt. The energy functional describing the ASt, given by eq. (7.8), acquires an additional contribution from the gravitational effects of the stellar mass,

$$E_{GS}(R) = m \int V_s(r)|\psi(r)|^2 \, d^3r. \tag{7.33}$$

Note that we have assumed that the external gravitational source has a radius R_s larger than the radius R of the ASt; this is appropriate for the types of QCD axions we discuss here, but could change in some more generic axion theory which produces very large ASts. Assuming a constant density for the OSt and requiring continuity of the full gravitational potential across each boundary gives the unique result

$$V_s(r) = \begin{cases} \dfrac{G\,M_s}{2\,R_s^3} r^2 - \dfrac{3}{2}\dfrac{G\,M_s}{R_s}, & r \le R_s \\ -\dfrac{G\,M_s}{r}, & r > R_s \end{cases} \tag{7.34}$$

where M_s is the mass of the star.

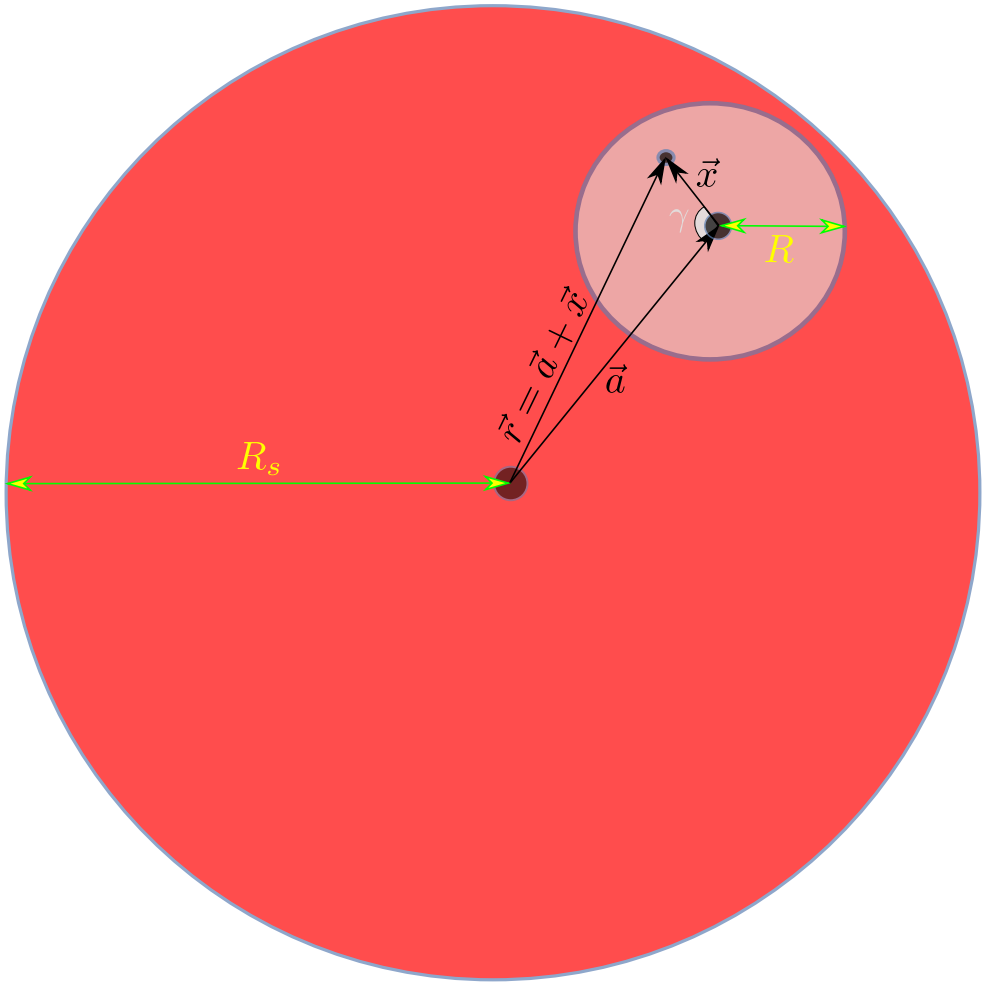

Figure 7.4.: An illustration of an ASt passing through an OSt. The relative radii of the ASt (R) and the OSt (R_s) are not to scale. Figure reproduced from [179].

In reality, ASts and OSts will collide with some relative velocity v_{rel} and the gravitational potential will be changing with time. However, the change in the total energy resulting from this effect is a function of the distance from the ASt to the center of the OSt (not of the variational parameter R), and so will not affect the existence or position of an energy minimum. To see that this is so, suppose the ASt sits at a point $\vec{a}$ away from the center of the OSt, and let $\vec{x}$ represent a position measured with respect to the

center of the ASt; then $\vec{r} = \vec{a} + \vec{x}$, as in Figure 7.4. Thus eqs. (7.33) and (7.34) give

$$\begin{aligned} E_{GS}(R) &= \frac{G\,m\,M_s}{2\,R_s^3}\int r^2|\psi(r)|^2 d^3r - \frac{3}{2}\frac{G\,m\,M_s}{R_s}\int |\psi(r)|^2 d^3r \\ &= \frac{G\,m\,M_s}{2\,R_s^3}\int (\vec{a}+\vec{x})^2|\psi(\vec{a}+\vec{x})|^2 d^3x - \frac{3}{2}\frac{G\,m\,M_s}{R_s}\,N \\ &= \frac{G\,m\,M_s}{2\,R_s^3}\int (a^2 + x^2 + 2\vec{a}\cdot\vec{x}\cos\gamma)|\psi(\vec{a}+\vec{x})|^2 d^3x - \frac{3}{2}\frac{G\,m\,M_s}{R_s}\,N \\ &= \frac{G\,m\,M_s}{2\,R_s^3}\int_0^R (x^2 + 2\vec{a}\cdot\vec{x}\cos\gamma)|\psi(\vec{a}+\vec{x})|^2 x^2\,dx\,d(\cos\gamma)d\phi \\ &\quad + \frac{G\,m\,M_s}{2\,R_s^3}\,a^2\,N - \frac{3}{2}\frac{G\,m\,M_s}{R_s}\,N, \end{aligned} \tag{7.35}$$

where in the third line we introduced the angle γ between the vectors $\vec{a}$ and $\vec{x}$. For a spherically symmetric ASt wavefunction, $\psi(\vec{x}) = \psi(x)$ does not depend on γ, and so the second integral vanishes. The last two terms of eq. (7.35) are constants with respect to R. For notational simplicity, we denote them by

$$\begin{aligned} C_1 &\equiv \frac{G\,m\,M_s}{2\,R_s^3}\,a^2\,N - \frac{3}{2}\frac{G\,m\,M_s}{R_s}\,N \\ &= m\,N\,\delta\Big[\frac{\mu_s\,\beta^2}{2\,\rho_s^3} - \frac{3\,\mu_s}{2\,\rho_s}\Big] \\ &= m\,N\,\delta\,c_1, \end{aligned} \tag{7.36}$$

where we defined the dimensionless quantities

$$\rho_s = \frac{m\,f}{M_P}\,R_s, \qquad \beta = \frac{m\,f}{M_P}\,a, \qquad \mu_s = \frac{m}{M_P\,f}\,M_s, \tag{7.37}$$

in analogy with the radius and mass of an ASt in eq. (6.4). The constant c_1 is always < 0, and very large: for the sun, $R_s = R_\odot = 7\times10^5$ km and $M_s = M_\odot = 2\times10^{30}$ kg, which implies $\rho_\odot = 1735$ and $\mu_\odot = 1.6\times10^{12}$, and then $c_1 \sim -10^9$ regardless of the value of β.

Evaluating the integral in eq. (7.35), we have

$$\begin{aligned} E_{GS}(R) &= \frac{3\,G\,M_s\,N\,m}{2\,R_s}\Big(\frac{2\pi^4 - 50\pi^2 + 315}{5\pi^2(2\pi^2-15)}\frac{R^2}{R_s^2}\Big) + C_1 \\ &= m\,N\,\delta\Big[\frac{\mu_s\,F}{\rho_s^3}\rho^2 + c_1\Big] \end{aligned} \tag{7.38}$$

where

$$F = \frac{3(2\pi^4 - 50\pi^2 + 315)}{10\pi^2(2\pi^2 - 15)} \approx .10. \tag{7.39}$$

Combining eqs. (7.8) and (7.38), we can write the rescaled total energy

$$E_s(\rho) = m\,N\,\delta\left[\frac{A}{\rho^2} - \frac{B\,n}{\rho} - \frac{C\,n}{\rho^3} + \frac{D\,\delta\,n^2}{\rho^6} + \frac{F\,\mu_s}{\rho_s^3}\rho^2 + c_1\right]. \tag{7.40}$$

The constant c_1 affects only the magnitude of $E_s(\rho)$, and not the existence of a minimum, i.e. it will have no effect on our analysis of collapse.

Recall that outside the OSt, an ASt can exist in a dilute state only for $n < n_c \approx 12.6$. During a collision, due to the change in the energy functional, this effective critical particle number changes as the ASt passes through an OSt. Taking the sun as an example, we find that the critical particle number decreases to $n_{c,\odot} \approx 11.29$, which implies that ASts with $n_{c,\odot} \leq n < n_c$, which are ordinarily stable, will collapse if they collide with the sun. For $n < n_{c,\odot}$, the dilute state binding energy increases as the ASt moves through the sun, though it remains stable (and it is still appropriate to consider it a weakly bound state).

More generally, the energy landscape in eq. (7.40) is a function of ASt particle number N, and a density parameter $\mathcal{D} \equiv M_s/R_s^3$ characterizing the OSt. In Figure 7.5, there exists a region in which ASts colliding with OSts remain stable, though with larger binding energy (shown in yellow), and one in which they collapse (red). In the red region, collapse proceeds via the mechanism outlined in [168] and described in Chapter 6: an initial slow roll, followed by a quick final collapse towards a strongly bound dense state. As the binding energy increases rapidly in the last moments, a large number of relativistic axions are emitted.

If the OSt has a sufficiently large radius, or if the relative velocity in the collision is sufficiently low, then collisions occurring in the red region of Figure 7.5 allow the ASt enough time to collapse fully before it passes fully through the OSt. To test whether this is plausible, we again use eq. (7.21) to calculate the time t_* needed for the ASt to sufficiently collapse. For axion stars with $N = .9\,N_c$ colliding with sun-like stars, this time is $t_* = 47$ minutes. We compare this to the time a colliding ASt spends inside the star, t_{in}. Averaging over the impact parameter of the collision, the average distance an ASt travels through an OSt is $\bar{d} = 4R_s/3$; the transit time of an ASt moving at a typical velocity $\bar{v} = 300$ km/s is roughly

$$t_{in} = \frac{\bar{d}}{\bar{v}} \approx \frac{4\,R_\odot/3}{\bar{v}} = 52\text{ min}, \tag{7.41}$$

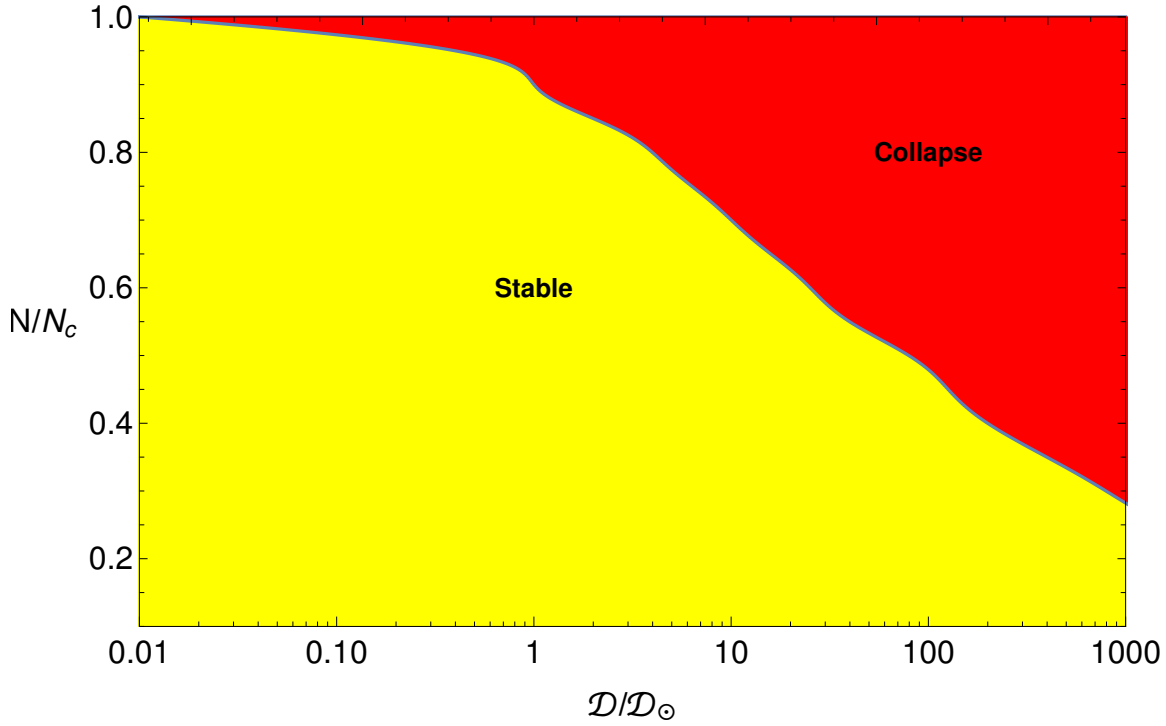

Figure 7.5.: The parameter space for ASt collapses induced by collisions with OSts. We identify two regions parameterized by the ratio of particle number to critical (N/N_c), and density compared to stellar density ($\mathcal{D}/\mathcal{D}_\odot$): A stable region with bound, dilute energy minima (yellow), and a collapse region with no dilute minimum (red). Figure reproduced from [179].

so $t_* < t_{in}$.

Thus, on the assumption that the sun is a "typical" star, and that a "typical" ASt has $N = .9\,N_c$, nearly all collisions represented by the rate in eq. (7.32) result in ASt collapse. This implies a collapse rate of[6]

$$\Gamma_{collapse} \sim 3000\,\frac{\mathcal{F}_{DM}}{\mathcal{F}_{AS}}\,\frac{\text{collapses}}{\text{year}\cdot\text{galaxy}}. \tag{7.42}$$

It should be emphasized that the estimation of the collapse rate above depends strongly on several assumptions, which may or may not hold true. Taking all stars to be roughly "sun-like" may not be a perfect approximation, but as we pointed out in Section 7.3, likely this approximation causes us to *under*estimate the size and mass of a "typical" star. On the other hand, we have mentioned that the mass distribution of ASts (both primordial and current) is very uncertain, so the assumption that most ASts have $N \sim .9N_c$ may break down. As a proof of concept, however, we feel that the estimates of this section work well: we have shown that in a reasonable range of parameters, it is possible that a very large number of ASts are caused to collapse

[6]Because this conclusion depends on the speed of ASts, we will again set $\eta = 1$ in this expression.

through repeated collisions with OSts. A precise determination of the rate of collapses beyond the assumptions of this chapter is beyond the scope of this work.

It is also worth noting that because axions have a coupling (albeit a weak one) to SM fields, ASts which do not collapse fully on a single pass through an OSt could dissipate kinetic energy through interactions with stellar matter. This could result in the ASt becoming bound to the OSt, resulting in repeated collisions and an increased probability for collapse.

Before we close this section, it may be useful to speculate about possible detection signatures related to these induced collapses. Recall from Chapter 6 that, as ASts collapse, they emit relativistic axions in the form of radiation [168, 173, 177], because the binding energy of a collapsing ASt increases rapidly. It is possible that all, or at least a large fraction of, the mass of the ASt would be converted to radiation in this way. If this is the case, then the total axion star contribution to dark matter in galactic halos could be decreasing with time, as relativistic axions escape from galaxies and galaxy clusters. If we take seriously our estimates of the rate of collapses induced in this way, this decrease could be substantial. If an $\mathcal{O}(1)$ fraction of a 10^{19} kg ASt is converted to radiation in each of $\mathcal{O}(1000)$ collisions per galaxy per year, then we would observe $\mathcal{O}(10^{22})$ kg of DM disappearing from a typical DM halo per year.[7] Over time, this could also lead to observable astrophysical or cosmological consequences, and it could constrain the hypothesis that axion stars constitute a large fraction of dark matter. Of course, a more detailed analysis would be required to determine more precisely the consequences, but in general this idea is very new and potentially exciting. We will return to these topics in a future work.

7.5. Collisions Between Axion Stars and Neutron Stars

7.5.1. Collision Rate

Axion star collisions with neutron stars are particularly interesting, because the strong magnetic fields in the latter can induce currents in the former, leading to stimulated axion conversion to radio-frequency photon bursts that could be observed. This mechanism has been proposed as the source of observed FRBs [189–192], and recent estimates suggest that the rate of collisions of ASts with NSts is compatible with the observed frequency of FRBs [187, 188, 193]. In this section we repeat the analysis of previous

[7] Of course, this estimate has *very very* large error bars.

authors using eq. (7.4), but also improve on these estimates by taking into account the NFW distribution of ASts, and a nontrivial distribution of neutron stars as well.

If ASts and NSts were distributed with uniform density in the galaxy, the rate of collisions is that of eq. (7.4). The gravitational enhancement of the cross section in eq. (7.5) is

$$\frac{2\,G\,(M_{NS}+M_{AS})}{\bar{v}^2\,(R_{NS}+R_{AS})} \approx 2\times 10^4, \tag{7.43}$$

where we used $R_{NS} = 10$ km and $M_{NS} = 1.4 M_\odot$. This is an enormous enhancement reflecting the fact that the neutron star is very compact and massive. The resulting cross section is

$$\sigma_{NS} = 2.7\times 10^9 \text{ km}^2. \tag{7.44}$$

Using a typical value $N_{NS} = 10^9$ for the number of NSts, we find a collision rate of

$$\hat{\Gamma}_{NS} = 1.5\times 10^{-3}\frac{\mathcal{F}_{DM}}{\mathcal{F}_{AS}}\frac{\text{collisions}}{\text{year}\cdot\text{galaxy}}. \tag{7.45}$$

This result was already known by previous authors [187, 188, 193] to be of the right order of magnitude to account for the reported frequency of observed FRBs.

As with the other astrophysical collisions considered in this chapter, we can improve on this estimate by taking nontrivial distributions into account. For ASts, we use (again) the NFW profile in eq. (7.14), while for neutron stars we use the phenomenological fit of [197]. The number density $n_{NS}(\ell,z)$ of neutron stars can be written in terms of two probability distributions $n_{NS}(\ell,z) = \mathcal{N}\,p_\ell(\ell)\,p_z(\ell,z)/2\pi\ell$, where

$$\begin{aligned} p_\ell(\ell) &= A_{0,\ell} + A\frac{\ell^{\alpha-1}}{\lambda^\alpha}e^{-\ell/\lambda} \text{ and} \\ p_z(\ell,z) &= A_{0,z}\,\Theta(z-.1\text{ kpc}) + A_1\,e^{-z/h_1(\ell)} + A_2\,e^{-z/h_2(\ell)}, \end{aligned} \tag{7.46}$$

where $\Theta(x)$ is a Heaviside step function. The scale heights $h_{1,2}(\ell)$ are defined by

$$\begin{aligned} h_1(\ell) &= k_1\,\ell + b_1 \\ h_2(\ell) &= \begin{cases} k_2^<\,\ell + b_2^<, & \ell \le 4.5\text{ kpc} \\ k_2^>\,\ell + b_2^>, & \ell \ge 4.5\text{ kpc} \end{cases} \end{aligned} \tag{7.47}$$

The cylindrical coordinates ℓ and z are defined as in Section 7.4, and the remaining constants are best-fit parameters from the analysis of [197], reproduced in Table 7.1. We

normalize the distribution using $\mathcal{N}$ by the requirement

$$2\int_0^{R_{vir}}\int_0^{2\pi}\int_0^{R_{vir}} \ell\, n_{NS}(\ell,z)\, d\ell\, d\theta\, dz = N_{NS} = 10^9. \tag{7.48}$$

We again use $v_{vir} = \eta\,\bar{v}$, and ignore velocity dispersion so that $\langle\sigma\, v\rangle_{NS} \approx \sigma_{NS}\, v_{vir}$. Finally, we find the total collision rate to be

$$\begin{aligned}\Gamma_{NS} &= 2\mathcal{N}\int_0^{R_{vir}} dz \int_0^{R_{vir}} d\ell\Big(\frac{\mathcal{F}_{DM}\rho_{NFW}(\sqrt{\ell^2+z^2})}{\mathcal{F}_{AS}M_{AS}}\Big)\, p_\ell(\ell)\, p_z(\ell,z)\langle\sigma\, v\rangle_{NS} \\ &= \frac{2\mathcal{N}\,\sigma_{NS}\,v_{vir}}{M_{AS}}\frac{\mathcal{F}_{DM}}{\mathcal{F}_{AS}}\int_0^{R_{vir}} dz \int_0^{R_{vir}} d\ell\,\rho_{NFW}(\sqrt{\ell^2+z^2})\, p_\ell(\ell)\, p_z(\ell,z) \\ &= 4\times 10^{-4}\,\eta\,\frac{\mathcal{F}_{DM}}{\mathcal{F}_{AS}}\frac{\text{collisions}}{\text{year}\cdot\text{galaxy}}.\end{aligned} \tag{7.49}$$

It should be noted that an estimate of this kind, using the NSt distribution found in [197], was first performed in [186] assuming spherical symmetry, whereas we have included the z-dependence in n_{NS}.

In this work we have remained agnostic about how axion stars form, preferring to parameterize our ignorance by the parameters $\mathcal{F}_{AS}$ and $\mathcal{F}_{DM}$. It is sometimes argued that all axion stars are formed in the early universe through the collapse of axion miniclusters. However, it is also possible that axion stars continually form as the dilute background of axions thermalizes and clumps together; such accretion of axions into condensates might be especially efficient if they form in the cores of ordinary stars. In this analysis, we have striven to correctly capture the relevant physics, as well as the astrophysical uncertainties regarding axion star formation. Because of these important uncertainties, we do not comment here on the interpretation of Fast Radio Bursts as originating in ASt collisions with neutron stars.

7.6. Summary

In this chapter, we have analyzed the consequences of axion stars as a component of dark matter halos. If they constitute a large fraction of the total dark matter mass, then they will exist in very copious quantities and will participate in astrophysical collisions with a large rate. We have attempted to quantify the most important astrophysical uncertainties using the parameters $\mathcal{F}_{DM}$ and $\mathcal{F}_{AS}$ defined in Section 7.2, which parameterize the total ASt contribution to DM and the average ASt mass (respectively).

In the parameter range analyzed here, we found that ASts may collide with OSts with a large rate, $\mathcal{O}(3000)$ collisions/year/galaxy. Further, by examining the response to a collision in the ASt energy functional, we estimated that a large fraction of these collisions could lead to collapse of otherwise stable ASts. This conclusion depends on somewhat tenuous assumptions about the ASt mass distribution. However, due to at least the possibility of such a large collapse rate, we conclude that this might be a promising area of future research, with more precise estimations leading to constraints on the hypothesis of ASts in DM halos.

Collisions between two ASts were estimated to occur with a much larger rate, $\mathcal{O}(10^7)$ collisions/year/galaxy. However, collapse will only occur if the relative velocity between the two colliding ASts is extremely small. As a result, it is probable that the effect of these collisions in a cosmological context is completely negligible.

Finally, collisions between ASts and neutron stars have been analyzed by a number of other authors [186, 188, 193]; we update the estimates of the collision rate here by using the full updated number distribution of NS, finding roughly commensurate results when uncertainties are taken into account. Though we do not analyze it in detail here, the hypothesis of FRBs originating in ASt collisions with NSts still appears viable.

Chapter 8.

Conclusions

"Nature's music is never over; her silences are pauses, not conclusions."
— Mary Webb

In this work, we have analyzed some of the consequences of the addition of scalar particles in extensions of the Standard Model. The SM, and its analogue in cosmology known as the ΛCDM model, each have a number of problems and lingering questions which allow the justification of such extensions. The Strong CP Problem in the QCD sector and the problem of Dark Matter in astrophysics and cosmology, which were at the forefront of this work, are two very different problems that could be solved simultaneously through the interactions of a new, very light boson: the axion.

Axions solve the Strong CP Problem through coupling to the strong interaction, and at the cosmological QCD phase transition, acquire a mass that can generate the correct relic abundance for DM. Being light scalars, produced sufficiently cold, they can coalesce into low-energy Bose-Einstein condensates, which can be large and massive enough to have novel astrophysical effects. We analyzed bosonic condensates through a number of methods, from classical field theory, to semiclassical quantization, to the nonrelativistic limit. These condensates are stabilized by a balance between kinetic (Heisenberg uncertainty) pressure, self-gravitation, and self-interactions.

By analyzing the low-energy limit of axion field theory, we derived the macroscopic properties of stable condensates formed from axions, usually called axion stars. In QCD, stable axion star states only exist up to a maximum mass which is $M = \mathcal{O}(10^{19})$ kg, and have a minimum radius which is $R = \mathcal{O}(100)$ km.[1] There exist energy extrema

[1] Due to their small size compared to an ordinary star, some prefer to refer to these states not as "axion stars", but rather as "axion drops" [93], "axitons" [137, 199], or (this author's favorite) "axteroids."

with smaller radii, but they are unstable to collapse. There are further no stable states with masses larger than the maximum.

We have analyzed the stability of axion stars. First, there exist number-changing transitions which can take place inside a condensate, where several bound axions convert to one or more high-energy axions which are emitted from the axion star. We found that the decay rate of axion stars through these processes was a function of their total mass, or through a simple variable change, their energy or chemical potential. Axion stars on the gravitationally stable, large-radius branch of solutions were found to be stable against decay with very long lifetimes.

We also analyzed the collapse of gravitationally unstable axion stars, finding that collapse proceeds from dilute to dense configurations in a timespan of $\mathcal{O}(few)$ minutes. The spectrum of states derived from the axion star energy indicated that collapsing axion stars do not form black holes, but are stabilized at a size larger than their Schwarzschild radius. In the last moments of collapse, the rate for the decay process increases rapidly, and a fraction of the axion star's energy is converted to relativistic particles.

Finally, we considered how axion stars might behave as a component of dark matter halos. In particular, if there exist a plenitude of axion stars in a typical halo, then they will participate in collisions with other astrophysical bodies. We calculated the rate for these collisions, and found them to be very frequent; we further showed that they can lead to collapse of otherwise stable axion stars. Because collapse leads to relativistic particle emission, we have speculated about possible novel detection signatures of axion stars in dark matter halos.

There are a number of open questions in the field of axion stars. First and foremost, the precise formation mechanism (both in the early universe and at late times) remains the subject of debate. Related to this is the mass distribution of axion stars, which is also not known with any precision. Of interest in recent literature is the possibility that individual axion condensates form entire dark matter halos; the consequences of this idea are still being explored. The answers to these questions will make precise the predictions of axion star models, and will be crucial in further developing an understanding of axion dark matter more generally.

Appendix A.

Expectation Values of the Axion Potential

A.1. N-particle Potential

The Ruffini-Bonazzola method consists in taking expectation values of the quantum equations of motion using an N-particle ground state. We detail the procedure here, using the axion potential of eq. (4.3) as our template. Other expectation values require a similar procedure (though most are calculationally less taxing).

Expand the axion wavefunction as in eq. (4.1); for simplicity, let $\mathcal{A} \equiv \mathcal{A}^+ + \mathcal{A}^-$, so that the axion potential has the form

$$V = m^2 f^2 \left[1 - \cos\left(\frac{\mathcal{A}^+ + \mathcal{A}^-}{f}\right)\right]. \tag{A.1}$$

Since $[\mathcal{A}^+, [\mathcal{A}^+, \mathcal{A}^-]] = 0$, we can use the Baker-Campbell-Hausdorff lemma to arrive at

$$\cos\left(\mathcal{A}^+ + \mathcal{A}^-\right) = e^{-[\mathcal{A}^+, \mathcal{A}^-]/2f^2}\, e^{i\mathcal{A}^+/f}\, e^{i\mathcal{A}^-/f}. \tag{A.2}$$

The expectation value of this potential between N-particle states is

$$\begin{aligned}\langle N|\cos\left(\frac{\mathcal{A}^+ + \mathcal{A}^-}{f}\right)|N\rangle &= e^{-[\mathcal{A}^+, \mathcal{A}^-]/2f^2}\,\langle N|e^{i\mathcal{A}^+/f}\, e^{i\mathcal{A}^-/f}|N\rangle \\ &= e^{-S(r)} \sum_{k=0}^{N} \frac{(-1)^k}{(k!)^2} \frac{N!}{(N-k)!} \left(\frac{R(r)}{f}\right)^{2k}\end{aligned} \tag{A.3}$$

where we have reinserted the definitions of the fields $\mathcal{A}^{\pm}$, and where

$$S(r) = \frac{R(r)^2}{2\,f^2}. \tag{A.4}$$

Because the wavefunction $R(r)$ scales with $N^{-1/2}$, the exponential $e^{-S} \to 1$ as the particle number $N \to \infty$. Further, in the same limit, the sum in eq. (A.3) is dominated by terms with $k \ll N$. Thus, in the large-N limit, we find the following result for the expectation value of the axion potential:

$$\begin{aligned}\langle N|V(\mathcal{A})|N\rangle &= m^2\,f^2\,\langle N|\left[1-\cos\left(\frac{\mathcal{A}}{f}\right)\right]|N\rangle \\ &= m^2\,f^2\left[1-J_0\Big(\frac{2\sqrt{N}\,R(r)}{f}\Big)\right],\end{aligned} \tag{A.5}$$

where J_k is the kth Bessel function of the first kind.

A.2. Number-Changing Operators

In Chapter 5, we also consider number-changing interactions. Using the method outlined above, we obtain in leading order in $1/N$,

$$\begin{aligned}\langle N|1-\cos\left(\frac{\mathcal{A}}{f}\right)|N-n\rangle &\approx \langle N|e^{i\,\mathcal{A}^+/f}e^{i\,\mathcal{A}^-/f}|N-n\rangle \\ &= -i^n\,J_n\left[Z(y)\right]e^{i\,n\,\mu_0}.\end{aligned} \tag{A.6}$$

These number-changing transitions generically lead to the emission of high energy axions, and so the analysis requires the extension of the field expansion in a complete set of both bound and scattering states, as in eq. (5.8). For the process (5.3), we find a transition matrix element

$$\langle N|1-\cos\left(\frac{\mathcal{A}}{f}\right)|N-n;\,p_1,...,p_\nu\rangle = -i^n\,J_n\left[Z(y)\right]\,e^{i\,n\,\mu_0}\left(\frac{i}{f}\right)^{\nu}\prod_{s=1}^{\nu}\frac{e^{i(\vec{p}_s\cdot\vec{r}-\mu_s\,t)}}{\sqrt{2\,\mu_s}}. \tag{A.7}$$

Each of the ν emitted axions are labeled by their energy eigenvalue μ_s and their momentum $\vec{p}_s$. Multiplying by the scale factor $m^2\,f^2$ and integrating over $d^3r\,dt$ gives the matrix element

$$\mathcal{M} = -2\,\pi\,m^2\,i^n\left(\frac{i}{f}\right)^{\nu-2}\delta(n\,\mu_0-\sum_s\mu_s)\int d^3r\,J_n(Z)\exp\left(i\,\vec{r}\cdot\left[\sum_s\vec{p}_s\right]\right)\prod_{s=1}^{\nu}\frac{1}{\sqrt{2\,\mu_s}}. \tag{A.8}$$

The application of (A.8) to the simplest case of $n = 3$ and $\nu = 1$ has been discussed in Chapter 5, which gave (5.19). Here we will discuss the next-to-leading order process, which involves the emission of two axions, $\nu = 2$. As shown by (A.8), $|\mathcal{M}|^2$ is proportional to $f^{4-2\nu}$. Since the remainder of the transition rate scales only with m, the rate of emission of μ axions compared to that of a single axion is $r_\nu = \Gamma^\nu \,/\, \Gamma^1 \sim (m \,/\, f)^{2\nu-2}$. This is a minuscule factor for almost every conceivable physical theory; for example, in QCD, $m^2 \,/\, f^2 \sim 10^{-50}$. In order to show that the coefficient is dominated by this small factor, and thus that higher-order contributions to the decay rate can be neglected, we sketch below the calculation of the rest of the matrix element for $\nu = 2$.

For $\nu = 2$, the most probable process has $n = 4$, i.e. 4 bound axions convert to 2 scattering state axions. In that case, the matrix element takes the form

$$\mathcal{M}_{4\to 2} = \frac{4\,\pi^2}{m\,K\,\sqrt{\mu_1\,\mu_2}}\, I_4(K)\,\delta(4\,\mu_0 - \mu_1 - \mu_2), \tag{A.9}$$

where $K = |\vec{p}_1 + \vec{p}_2| \,/\, m$ and where $I_4(K)$ was defined in (5.21). Then the transition rate per unit time is

$$\Gamma_{4\to 2} = \frac{1}{2\,\pi^4\,m^2} \int \frac{d^3p_1}{\mu_1}\,\frac{d^3p_2}{\mu_2}\,\frac{1}{K^2}\,[I_4(K)]^2\,\delta(4\,\mu_0 - \mu_1 - \mu_2), \tag{A.10}$$

where $\Gamma_{n\to\nu}$ is the transition rate of the process $N\,a_c \to (N-n)\,a_c + a_{k_1} + ... + a_{k_\nu}$. The integration over every variable but K can be performed analytically, to give

$$\Gamma_{4\to 2} = \frac{m}{16\pi^3} \int_0^{\sqrt{16\,(\mu_0/m)^2 - 4}} dK\, f(K)\,[I_4(K)]^2, \tag{A.11}$$

where $f(K)$ is a complicated function involving logarithms of expression containing K. However, at very weak binding $\mu_0 \to m$, $f(K)$ simplifies to

$$f(K) \simeq \frac{K\,(12 - K^2)}{16 - K^2}, \tag{A.12}$$

while the upper limit of integration over K becomes $\sqrt{12}$.

We calculated the the ratio of $\Gamma_{4\to 2}\,/\Gamma_{3\to 1}$, where $\Gamma_{3\to 1}$ is given in (5.19), at several choices of the input parameters and found that

$$\frac{\Gamma_{4\to 2}}{\Gamma_{3\to 1}} = C\,\frac{m^2}{f^2}, \tag{A.13}$$

where C is a constant of $\mathcal{O}(1) - \mathcal{O}(10)$. Thus, the ratio $m^2 \,/\, f^2 \ll 1$ makes the contribution of the process of emission of more than 1 axion to the decay of axion stars negligible.

Appendix B.

Binding Energy Corrections to the Axion Star Mass

In this appendix we estimate the binding energy in an axion star using leading corrections away from the infrared limit of Chapter 4. The lowest order corrections to the calculation of the mass M and particle number N in that chapter come at $\mathcal{O}(\delta)$ and $\mathcal{O}(\Delta^2)$, and in the interesting range $\kappa \equiv \delta/\Delta^2 = \mathcal{O}(1)$, these corrections are of the same order.

Recall from eq. (4.6) that the expectation value of the stress-energy tensor gives

$$\begin{aligned}\langle N|T_{00}|N\rangle &= f^2\left[\frac{{\mu_0}^2 N R^2}{B f^2} + \frac{N R'^2}{A f^2} - m^2\,[1 - J_0(X)]\right] \\ &= f^2\left[\frac{{\mu_0}^2 Z^2}{4B} + \frac{m^2 Z'^2}{4A} + \frac{m^2}{4}Z^2 - \frac{m^2}{64}Z^4 + ...\right] \\ &\approx m^2 f^2\left[\frac{{\epsilon_\mu}^2}{4B}\Delta^2 Y^2 + \frac{1}{4}\Delta^2 Y^2 + \frac{\Delta^4 Y'^2}{4A} - \frac{\Delta^4 Y^4}{64}\right],\end{aligned} \tag{B.1}$$

where in the last step we have dropped terms higher-order in $\Delta \ll 1$. Thus the mass is

$$\begin{aligned}M &= \int \langle N|T_{00}|N\rangle \sqrt{|g|}\, d^3r \\ &= \frac{1}{m^3\Delta^3}\int \langle N|T_{00}|N\rangle \sqrt{A\,B}\, d^3x \\ &= \frac{f^2}{m\,\Delta}\pi \int \left[\frac{{\epsilon_\mu}^2}{B} Y^2 + Y^2 + \frac{\Delta^2 Y'^2}{A} - \frac{\Delta^2 Y^4}{16}\right] \sqrt{A\,B}\, x^2 dx.\end{aligned} \tag{B.2}$$

Next, we will use $A = 1 + \delta\, a$ and $B = 1 + \delta\, b$ as in Chapter 4, which give further corrections of $\mathcal{O}(\delta)$; we need to expand also ${\epsilon_\mu}^2 = 1 - \Delta^2$ in the first term. Finally, there are corrections also to the wavefunction $Y(x)$, because the solutions we computed in that chapter neglected $\mathcal{O}(\delta, \Delta^2)$ terms in the equations of motion. Let's write $Y = Y_0 +$

Υ_1, where Υ_0 are the solutions found at leading order and Υ_1 represents the correction; we will take the correction term Υ_1 to be of the same order as δ, Δ^2, i.e. we drop ${\Upsilon_1}^2$ pieces. The leading order corrections are

$$\begin{aligned} M &= \frac{f^2}{m\,\Delta}\pi \int \left[(1-\Delta^2)(1-\delta\, b)\,\Upsilon^2 + \Upsilon^2 + \frac{\Delta^2\,\Upsilon'^2}{A} - \frac{\Delta^2\,\Upsilon^4}{16}\right] \sqrt{A\,B}\, x^2 dx \\ &\approx \frac{f^2}{m\,\Delta}\,\pi \int \left[2\,\Upsilon^2 - \Delta^2\,\Upsilon^2 - \delta\, b\,\Upsilon^2 + \Delta^2\,\Upsilon'^2 - \frac{\Delta^2\,\Upsilon^4}{16}\right]\left[1 + \frac{\delta}{2}(a+b)\right] x^2 dx \\ &= \frac{f^2}{m\,\Delta}\,\pi \int \left[2\,\Upsilon^2 + \delta(a+b)\Upsilon^2 - \Delta^2\,\Upsilon^2 - \delta\, b\,\Upsilon^2 + \Delta^2\,\Upsilon'^2 - \frac{\Delta^2\,\Upsilon^4}{16}\right] x^2 dx \\ &\approx \frac{f^2}{m\,\Delta}\,2\,\pi \int \left[\Upsilon_0^2 + 2\,\Upsilon_0\,\Upsilon_1 + \frac{\delta\, a}{2}\,\Upsilon_0^2 - \frac{\Delta^2}{2}\,\Upsilon_0^2 + \frac{\Delta^2}{2}\,\Upsilon_0'^2 - \frac{\Delta^2\,\Upsilon_0^4}{32}\right] x^2 dx. \end{aligned} \tag{B.3}$$

Observe that every term in eq. (B.3) is proportional to one of the following integrals:

$$\begin{aligned} I_0 &= \int {\Upsilon_0}^2\, x^2\, dx & I_1 &= \int \Upsilon_0\,\Upsilon_1\, x^2\, dx \\ I_a &= \int a\,{\Upsilon_0}^2\, x^2\, dx & I_b &= \int b\,{\Upsilon_0}^2\, x^2\, dx \\ I_p &= \int {\Upsilon_0}'^2\, x^2\, dx & I_4 &= \int {\Upsilon_0}^4\, x^2\, dx \end{aligned} \tag{B.4}$$

As a result, we can write the mass as

$$M = \frac{f^2}{m\,\Delta}\,2\,\pi\left[I_0 + 2\,I_1 + \frac{\delta}{2}\,I_a - \frac{\Delta^2}{2}\,I_0 + \frac{\Delta^2}{2}\,I_p - \frac{\Delta^2}{32}\,I_4\right]. \tag{B.5}$$

The leading-order expression recovers eq. (4.18) because the integral $U(\infty) = 2\,\pi\, I_0$.

Performing a similar analysis for the corrections to the particle number N, beginning with the first equality of eq. (4.23), we obtain

$$\begin{aligned} N &= \frac{f^2}{m^2\,\Delta}\,2\,\pi\,\sqrt{1-\Delta^2}\int \sqrt{\frac{1+\delta a(x)}{1+\delta b(x)}}\,\Upsilon(x)^2\, x^2\, dx \\ &\approx \frac{f^2}{m^2\,\Delta}\,2\,\pi\left[1 - \frac{\Delta^2}{2}\right]\int \left[1 + \frac{\delta}{2}(a-b)\right]\Upsilon(x)^2\, x^2\, dx \\ &\approx \frac{f^2}{m^2\,\Delta}\,2\,\pi\left[\Upsilon_0^2 + 2\,\Upsilon_0\,\Upsilon_1 - \frac{\Delta^2}{2}\,\Upsilon_0^2 + \frac{\delta}{2}(a-b)\,\Upsilon_0^2\right] x^2\, dx \\ &= \frac{f^2}{m^2\,\Delta}\,2\,\pi\left[I_0 + 2\,I_1 + \frac{\delta}{2}\,I_a - \frac{\delta}{2}\,I_b - \frac{\Delta^2}{2}\,I_0\right] \end{aligned} \tag{B.6}$$

The binding energy, defined in eq. (4.28), is

$$\begin{aligned} E_B = M - m\,N &= \frac{f^2}{m\,\Delta}\,2\,\pi\left[\frac{\delta}{2}\,I_b + \frac{\Delta^2}{2}\,I_p - \frac{\Delta^2}{32}\,I_4\right] \\ &= \frac{f^2}{m}\,2\,\pi\,\sqrt{\frac{\kappa}{\delta}}\left[\frac{\delta}{2}\,I_b + \frac{\Delta^2}{2}\,I_p - \frac{\Delta^2}{32}\,I_4\right], \end{aligned} \tag{B.7}$$

to leading order in $\mathcal{O}(\delta, \Delta^2)$. Note that the wavefunction correction Υ_1 cancels in the computation of E_B. To compute the binding energy per particle, we simply divide by the leading expression for N, given in eq. (4.23). The result, in units of particle mass, is

$$\frac{E_B}{m\,N} = \frac{1}{I_0}\left[\frac{\delta}{2}\,I_b + \frac{\Delta^2}{2}\,I_p - \frac{\Delta^2}{32}\,I_4\right]. \tag{B.8}$$

For each of the solutions $\Upsilon_0(x)$ we calculated in Chapter 4, we calculated $E_B/m\,N$ by evaluating the integrals in eq. (B.8). The results are illustrated in Figure 4.2.

Appendix C.

Computation of the Integral I_3

Regular solutions of eqs. (4.12) quite likely form a complete set of functions. In the region of parameter space where $\kappa \ll 1$, the axion wavefunction $Y(x)$ is effectively decoupled from gravity. Solutions of the resulting gravity-decoupled eq. (5.15) which are regular at $x = 0$ and vanish at infinity are uniquely defined and are real analytic, but have singularities at pairs of complex conjugate points.

Consequently, the contour of integration in I_3, which using eq. (5.14) we cast in the form

$$I_3 = \frac{\Delta}{48\, i} \int_{-\infty}^{\infty} dx\, x\, \exp\left(\frac{i\, k\, x}{\Delta}\right)\, Y(x)^3, \tag{C.1}$$

can be deformed until we encounter the first singularity, at $x = i\, y_I$, in the upper half complex plane. The contribution of the first pole in the upper half plane dominates the integral. To find the nature of these singularities, we expand the equation of motion (5.15) around the singular term, taking the ansatz

$$Y_{\text{sing}} \simeq \frac{A}{(x^2 + {y_I}^2)^{\alpha}}. \tag{C.2}$$

The only nontrivial solution is found if $\alpha = 1$, which implies that the singularities are first-order poles. In leading-order of the Laurent series expansion around $x^2 = -{y_I}^2$, we obtain the constraint $A = \pm\, 8\, y_I$.

The nature and location of the singularities with the smallest distance from the real axis, i.e. at $x = \pm\, i\, y_I$, can also be found out from examining the Taylor series expansion of the solution $Y(x)$ around $x = 0$

$$Y(x) = \sum_{n=0}^{\infty} \eta(n)\, x^{2\, n}. \tag{C.3}$$

Assuming a leading singularity of the form (C.2), it is easy to deduce the value of α, A, and y_I by using the asymptotic expansions in n,

$$\alpha = 1 + n^2 \left(1 - \frac{\eta(n+1)\,\eta(n-1)}{\eta(n)^2}\right) + O(n^{-4}), \tag{C.4}$$

$$y_I = \sqrt{-\frac{\eta(n-1)}{\eta(n)}} \left(1 + \frac{1-\alpha}{n} + \mathcal{O}(n^{-2})\right), \tag{C.5}$$

$$A = (-1)^n\, \eta(n)\, {y_I}^{2n+2}\, \alpha\, \frac{\alpha+1}{2}\, \frac{\alpha+2}{3} \left(1 + \frac{\alpha-1}{n}\right). \tag{C.6}$$

The expression (C.4), evaluated at large n, give

$$\alpha - 1 \approx \begin{cases} 3.2 \times 10^{-6}, & \text{for } n = 18 \\ 2.6 \times 10^{-6}, & \text{for } n = 19 \\ 2.1 \times 10^{-6}, & \text{for } n = 20 \end{cases} \tag{C.7}$$

This implies that $\alpha = 1$ (the singularity is a single pole) with a very high confidence. Then (C.6) reduces to $A = (-1)^n\, \eta(n)\, {y_I}^{2n+2}$, and we find

$$A \approx 4.81747, \qquad y_I \approx 0.602184. \tag{C.8}$$

Using the expression (C.2) and the fact that the pole at $x = i\,y_I$ dominates the integral, I_3 evaluates to the following simplified expression in leading order of Δ:

$$I_3 \approx \frac{32\, i\, \pi\, y_I}{3\,\Delta} \exp\left(-\frac{\sqrt{8}\, y_I}{\Delta}\right). \tag{C.9}$$

We also calculated I_3 by brute force, using the wave function obtained from numerical integration of eq. (5.15). This can only be done for moderately small (but not too small) values of Δ due to the rapidly oscillating integrand $\sim \sin(k\,x/\Delta)$. The expression of eq. (C.9) fits those calculations with the choice $y_I \approx 0.6$ extremely well.

Appendix D.

Boundedness of the Instanton Potential

In our original work on the topic of axion star collapse [168], the proof that the axion star energy had a dense global minimum depended on the boundedness of the axion self-interaction potential; in the Appendix of that paper, we provided a proof for the specific case of a Gaussian wavefunction. This proof can be generalized to any wavefunction which falls into one of two categories. For $F(\xi)$ defined in eq. (6.5), either: (a) ξ has a finite range, such that $F(\xi) = 0$ at $\xi \geq 1$ (i.e. the axion star has compact support on radius R); or (b) ξ has an infinite range but $F(\xi) \to 0$ as $\xi \to \infty$.[1] In this section we prove, under general conditions on the ansatz, that the self-interaction term in the axion star energy is bounded, and the kinetic energy term $1/\rho^2$ is dominant as $\rho \to 0$. This proof was originally provided in our follow-up work [169].

The general form of ansätze for the wave function, which we and other authors use, is of the form in eq. (6.5). We can see by using eqs. (6.7) and (6.14) that such an ansatz leads to the following equation for the self-interaction energy:

$$\frac{E_{SI}}{m\,N} = -\frac{\delta\, n}{\rho^3}\, v_I = -\frac{4\,\pi}{\zeta^2\, C_2} \int d\xi\, \xi^2 \left\{ 1 - J_0[\sqrt{2}\zeta\, F(\xi)] - \frac{\zeta^2}{2} F(\xi)^2 \right\}. \tag{D.1}$$

The $\rho \to 0$ limit of the self-energy is given by the $\zeta \to \infty$ limit, as in the definition (6.6). Then, dropping for now the numerical coefficients in the self-energy, we can write the integral in question as

$$K = \frac{1}{\zeta^2} \int d\xi\, \xi^2 \left\{ 1 - J_0[\sqrt{2}\zeta\, F(\xi)] - \frac{\zeta^2}{2} F(\xi)^2 \right\}. \tag{D.2}$$

The last term of K

$$-\frac{1}{\zeta^2} \int d\xi\, \xi^2\, \frac{\zeta^2}{2} F(\xi)^2 = -\frac{C_2}{8\,\pi} \tag{D.3}$$

[1] To our knowledge, all relevant ansätze used by other authors fall into one of these categories as well.

is always finite, since we must have[2]

$$C_2 = 4\,\pi \int_0^\infty d\xi\, \xi^2\, F(\xi)^2 < \infty, \tag{D.4}$$

convergent for a normalizable wavefunction. Consequently, we can restrict ourselves to investigate the $\zeta \to \infty$ behavior of the remainder of the integral

$$K' = \frac{1}{\zeta^2} \int d\xi\, \xi^2 \left\{1 - J_0[\sqrt{2}\,\zeta\, F(\xi)]\right\}. \tag{D.5}$$

The multiplier $1 - J_0[\sqrt{2}\,\zeta\, F(\xi)]$ of the integrand of K is positive, and bounded by its value taken at $\sqrt{2}\,\zeta\, F(\xi) = j_{1,1} = 3.83171$, where $j_{1,1}$ is the first zero of $J_1(x)$. Then we have the inequality

$$1 - J_0[\sqrt{2}\,\zeta\, F(\xi)] \leq B \equiv 1 - J_0(j_{1,1}) = 1.40276. \tag{D.6}$$

Let us consider ansätze in the first class (a). In that case, using the bound B in eq. (D.6), we have

$$K' = \frac{1}{\zeta^2} \int_0^1 d\xi\, \xi^2 \left\{1 - J_0[\sqrt{2}\,\zeta\, F(\xi)]\right\} \leq \frac{1}{\zeta^2} \int_0^1 d\xi\, \xi^2 B = \frac{B}{3\,\zeta^2} \sim \rho^3. \tag{D.7}$$

Clearly, $K' \to 0$ as $\rho \to 0$.

Now consider ansätze in class (b). We break up integral K' of eq. (D.5) such that in K'_1 the region of integration is $0 \leq \xi \leq \xi_1$ while in K'_2 it is $\xi > \xi_1$. We fix ξ_1 such that $\sqrt{2}\,\zeta\, F(\xi_1) = \nu$, where $\nu \ll 1$, a constant. Then using again the bound in eq. (D.6), we certainly have

$$K'_1 \leq \frac{{\xi_1}^3\, B}{3\,\zeta^2}. \tag{D.8}$$

Then it is easy to see that there is an $a > 0$ such that

$$F(\xi) < \frac{a}{\xi^{3/2}}. \tag{D.9}$$

Taken at $\xi = \xi_1$, eq. (D.9) can be inverted as

$${\xi_1}^3 < \frac{a^2}{F(\xi_1)^2} = \frac{2\,a^2\,\zeta^2}{\nu^2}. \tag{D.10}$$

[2]For example, in [168], we had $C_2 = \pi^{3/2}$, evaluated using the Gaussian ansatz.

Substituting ξ_1 into eq. (D.8) we obtain that $K_1' < 2\,a^2\,B\,/\,3\,\nu^2$, i.e. it has a finite limit as $\zeta \to \infty$.

Now consider integral

$$K_2' = \frac{1}{\zeta^2}\int_{\xi_1}^{\infty} d\xi\,\xi^2\left\{1 - J_0[\sqrt{2}\,\zeta\,F(\xi)]\right\}. \tag{D.11}$$

As $\sqrt{2}\,\zeta\,F(\xi_1) = \nu \ll 1$ and as $F(\xi)$ is monotonically decreasing as a function of ξ, the argument of the Bessel function in eq. (D.11), $\sqrt{2}\,\zeta\,F(\xi) \ll 1$ at all ξ. Then we can safely expand the Bessel function and keep terms only up to the second order, to get

$$K_2' \simeq \frac{1}{\zeta^2}\int_{\xi_1}^{\infty} d\xi\,\xi^2\,\frac{\zeta^2}{2}\,F(\xi)^2 < \frac{C_2}{8\,\pi}, \tag{D.12}$$

bounded. Then $K' = K_1' + K_2'$ is also bounded. We conclude that for any generic, monotonically decreasing ansatz for the axion star wavefunction, the instanton potential self-energy is bounded below. Because the chiral potential, as a function of z, is bounded below by the instanton potential (as shown in Chapter 6), we conclude that the chiral potential is also bounded.

Bibliography

[1] Mary K. Gaillard, Paul D. Grannis, and Frank J. Sciulli. The Standard Model of Particle Physics. *Reviews of Modern Physics*, 71(2):S96–S111, March 1999, hep-ph/9812285.

[2] Tom W. B. Kibble. The Standard Model of Particle Physics. *arXiv:1412.4094 [hep-ph, physics:hep-th, physics:physics]*, December 2014, 1412.4094.

[3] The CMS Collaboration. Observation of a new boson at a mass of 125 GeV with the CMS experiment at the LHC. *Physics Letters B*, 716(1):30–61, September 2012, 1207.7235.

[4] The ATLAS Collaboration. Observation of a new particle in the search for the Standard Model Higgs boson with the ATLAS detector at the LHC. *Physics Letters B*, 716(1):1–29, September 2012, 1207.7214.

[5] Peter W. Higgs. Broken Symmetries and the Masses of Gauge Bosons. *Phys. Rev. Lett.*, 13(16):508–509, October 1964.

[6] F. Englert and R. Brout. Broken Symmetry and the Mass of Gauge Vector Mesons. *Phys. Rev. Lett.*, 13(9):321–323, August 1964.

[7] N. Brambilla, S. Eidelman, P. Foka, S. Gardner, A. S. Kronfeld, M. G. Alford, R. Alkofer, M. Butenschoen, T. D. Cohen, J. Erdmenger, L. Fabbietti, M. Faber, J. L. Goity, B. Ketzer, H. W. Lin, F. J. Llanes-Estrada, H. Meyer, P. Pakhlov, E. Pallante, M. I. Polikarpov, H. Sazdjian, A. Schmitt, W. M. Snow, A. Vairo, R. Vogt, A. Vuorinen, H. Wittig, P. Arnold, P. Christakoglou, P. Di Nezza, Z. Fodor, X. Garcia i Tormo, R. Höllwieser, A. Kalwait, D. Keane, E. Kiritsis, A. Mischke, R. Mizuk, G. Odyniec, K. Papadodimas, A. Pich, R. Pittau, Jian-Wei Qiu, G. Ricciardi, C. A. Salgado, K. Schwenzer, N. G. Stefanis, G. M. von Hippel, and V. I. Zakharov. QCD and strongly coupled gauge theories: Challenges and perspectives. *The European Physical Journal C*, 74(10), October 2014, 1404.3723.

[8] A. Pich. The Standard Model of Electroweak Interactions. *arXiv:hep-ph/0502010*, February 2005, hep-ph/0502010.

[9] Paul Langacker. Introduction to the Standard Model and Electroweak Physics. *arXiv:0901.0241 [hep-ph]*, January 2009, 0901.0241.

[10] Edward Kolb and Michael Turner. The Early Universe. *Front. Phys.*, 69:1–547, 1990.

[11] D. Semikoz. High-energy astroparticle physics. *arXiv:1010.2647 [astro-ph, physics:hep-ph]*, October 2010, 1010.2647.

[12] P. Pralavorio. Particle Physics and Cosmology. *arXiv:1311.1769 [astro-ph, physics:hep-ex, physics:hep-ph]*, November 2013, 1311.1769.

[13] C. Patrignani and Particle Data Group. Review of Particle Physics. *Chinese Phys. C*, 40(10):100001, 2016.

[14] Michael Peskin and Daniel Schroeder. *An Introduction to Quantum Field Theory*. Westview, Boulder, CO, 1995.

[15] Mark Srednicki. *Quantum Field Theory*. Cambridge Univ. Press, Cambridge, 2007.

[16] Steven Weinberg. *Gravitation and Cosmology: Principles and Applications of the General Theory of Relativity*. Wiley, New York, NY, 1971.

[17] Bernard Schutz. *A First Course in General Relativity*. Cambridge University Press, 2nd edition, June 2009.

[18] Satyendra Bose. Plancks Gesetz und Lichtquantenhypothese. *Z. Phys.*, 26:178, 1924.

[19] Albert Einstein. Quantentheorie des einatomigen idealen Gases. *Sitzungsber. Kgl. Preuss. Akad. Wiss.*, page 261, 1924.

[20] Christopher Pethik and Henrik Smith. *Bose-Einstein Condensation in Dilute Gases*. Cambridge Univ. Press, Cambridge, 2001.

[21] M. H. Anderson, J. R. Ensher, M. R. Matthews, C. E. Wieman, and E. A. Cornell. Observation of Bose-Einstein Condensation in a Dilute Atomic Vapor. *Science*, 269(5221):198–201, July 1995.

[22] Dallin S. Durfee and Wolfgang Ketterle. Experimental studies of Bose-Einstein condensation. *Opt. Express, OE*, 2(8):299–313, April 1998.

[23] Qizhong Zhu and Biao Wu. Superfluidity of Bose-Einstein condensates in ultracold atomic gases. *Chinese Physics B*, 24(5):050507, May 2015, 1501.04153.

[24] M. R. Matthews, B. P. Anderson, P. C. Haljan, D. S. Hall, C. E. Wieman, and E. A. Cornell. Vortices in a Bose-Einstein Condensate. *Phys. Rev. Lett.*, 83(13):2498–2501,

September 1999.

[25] Chad N. Weiler, Tyler W. Neely, David R. Scherer, Ashton S. Bradley, Matthew J. Davis, and Brian P. Anderson. Spontaneous vortices in the formation of Bose–Einstein condensates. *Nature*, 455(7215):948–951, October 2008.

[26] N. G. Parker, B. Jackson, A. M. Martin, and C. S. Adams. Vortices in Bose-Einstein Condensates: Theory. *arXiv:0704.0146 [cond-mat]*, 45:173–189, 2008, 0704.0146.

[27] Jordan M. Gerton, Dmitry Strekalov, Ionut Prodan, and Randall G. Hulet. Direct observation of growth and collapse of a Bose–Einstein condensate with attractive interactions. *Nature*, 408(6813):692–695, December 2000.

[28] J. L. Roberts, N. R. Claussen, S. L. Cornish, E. A. Donley, E. A. Cornell, and C. E. Wieman. Controlled Collapse of a Bose-Einstein Condensate. *Phys. Rev. Lett.*, 86(19):4211–4214, May 2001.

[29] Elizabeth A. Donley, Neil R. Claussen, Simon L. Cornish, Jacob L. Roberts, Eric A. Cornell, and Carl E. Wieman. Dynamics of collapsing and exploding Bose-Einstein condensates. *Nature*, 412(6844):295–299, July 2001, cond-mat/0105019.

[30] Jihn E. Kim and Gianpaolo Carosi. Axions and the Strong CP Problem. *Reviews of Modern Physics*, 82(1):557–601, March 2010, 0807.3125.

[31] F. Zwicky. Die Rotverschiebung von extragalaktischen Nebeln. *Helvetica Physica Acta*, 6:110–127, 1933.

[32] F. Zwicky. Republication of: The redshift of extragalactic nebulae. *Gen Relativ Gravit*, 41(1):207–224, January 2009.

[33] E. Margaret Burbidge, G. R. Burbidge, D. J. Crampin, V. C. Rubin, and K. H. Prendergast. The Rotation and Mass of NGC 6503. *The Astrophysical Journal*, 139:539, February 1964.

[34] Vera C. Rubin and W. Kent Ford. Rotation of the Andromeda Nebula from a Spectroscopic Survey of Emission Regions. *The Astrophysical Journal*, 159:379, February 1970.

[35] Yoshiaki Sofue. Rotation Curve Decomposition for Size-Mass Relations of Bulge, Disk, and Dark Halo in Spiral Galaxies. *Publications of the Astronomical Society of Japan*, 68(1):2, February 2016, 1510.05752.

[36] M. Markevitch, A. H. Gonzalez, D. Clowe, A. Vikhlinin, L. David, W. Forman, C. Jones, S. Murray, and W. Tucker. Direct constraints on the dark matter self-interaction cross-section from the merging galaxy cluster 1E0657-56. *The Astro-*

physical Journal, 606(2):819–824, May 2004, astro-ph/0309303.

[37] Planck Collaboration, P. A. R. Ade, N. Aghanim, M. Arnaud, M. Ashdown, J. Aumont, C. Baccigalupi, A. J. Banday, R. B. Barreiro, J. G. Bartlett, N. Bartolo, E. Battaner, R. Battye, K. Benabed, A. Benoit, A. Benoit-Levy, J.-P. Bernard, M. Bersanelli, P. Bielewicz, J. J. Bock, A. Bonaldi, L. Bonavera, J. R. Bond, J. Borrill, F. R. Bouchet, F. Boulanger, M. Bucher, C. Burigana, R. C. Butler, E. Calabrese, J.-F. Cardoso, A. Catalano, A. Challinor, A. Chamballu, R.-R. Chary, H. C. Chiang, J. Chluba, P. R. Christensen, S. Church, D. L. Clements, S. Colombi, L. P. L. Colombo, C. Combet, A. Coulais, B. P. Crill, A. Curto, F. Cuttaia, L. Danese, R. D. Davies, R. J. Davis, P. de Bernardis, A. de Rosa, G. de Zotti, J. Delabrouille, F.-X. Desert, E. Di Valentino, C. Dickinson, J. M. Diego, K. Dolag, H. Dole, S. Donzelli, O. Dore, M. Douspis, A. Ducout, J. Dunkley, X. Dupac, G. Efstathiou, F. Elsner, T. A. Ensslin, H. K. Eriksen, M. Farhang, J. Fergusson, F. Finelli, O. Forni, M. Frailis, A. A. Fraisse, E. Franceschi, A. Frejsel, S. Galeotta, S. Galli, K. Ganga, C. Gauthier, M. Gerbino, T. Ghosh, M. Giard, Y. Giraud-Heraud, E. Giusarma, E. Gjerlow, J. Gonzalez-Nuevo, K. M. Gorski, S. Gratton, A. Gregorio, A. Gruppuso, J. E. Gudmundsson, J. Hamann, F. K. Hansen, D. Hanson, D. L. Harrison, G. Helou, S. Henrot-Versille, C. Hernandez-Monteagudo, D. Herranz, S. R. Hildebrandt, E. Hivon, M. Hobson, W. A. Holmes, A. Hornstrup, W. Hovest, Z. Huang, K. M. Huffenberger, G. Hurier, A. H. Jaffe, T. R. Jaffe, W. C. Jones, M. Juvela, E. Keihanen, R. Keskitalo, T. S. Kisner, R. Kneissl, J. Knoche, L. Knox, M. Kunz, H. Kurki-Suonio, G. Lagache, A. Lahteenmaki, J.-M. Lamarre, A. Lasenby, M. Lattanzi, C. R. Lawrence, J. P. Leahy, R. Leonardi, J. Lesgourgues, F. Levrier, A. Lewis, M. Liguori, P. B. Lilje, M. Linden-Vornle, M. Lopez-Caniego, P. M. Lubin, J. F. Macias-Perez, G. Maggio, D. Maino, N. Mandolesi, A. Mangilli, A. Marchini, P. G. Martin, M. Martinelli, E. Martinez-Gonzalez, S. Masi, S. Matarrese, P. Mazzotta, P. McGehee, P. R. Meinhold, A. Melchiorri, J.-B. Melin, L. Mendes, A. Mennella, M. Migliaccio, M. Millea, S. Mitra, M.-A. Miville-Deschenes, A. Moneti, L. Montier, G. Morgante, D. Mortlock, A. Moss, D. Munshi, J. A. Murphy, P. Naselsky, F. Nati, P. Natoli, C. B. Netterfield, H. U. Norgaard-Nielsen, F. Noviello, D. Novikov, I. Novikov, C. A. Oxborrow, F. Paci, L. Pagano, F. Pajot, R. Paladini, D. Paoletti, B. Partridge, F. Pasian, G. Patanchon, T. J. Pearson, O. Perdereau, L. Perotto, F. Perrotta, V. Pettorino, F. Piacentini, M. Piat, E. Pierpaoli, D. Pietrobon, S. Plaszczynski, E. Pointecouteau, G. Polenta, L. Popa, G. W. Pratt, G. Prezeau, S. Prunet, J.-L. Puget, J. P. Rachen, W. T. Reach, R. Rebolo, M. Reinecke, M. Remazeilles, C. Renault, A. Renzi, I. Ristorcelli, G. Rocha, C. Rosset, M. Rossetti, G. Roudier, B. Rouille d'Orfeuil, M. Rowan-Robinson, J. A. Rubino-Martin, B. Rusholme, N. Said, V. Salvatelli, L. Salvati, M. Sandri, D. Santos, M. Savelainen, G. Savini,

D. Scott, M. D. Seiffert, P. Serra, E. P. S. Shellard, L. D. Spencer, M. Spinelli, V. Stolyarov, R. Stompor, R. Sudiwala, R. Sunyaev, D. Sutton, A.-S. Suur-Uski, J.-F. Sygnet, J. A. Tauber, L. Terenzi, L. Toffolatti, M. Tomasi, M. Tristram, T. Trombetti, M. Tucci, J. Tuovinen, M. Turler, G. Umana, L. Valenziano, J. Valiviita, B. Van Tent, P. Vielva, F. Villa, L. A. Wade, B. D. Wandelt, I. K. Wehus, M. White, S. D. M. White, A. Wilkinson, D. Yvon, A. Zacchei, and A. Zonca. Planck 2015 results. XIII. Cosmological parameters. *Astronomy & Astrophysics*, 594:A13, October 2016, 1502.01589.

[38] Mario G. Abadi, Julio F. Navarro, Matthias Steinmetz, and Vincent R. Eke. Simulations of Galaxy Formation in a Λ Cold Dark Matter Universe. I. Dynamical and Photometric Properties of a Simulated Disk Galaxy. *ApJ*, 591(2):499, July 2003.

[39] Julio F. Navarro, Carlos S. Frenk, and Simon D. M. White. The Structure of Cold Dark Matter Halos. *The Astrophysical Journal*, 462:563, May 1996, astro-ph/9508025.

[40] Julio F. Navarro, Carlos S. Frenk, and Simon D. M. White. A Universal Density Profile from Hierarchical Clustering. *ApJ*, 490(2):493, 1997.

[41] Teresa Undagoitia and Ludwig Rauch. Dark matter direct-detection experiments. *J. Phys. G*, 43(1), 2016.

[42] Miguel Rocha, Annika H. G. Peter, James S. Bullock, Manoj Kaplinghat, Shea Garrison-Kimmel, Jose Onorbe, and Leonidas A. Moustakas. Cosmological Simulations with Self-Interacting Dark Matter I: Constant Density Cores and Substructure. *Monthly Notices of the Royal Astronomical Society*, 430(1):81–104, March 2013, 1208.3025.

[43] B. Moore, V. Quilis, S. Gelato, A. Jenkins, and F. R. Pearce. Collisional versus Collisionless Dark Matter. http://cds.cern.ch/record/427279, 2000.

[44] Romeel Davé, David N. Spergel, Paul J. Steinhardt, and Benjamin D. Wandelt. Halo Properties in Cosmological Simulations of Self-interacting Cold Dark Matter. *ApJ*, 547(2):574, 2001.

[45] Ben Moore. Evidence against dissipation-less dark matter from observations of galaxy haloes. *Nature*, 370(6491):629–631, August 1994.

[46] Ricardo A. Flores and Joel R. Primack. Observational and Theoretical Constraints on Singular Dark Matter Halos. *The Astrophysical Journal*, 427:L1, May 1994, astro-ph/9402004.

[47] G. Kauffmann, S. D. M. White, and B. Guiderdoni. The Formation and Evolution

of Galaxies Within Merging Dark Matter Haloes. *Monthly Notices of the Royal Astronomical Society*, 264:201, September 1993.

[48] Ben Moore, Sebastiano Ghigna, Fabio Governato, George Lake, Tom Quinn, Joachim Stadel, and Paolo Tozzi. Dark Matter Substructure in Galactic Halos. *The Astrophysical Journal*, 524(1):L19–L22, October 1999, astro-ph/9907411.

[49] Anatoly A. Klypin, Andrey V. Kravtsov, Octavio Valenzuela, and Francisco Prada. Where are the missing galactic satellites? *The Astrophysical Journal*, 522(1):82–92, September 1999, astro-ph/9901240.

[50] Lulu Liu, Brian F. Gerke, Risa H. Wechsler, Peter S. Behroozi, and Michael T. Busha. How Common are the Magellanic Clouds? *The Astrophysical Journal*, 733(1):62, May 2011, 1011.2255.

[51] Erik J. Tollerud, Michael Boylan-Kolchin, Elizabeth J. Barton, James S. Bullock, and Christopher Q. Trinh. Small-Scale Structure in the SDSS and LCDM: Isolated L* Galaxies with Bright Satellites. *The Astrophysical Journal*, 738(1):102, September 2011, 1103.1875.

[52] Louis E. Strigari and Risa H. Wechsler. The Cosmic Abundance of Classical Milky Way Satellites. *The Astrophysical Journal*, 749(1):75, April 2012, 1111.2611.

[53] Michael Boylan-Kolchin, James S. Bullock, and Manoj Kaplinghat. Too big to fail? The puzzling darkness of massive Milky Way subhaloes. *Monthly Notices of the Royal Astronomical Society: Letters*, 415(1):L40–L44, July 2011, 1103.0007.

[54] David H. Weinberg, James S. Bullock, Fabio Governato, Rachel Kuzio de Naray, and Annika H. G. Peter. Cold dark matter: Controversies on small scales. *Proceedings of the National Academy of Sciences*, 112(40):12249–12255, October 2015, 1306.0913.

[55] Mark Vogelsberger, Shy Genel, Debora Sijacki, Paul Torrey, Volker Springel, and Lars Hernquist. A model for cosmological simulations of galaxy formation physics. *Monthly Notices of the Royal Astronomical Society*, 436(4):3031–3067, December 2013, 1305.2913.

[56] Gianfranco Bertone, Dan Hooper, and Joseph Silk. Particle Dark Matter: Evidence, Candidates and Constraints. *Physics Reports*, 405(5-6):279–390, January 2005, hep-ph/0404175.

[57] Katherine Garrett and Gintaras Duda. Dark Matter: A Primer. *Advances in Astronomy*, 2011:1–22, 2011, 1006.2483.

[58] Adam G. Riess, Alexei V. Filippenko, Peter Challis, Alejandro Clocchiattia,

Alan Diercks, Peter M. Garnavich, Ron L. Gilliland, Craig J. Hogan, Saurabh Jha, Robert P. Kirshner, B. Leibundgut, M. M. Phillips, David Reiss, Brian P. Schmidt, Robert A. Schommer, R. Chris Smith, J. Spyromilio, Christopher Stubbs, Nicholas B. Suntzeff, and John Tonry. Observational Evidence from Supernovae for an Accelerating Universe and a Cosmological Constant. *The Astronomical Journal*, 116(3):1009–1038, September 1998, astro-ph/9805201.

[59] S. Perlmutter, G. Aldering, G. Goldhaber, R. A. Knop, P. Nugent, P. G. Castro, S. Deustua, S. Fabbro, A. Goobar, D. E. Groom, I. M. Hook, A. G. Kim, M. Y. Kim, J. C. Lee, N. J. Nunes, R. Pain, C. R. Pennypacker, R. Quimby, C. Lidman, R. S. Ellis, M. Irwin, R. G. McMahon, P. Ruiz-Lapuente, N. Walton, B. Schaefer, B. J. Boyle, A. V. Filippenko, T. Matheson, A. S. Fruchter, N. Panagia, H. J. M. Newberg, and W. J. Couch. Measurements of Omega and Lambda from 42 High-Redshift Supernovae. *The Astrophysical Journal*, 517(2):565–586, June 1999, astro-ph/9812133.

[60] Joshua Frieman, Michael Turner, and Dragan Huterer. Dark Energy and the Accelerating Universe. *Annual Review of Astronomy and Astrophysics*, 46(1):385–432, September 2008, 0803.0982.

[61] Michael J. Mortonson, David H. Weinberg, and Martin White. Dark Energy: A Short Review. *arXiv:1401.0046 [astro-ph]*, December 2013, 1401.0046.

[62] R. D. Peccei. The Strong CP Problem and Axions. *arXiv:hep-ph/0607268*, 741:3–17, 2008, hep-ph/0607268.

[63] Jihn E. Kim and Gianpaolo Carosi. Axions and the Strong CP Problem. *Reviews of Modern Physics*, 82(1):557–601, March 2010, 0807.3125.

[64] G. F. Giudice. Naturally Speaking: The Naturalness Criterion and Physics at the LHC. *arXiv:0801.2562 [hep-ph, physics:hep-th]*, June 2008, 0801.2562.

[65] Fred Jegerlehner. The hierarchy problem of the electroweak Standard Model revisited. *arXiv:1305.6652 [hep-ph]*, May 2013, 1305.6652.

[66] Antonio Padilla. Lectures on the Cosmological Constant Problem. *arXiv:1502.05296 [astro-ph, physics:gr-qc, physics:hep-ph, physics:hep-th]*, February 2015, 1502.05296.

[67] B. Borasoy. The electric dipole moment of the neutron in chiral perturbation theory. *Physical Review D*, 61(11), May 2000, hep-ph/0004011.

[68] Maxim Pospelov and Adam Ritz. Theta Vacua, QCD Sum Rules, and the Neutron Electric Dipole Moment. *Nuclear Physics B*, 573(1-2):177–200, May 2000, hep-

ph/9908508.

[69] Ralf Lehnert. CPT- and Lorentz-symmetry breaking: A review. *arXiv:hep-ph/0611177*, November 2006, hep-ph/0611177.

[70] R. J. Crewther, P. Di Vecchia, G. Veneziano, and Edward Witten. Chiral Estimate of the Electric Dipole Moment of the Neutron in Quantum Chromodynamics. *Phys.Lett.*, 88B:123, 1980.

[71] P. G. Harris. The Neutron EDM Experiment. *arXiv:0709.3100 [hep-ex]*, September 2007, 0709.3100.

[72] A. P. Serebrov, E. A. Kolomenskiy, A. N. Pirozhkov, I. A. Krasnoshekova, A. V. Vasiliev, A. O. Polyushkin, M. S. Lasakov, A. K. Fomin, I. V. Shoka, V. A. Solovey, O. M. Zherebtsov, P. Geltenbort, O. Zimmer, S. N. Ivanov, E. B. Alexandrov, S. P. Dmitriev, and N. A. Dovator. New measurements of neutron electric dipole moment. *JETP Letters*, 99(1):4–8, March 2014, 1310.5588.

[73] J. M. Pendlebury, S. Afach, N. J. Ayres, C. A. Baker, G. Ban, G. Bison, K. Bodek, M. Burghoff, P. Geltenbort, K. Green, W. C. Griffith, M. van der Grinten, Z. D. Grujic, P. G. Harris, V. Helaine, P. Iaydjiev, S. N. Ivanov, M. Kasprzak, Y. Kermaidic, K. Kirch, H.-C. Koch, S. Komposch, A. Kozela, J. Krempel, B. Lauss, T. Lefort, Y. Lemiere, D. J. R. May, M. Musgrave, O. Naviliat-Cuncic, F. M. Piegsa, G. Pignol, P. N. Prashanth, G. Quemener, M. Rawlik, D. Rebreyend, J. D. Richardson, D. Ries, S. Roccia, D. Rozpedzik, A. Schnabel, P. Schmidt-Wellenburg, N. Severijns, D. Shiers, J. A. Thorne, A. Weis, O. J. Winston, E. Wursten, J. Zejma, and G. Zsigmond. A Revised Experimental Upper Limit on the Electric Dipole Moment of the Neutron. *Physical Review D*, 92(9), November 2015, 1509.04411.

[74] A. C Irving, C McNeile, C Michael, K. J Sharkey, and H Wittig. Is the up-quark massless? *Physics Letters B*, 518(3–4):243–251, October 2001.

[75] Anson Hook. Anomalous solutions to the strong CP problem. *Physical Review Letters*, 114(14), April 2015, 1411.3325.

[76] R. D. Peccei and Helen R. Quinn. CP Conservation in the Presence of Pseudoparticles. *Phys. Rev. Lett.*, 38(25):1440–1443, June 1977.

[77] R. D. Peccei and Helen R. Quinn. Constraints imposed by CP conservation in the presence of pseudoparticles. *Phys. Rev. D*, 16(6):1791–1797, September 1977.

[78] Steven Weinberg. A New Light Boson? *Phys. Rev. Lett.*, 40(4):223–226, January 1978.

[79] F. Wilczek. Problem of Strong P and T Invariance in the Presence of Instantons. *Phys. Rev. Lett.*, 40(5):279–282, January 1978.

[80] Giovanni Grilli di Cortona, Edward Hardy, Javier Pardo Vega, and Giovanni Villadoro. The QCD axion, precisely. *arXiv:1511.02867 [hep-ex, physics:hep-lat, physics:hep-ph]*, November 2015, 1511.02867.

[81] Jihn E. Kim. Weak-Interaction Singlet and Strong CP Invariance. *Phys. Rev. Lett.*, 43(2):103–107, July 1979.

[82] M. A. Shifman, A. I. Vainshtein, and V. I. Zakharov. Can confinement ensure natural CP invariance of strong interactions? *Nuclear Physics B*, 166(3):493–506, April 1980.

[83] Michael Dine, Willy Fischler, and Mark Srednicki. A simple solution to the strong CP problem with a harmless axion. *Physics Letters B*, 104(3):199–202, August 1981.

[84] A. P. Zhitnitskii. Possible Suppression of Axion-Hadron Interactions. *Sov. J. Nucl. Phys. (Engl. Transl.); (United States)*, 31:2, February 1980.

[85] Pierre Sikivie. Axion Cosmology. *arXiv:astro-ph/0610440*, 741:19–50, 2008, astro-ph/0610440.

[86] David J. Gross, Robert D. Pisarski, and Laurence G. Yaffe. QCD and instantons at finite temperature. *Rev. Mod. Phys.*, 53(1):43–80, January 1981.

[87] Takashi Hiramatsu, Masahiro Kawasaki, Ken'ichi Saikawa, and Toyokazu Sekiguchi. Production of dark matter axions from collapse of string-wall systems. *Physical Review D*, 86(8), October 2012, 1202.5851.

[88] Masahiro Kawasaki, Ken'ichi Saikawa, and Toyokazu Sekiguchi. Axion dark matter from topological defects. *Physical Review D*, 91(6), March 2015, 1412.0789.

[89] C. J. Hogan and M. J. Rees. Axion miniclusters. *Physics Letters B*, 205(2):228–230, April 1988.

[90] Edward W. Kolb and Igor I. Tkachev. Axion miniclusters and Bose stars. *Phys. Rev. Lett.*, 71(19):3051–3054, November 1993.

[91] Kathryn M. Zurek, Craig J. Hogan, and Thomas R. Quinn. Astrophysical Effects of Scalar Dark Matter Miniclusters. *Physical Review D*, 75(4), February 2007, astro-ph/0607341.

[92] Edward Hardy. Miniclusters in the Axiverse. *Journal of High Energy Physics*, 2017(2), February 2017, 1609.00208.

[93] Sacha Davidson and Thomas Schwetz. Rotating Drops of Axion Dark Matter. *Physical Review D*, 93(12), June 2016, 1603.04249.

[94] Adam Burrows, M. Ted Ressell, and Michael S. Turner. Axions and SN 1987A: Axion trapping. *Phys. Rev. D*, 42(10):3297–3309, November 1990.

[95] Georg G. Raffelt, Javier Redondo, and Nicolás Viaux. The meV mass frontier of axion physics. *Physical Review D*, 84(10), November 2011, 1110.6397.

[96] Bijan Berenji, Jennifer Gaskins, and Manuel Meyer. Constraints on Axions and Axionlike Particles from Fermi Large Area Telescope Observations of Neutron Stars. *Physical Review D*, 93(4), February 2016, 1602.00091.

[97] Kyu Jung Bae, Ji-Haeng Huh, and Jihn E. Kim. Update of axion CDM energy density. *Journal of Cosmology and Astroparticle Physics*, 2008(09):005, September 2008, 0806.0497.

[98] Asimina Arvanitaki, Masha Baryakhtar, and Xinlu Huang. Discovering the QCD Axion with Black Holes and Gravitational Waves. *Physical Review D*, 91(8), April 2015, 1411.2263.

[99] Asimina Arvanitaki, Masha Baryakhtar, Savas Dimopoulos, Sergei Dubovsky, and Robert Lasenby. Black Hole Mergers and the QCD Axion at Advanced LIGO. *Physical Review D*, 95(4), February 2017, 1604.03958.

[100] Richard Brito, Vitor Cardoso, and Paolo Pani. Superradiance. *arXiv:1501.06570 [astro-ph, physics:gr-qc, physics:hep-ph, physics:hep-th, physics:physics]*, 906, 2015, 1501.06570.

[101] The LIGO Scientific Collaboration and the Virgo Collaboration. Observation of Gravitational Waves from a Binary Black Hole Merger. *Physical Review Letters*, 116(6), February 2016, 1602.03837.

[102] The LIGO Scientific Collaboration and the Virgo Collaboration. GW151226: Observation of Gravitational Waves from a 22-Solar-Mass Binary Black Hole Coalescence. *Physical Review Letters*, 116(24), June 2016, 1606.04855.

[103] Antoine Klein, Enrico Barausse, Alberto Sesana, Antoine Petiteau, Emanuele Berti, Stanislav Babak, Jonathan Gair, Sofiane Aoudia, Ian Hinder, Frank Ohme, and Barry Wardell. Science with the space-based interferometer eLISA. I: Supermassive black hole binaries. *Physical Review D*, 93(2), January 2016, 1511.05581.

[104] Edward Witten. Some properties of O(32) superstrings. *Physics Letters B*, 149(4):351–356, December 1984.

[105] Peter Svrcek and Edward Witten. Axions In String Theory. *Journal of High Energy Physics*, 2006(06):051–051, June 2006, hep-th/0605206.

[106] Asimina Arvanitaki, Savas Dimopoulos, Sergei Dubovsky, Nemanja Kaloper, and John March-Russell. String Axiverse. *Physical Review D*, 81(12), June 2010, 0905.4720.

[107] Bobby Samir Acharya, Konstantin Bobkov, and Piyush Kumar. An M Theory Solution to the Strong CP Problem and Constraints on the Axiverse. *Journal of High Energy Physics*, 2010(11), November 2010, 1004.5138.

[108] Michele Cicoli, Mark Goodsell, and Andreas Ringwald. The type IIB string axiverse and its low-energy phenomenology. *Journal of High Energy Physics*, 2012(10), October 2012, 1206.0819.

[109] Michael S. Turner. Coherent scalar-field oscillations in an expanding universe. *Phys. Rev. D*, 28(6):1243–1247, September 1983.

[110] William H. Press, Barbara S. Ryden, and David N. Spergel. Single mechanism for generating large-scale structure and providing dark missing matter. *Phys. Rev. Lett.*, 64(10):1084–1087, March 1990.

[111] Sang-Jin Sin. Late time Cosmological Phase Transition and Galactic Halo as Bose-liquid. *Physical Review D*, 50(6):3650–3654, September 1994, hep-ph/9205208.

[112] Wayne Hu, Rennan Barkana, and Andrei Gruzinov. Cold and Fuzzy Dark Matter. *Physical Review Letters*, 85(6):1158–1161, August 2000, astro-ph/0003365.

[113] Jeremy Goodman. Repulsive Dark Matter. *New Astronomy*, 5(2):103–107, April 2000, astro-ph/0003018.

[114] Luca Amendola and Riccardo Barbieri. Dark Matter from an ultra-light pseudo-Goldsone-boson. *Physics Letters B*, 642(3):192–196, November 2006, hep-ph/0509257.

[115] Bohua Li, Tanja Rindler-Daller, and Paul R. Shapiro. Cosmological Constraints on Bose-Einstein-Condensed Scalar Field Dark Matter. *Physical Review D*, 89(8), April 2014, 1310.6061.

[116] Hsi-Yu Schive, Tzihong Chiueh, and Tom Broadhurst. Cosmic Structure as the Quantum Interference of a Coherent Dark Wave. *Nature Physics*, 10(7):496–499, June 2014, 1406.6586.

[117] Lam Hui, Jeremiah P. Ostriker, Scott Tremaine, and Edward Witten. Ultralight scalars as cosmological dark matter. *Physical Review D*, 95(4), February 2017,

1610.08297.

[118] Monica Colpi, Stuart L. Shapiro, and Ira Wasserman. Boson Stars: Gravitational Equilibria of Self-Interacting Scalar Fields. *Phys. Rev. Lett.*, 57(20):2485–2488, November 1986.

[119] Andrea Maselli, Pantelis Pnigouras, Niklas Gronlund Nielsen, Chris Kouvaris, and Kostas D. Kokkotas. Dark stars: Gravitational and electromagnetic observables. *arXiv:1704.07286 [astro-ph]*, April 2017, 1704.07286.

[120] Joshua Eby, Chris Kouvaris, Niklas Gronlund Nielsen, and L. C. R. Wijewardhana. Boson Stars from Self-Interacting Dark Matter. *Journal of High Energy Physics*, 2016(2), February 2016, 1511.04474.

[121] John Archibald Wheeler. Geons. *Phys. Rev.*, 97(2):511–536, January 1955.

[122] Jan Klaers, Julian Schmitt, Frank Vewinger, and Martin Weitz. Bose-Einstein condensation of photons in an optical microcavity. *Nature*, 468(7323):545–548, November 2010, 1007.4088.

[123] David J. Kaup. Klein-Gordon Geon. *Phys. Rev.*, 172(5):1331–1342, August 1968.

[124] Eckehard W. Mielke and Reinhard Scherzer. Geon Type Solutions of the Nonlinear {Heisenberg-Klein-Gordon} Equation. *Phys.Rev.*, D24:2111, 1981.

[125] Remo Ruffini and Silvano Bonazzola. Systems of Self-Gravitating Particles in General Relativity and the Concept of an Equation of State. *Phys. Rev.*, 187(5):1767–1783, November 1969.

[126] Pierre-Henri Chavanis. Mass-radius relation of Newtonian self-gravitating Bose-Einstein condensates with short-range interactions: I. Analytical results. *Physical Review D*, 84(4), August 2011, 1103.2050.

[127] S. Chandrasekhar. The Maximum Mass of Ideal White Dwarfs. *The Astrophysical Journal*, 74:81, July 1931.

[128] S. Chandrasekhar. The highly collapsed configurations of a stellar mass (Second paper). *Monthly Notices of the Royal Astronomical Society*, 95:207–225, January 1935.

[129] Eckehard W. Mielke and Franz E. Schunck. Boson Stars: Alternatives to primordial black holes? *Nuclear Physics B*, 564(1-2):185–203, January 2000, gr-qc/0001061.

[130] Franz E. Schunck and Eckehard W. Mielke. TOPICAL REVIEW: General relativistic boson stars. *arXiv:0801.0307 [astro-ph]*, January 2008, 0801.0307.

[131] Sacha Davidson. Axions: Bose Einstein Condensate or Classical Field? *Astroparti-*

cle Physics, 65:101–107, May 2015, 1405.1139.

[132] David J. E. Marsh. Axion Cosmology. *Physics Reports*, 643:1–79, July 2016, 1510.07633.

[133] Pierre Sikivie and Elisa M. Todarello. Duration of classicality in highly degenerate interacting Bosonic systems. *arXiv:1607.00949 [astro-ph, physics:cond-mat, physics:hep-ph, physics:hep-th]*, July 2016, 1607.00949.

[134] Mark P. Hertzberg. Quantum and Classical Behavior in Interacting Bosonic Systems. *Journal of Cosmology and Astroparticle Physics*, 2016(11):037–037, November 2016, 1609.01342.

[135] J. D. Breit, S. Gupta, and A. Zaks. Cold Bose stars. *Physics Letters B*, 140:329–332, June 1984.

[136] Yasusada Nambu and Misao Sasaki. Quantum treatment of cosmological axion perturbations. *Phys. Rev. D*, 42(12):3918–3924, December 1990.

[137] Alan H. Guth, Mark P. Hertzberg, and C. Prescod-Weinstein. Do Dark Matter Axions Form a Condensate with Long-Range Correlation? *Physical Review D*, 92(10), November 2015, 1412.5930.

[138] Eniko J. M. Madarassy and Viktor T. Toth. Evolution and dynamical properties of Bose-Einstein condensate dark matter stars. *Physical Review D*, 91(4), February 2015, 1412.7152.

[139] E. P. Gross. Structure of a quantized vortex in boson systems. *Nuovo Cim*, 20(3):454–477, May 1961.

[140] L. P. Pitaevskii. Vortex lines in an imperfect Bose gas. *Sov. Phys. JETP*, 13(2):451–454, 1961.

[141] L. Landau and E. Lifshitz. *Course of Theoretical Physics, Volume 6: Fluid Mechanics*, volume 6. Pergamon Press, Oxford, 1980.

[142] Felix Kling and Arvind Rajaraman. Towards an Analytic Construction of the Wavefunction of Boson Stars. *arXiv:1706.04272 [astro-ph, physics:gr-qc, physics:hep-th]*, June 2017, 1706.04272.

[143] C. G. Boehmer and T. Harko. Can dark matter be a Bose-Einstein condensate? *Journal of Cosmology and Astroparticle Physics*, 2007(06):025–025, June 2007, 0705.4158.

[144] P. Schuck and X. Viñas. Thomas-Fermi approximation for Bose-Einstein condensates in traps. *Phys. Rev. A*, 61(4):043603, March 2000.

[145] P. H. Chavanis and L. Delfini. Mass-radius relation of Newtonian self-gravitating Bose-Einstein condensates with short-range interactions: II. Numerical results. *Physical Review D*, 84(4), August 2011, 1103.2054.

[146] H. T. C. Stoof. Macroscopic Quantum Tunneling of a Bose Condensate. *Journal of Statistical Physics*, 87(5-6):1353–1366, June 1997, cond-mat/9601150.

[147] Jose A. Freire and Daniel P. Arovas. Collapse of a Bose Condensate with Attractive Interactions. *Physical Review A*, 59(2):1461–1467, February 1999, cond-mat/9803280.

[148] M. Membrado, A. F. Pacheco, and J. Sañudo. Hartree solutions for the self-Yukawian boson sphere. *Phys. Rev. A*, 39(8):4207–4211, April 1989.

[149] Fabio Governato, Chris Brook, Lucio Mayer, Alyson Brooks, George Rhee, James Wadsley, Patrik Jonsson, Beth Willman, Greg Stinson, Thomas Quinn, and Piero Madau. At the heart of the matter: The origin of bulgeless dwarf galaxies and Dark Matter cores. *Nature*, 463(7278):203–206, January 2010, 0911.2237.

[150] A. Del Popolo and F. Pace. The Cusp/Core problem: Supernovae feedback versus the baryonic clumps and dynamical friction model. *Astrophysics and Space Science*, 361(5), May 2016, 1502.01947.

[151] Joshua Eby, Peter Suranyi, Cenalo Vaz, and L. C. R. Wijewardhana. Axion Stars in the Infrared Limit. *Journal of High Energy Physics*, 2015(3), March 2015, 1412.3430.

[152] J. Barranco and A. Bernal. Towards a realistic axion star. *arXiv:0808.0081 [astro-ph]*, 1026:245–247, 2008, 0808.0081.

[153] J. Barranco and A. Bernal. Self-gravitating system made of axions. *Phys. Rev. D*, 83(4):043525, February 2011.

[154] Eric Braaten, Abhishek Mohapatra, and Hong Zhang. Dense Axion Stars. *Physical Review Letters*, 117(12), September 2016, 1512.00108.

[155] Joshua Eby, Peter Suranyi, and L. C. R. Wijewardhana. The lifetime of axion stars. *Mod. Phys. Lett. A*, 31(15):1650090, May 2016, 1512.01709.

[156] Joshua Eby, Michael Ma, Peter Suranyi, and L. C. R. Wijewardhana. Decay of Ultralight Axion Condensates. *arXiv:1705.05385 [astro-ph, physics:hep-ph]*, May 2017, 1705.05385.

[157] M. Gell-Mann. The interpretation of the new particles as displaced charge multiplets. *Nuovo Cim*, 4(2):848–866, April 1956.

[158] Gordon Kane. *Modern Elementary Particle Physics*. Addison Wesley, Redwood

City, CA, 1987.

[159] David J. Griffiths. *Introduction to Elementary Particles*. Wiley, New York, NY, 2nd edition, 2008.

[160] E. Fermi. Versuch einer Theorie der β-Strahlen. I. *Z. Physik*, 88(3-4):161–177, March 1934.

[161] M. Gell-Mann. The Eightfold Way: A Theory of Strong Interaction Symmetry. Technical Report TID-12608; CTSL-20, California Inst. of Tech., Pasadena. Synchrotron Lab., March 1961.

[162] M. Gell-Mann. Strange Particle Physics. Strong Interactions. *Proc. Int. Conf. High Energy Phys. (CERN)*, page 805, 1962.

[163] I. I. Tkachev. On the possibility of Bose-star formation. *Physics Letters B*, 261(3):289–293, May 1991.

[164] Eric Braaten, Abhishek Mohapatra, and Hong Zhang. Emission of Photons and Relativistic Axions from Axion Stars. *arXiv:1609.05182 [astro-ph, physics:hep-ph]*, September 2016, 1609.05182.

[165] Eric Braaten, Hans-Werner Hammer, and G. Peter Lepage. Open Effective Field Theories from Highly Inelastic Reactions. *arXiv:1612.08047 [hep-ph]*, December 2016, 1612.08047.

[166] Kyohei Mukaida, Masahiro Takimoto, and Masaki Yamada. On Longevity of I-ball/Oscillon. *arXiv:1612.07750 [astro-ph, physics:hep-ph, physics:hep-th]*, December 2016, 1612.07750.

[167] Mark P. Hertzberg. Quantum Radiation of Oscillons. *Physical Review D*, 82(4), August 2010, 1003.3459.

[168] Joshua Eby, Madelyn Leembruggen, Peter Suranyi, and L. C. R. Wijewardhana. Collapse of Axion Stars. *Journal of High Energy Physics*, 2016(12), December 2016, 1608.06911.

[169] Joshua Eby, Madelyn Leembruggen, Peter Suranyi, and L. C. R. Wijewardhana. QCD Axion Star Collapse with the Chiral Potential. *arXiv:1702.05504 [hep-ph]*, February 2017, 1702.05504.

[170] Eric Braaten, Abhishek Mohapatra, and Hong Zhang. Nonrelativistic Effective Field Theory for Axions. *Physical Review D*, 94(7), October 2016, 1604.00669.

[171] Pierre-Henri Chavanis. Collapse of a self-gravitating Bose-Einstein condensate with attractive self-interaction. *Physical Review D*, 94(8), October 2016, 1604.05904.

[172] Yang Bai, Vernon Barger, and Joshua Berger. Hydrogen Axion Star: Metallic Hydrogen Bound to a QCD Axion BEC. *Journal of High Energy Physics*, 2016(12), December 2016, 1612.00438.

[173] Thomas Helfer, David J. E. Marsh, Katy Clough, Malcolm Fairbairn, Eugene A. Lim, and Ricardo Becerril. Black hole formation from axion stars. *Journal of Cosmology and Astroparticle Physics*, 2017(03):055–055, March 2017, 1609.04724.

[174] Tiberiu Harko. Gravitational collapse of Bose-Einstein condensate dark matter halos. *Physical Review D*, 89(8), April 2014, 1403.3358.

[175] Víctor M. Pérez-García, Humberto Michinel, J. I. Cirac, M. Lewenstein, and P. Zoller. Dynamics of Bose-Einstein condensates: Variational solutions of the Gross-Pitaevskii equations. *Phys. Rev. A*, 56(2):1424–1432, August 1997.

[176] Lay Nam Chang, Djordje Minic, Chen Sun, and Tatsu Takeuchi. Observable Effects of Quantum Gravity. *arXiv:1605.04361 [gr-qc, physics:hep-th]*, May 2016, 1605.04361.

[177] D. G. Levkov, A. G. Panin, and I. I. Tkachev. Relativistic axions from collapsing Bose stars. *Physical Review Letters*, 118(1), January 2017, 1609.03611.

[178] P. Di Vecchia and G. Veneziano. Chiral dynamics in the large N limit. *Nuclear Physics B*, 171:253–272, January 1980.

[179] Joshua Eby, Madelyn Leembruggen, Joseph Leeney, Peter Suranyi, and L. C. R. Wijewardhana. Collisions of Dark Matter Axion Stars with Astrophysical Sources. *arXiv:1701.01476 [astro-ph, physics:hep-ph]*, January 2017, 1701.01476.

[180] B. J. Carr and M. Sakellariadou. Dynamical Constraints on Dark Matter in Compact Objects. *ApJ*, 516(1):195, 1999.

[181] Nilanjan Banik, Adam Christopherson, Pierre Sikivie, and Elisa Maria Todarello. The Rethermalizing Bose-Einstein Condensate of Dark Matter Axions. *arXiv:1509.02081 [astro-ph, physics:hep-ph]*, September 2015, 1509.02081.

[182] Chris Kouvaris and Peter Tinyakov. Excluding Light Asymmetric Bosonic Dark Matter. *Physical Review Letters*, 107(9), August 2011, 1104.0382.

[183] Xinyu Li, Fayin Wang, and K. S. Cheng. Gravitational effects of condensate dark matter on compact stellar objects. *Journal of Cosmology and Astroparticle Physics*, 2012(10):031–031, October 2012, 1210.1748.

[184] Chris Kouvaris and Peter Tinyakov. On (Not)-Constraining Heavy Asymmetric Bosonic Dark Matter. *Physical Review D*, 87(12), June 2013, 1212.4075.

[185] Aiichi Iwazaki. Axionic Boson Stars in Magnetized Conducting Media. *Physical Review D*, 60(2), June 1999, hep-ph/9901396.

[186] J. Barranco, A. Carrillo Monteverde, and D. Delepine. Can the dark matter halo be a collisionless ensemble of axion stars? *Physical Review D*, 87(10), May 2013, 1212.2254.

[187] Igor I. Tkachev. Fast Radio Bursts and Axion Miniclusters. *JETP Letters*, 101(1):1–6, January 2015, 1411.3900.

[188] A. Iwazaki. Axion Stars and Fast Radio Bursts. *Physical Review D*, 91(2), January 2015, 1410.4323.

[189] D. R. Lorimer, M. Bailes, M. A. McLaughlin, D. J. Narkevic, and F. Crawford. A bright millisecond radio burst of extragalactic origin. *Science*, 318(5851):777–780, November 2007, 0709.4301.

[190] E. F. Keane, D. A. Ludovici, R. P. Eatough, M. Kramer, A. G. Lyne, M. A. McLaughlin, and B. W. Stappers. Further Searches for RRATs in the Parkes Multi-Beam Pulsar Survey. *Monthly Notices of the Royal Astronomical Society*, 401(2):1057–1068, January 2010, 0909.1924.

[191] D. Thornton, B. Stappers, M. Bailes, B. R. Barsdell, S. D. Bates, N. D. R. Bhat, M. Burgay, S. Burke-Spolaor, D. J. Champion, P. Coster, N. D'Amico, A. Jameson, S. Johnston, M. J. Keith, M. Kramer, L. Levin, S. Milia, C. Ng, A. Possenti, and W. van Straten. A Population of Fast Radio Bursts at Cosmological Distances. *Science*, 341(6141):53–56, July 2013, 1307.1628.

[192] L. G. Spitler, J. M. Cordes, J. W. T. Hessels, D. R. Lorimer, M. A. McLaughlin, S. Chatterjee, F. Crawford, J. S. Deneva, V. M. Kaspi, R. S. Wharton, B. Allen, S. Bogdanov, A. Brazier, F. Camilo, P. C. C. Freire, F. A. Jenet, C. Karako-Argaman, B. Knispel, P. Lazarus, K. J. Lee, J. van Leeuwen, R. Lynch, A. G. Lyne, S. M. Ransom, P. Scholz, X. Siemens, I. H. Stairs, K. Stovall, J. K. Swiggum, A. Venkataraman, W. W. Zhu, C. Aulbert, and H. Fehrmann. Fast Radio Burst Discovered in the Arecibo Pulsar ALFA Survey. *The Astrophysical Journal*, 790(2):101, July 2014, 1404.2934.

[193] Stuart Raby. Axion star collisions with Neutron stars and Fast Radio Bursts. *Physical Review D*, 94(10), November 2016, 1609.01694.

[194] Simeon Bird, Ilias Cholis, Julian B. Muñoz, Yacine Ali-Haïmoud, Marc Kamionkowski, Ely D. Kovetz, Alvise Raccanelli, and Adam G. Riess. Did LIGO detect dark matter? *Physical Review Letters*, 116(20), May 2016, 1603.00464.

[195] Fabrizio Nesti and Paolo Salucci. The Dark Matter Halo of the Milky Way, AD 2013. *Journal of Cosmology and Astroparticle Physics*, 2013(07):016–016, July 2013, 1304.5127.

[196] Mario Juric, Zeljko Ivezic, Alyson Brooks, Robert H. Lupton, David Schlegel, Douglas Finkbeiner, Nikhil Padmanabhan, Nicholas Bond, Branimir Sesar, Constance M. Rockosi, Gillian R. Knapp, James E. Gunn, Takahiro Sumi, Donald Schneider, J. C. Barentine, Howard J. Brewington, J. Brinkmann, Masataka Fukugita, Michael Harvanek, S. J. Kleinman, Jurek Krzesinski, Dan Long, Jr Neilsen, Atsuko Nitta, Stephanie A. Snedden, and Donald G. York. The Milky Way Tomography with SDSS: I. Stellar Number Density Distribution. *The Astrophysical Journal*, 673(2):864–914, February 2008, astro-ph/0510520.

[197] Ali Taani, Luca Naso, Yingchun Wei, Chengmin Zhang, and Yongheng Zhao. Modeling the Spatial Distribution of Neutron Stars in the Galaxy. *arXiv:1205.4307 [astro-ph]*, May 2012, 1205.4307.

[198] Eric Cotner. Collisional interactions between self-interacting non-relativistic boson stars: Effective potential analysis and numerical simulations. *Physical Review D*, 94(6), September 2016, 1608.00547.

[199] Edward W. Kolb and Igor I. Tkachev. Non-Linear Axion Dynamics and Formation of Cosmological Pseudo-Solitons. *Physical Review D*, 49(10):5040–5051, May 1994, astro-ph/9311037.